A CONSTRAINT-STABILIZED TIME-STEPPING APPROACH FOR PIECEWISE SMOOTH MULTIBODY DYNAMICS

by

Gary D. Hart

M.S., University of Pittsburgh, 2004

Submitted to the Graduate Faculty of

the University of Pittsburgh in partial fulfillment

of the requirements for the degree of

Doctor of Philosophy

University of Pittsburgh

2007

UNIVERSITY OF PITTSBURGH

DEPARTMENT OF MATHEMATICS

This dissertation was presented

by

Gary D. Hart

It was defended on

April 4th 2007

and approved by

Dr. Mihai Anitescu, Department of Mathematics

Dr. William J. Layton, Department of Mathematics

Dr. Beatrice M. Riviere, Department of Mathematics

Dr. Andrew J. Schaefer, Department of Industrial Engineering

Dr. Ivan P. Yotov, Department of Mathematics

Dissertation Advisors: Dr. Mihai Anitescu, Department of Mathematics,

Dr. William J. Layton, Department of Mathematics

A CONSTRAINT-STABILIZED TIME-STEPPING APPROACH FOR PIECEWISE SMOOTH MULTIBODY DYNAMICS

Gary D. Hart, PhD

University of Pittsburgh, 2007

Rigid multibody dynamics is an important area of mathematical modeling which attempts to predict the position and velocity of a system of rigid bodies. Many methods will use smooth bodies without friction. The task is made especially more difficult in the face of noninterpenetration constraints, joint constraints, and friction forces.

The difficulty that arises when noninterpenetration constraints are enforced is directly related to the fact that the usual methods of computing the distance between bodies do not give any indication of the amount of penetration when two bodies interpenetrate. Because we wish to calculate vectors that are normal to contact, and because it is necessary to determine the amount of penetration, when it exists, the classical computation of the depth of penetration when applied to convex polyhedral bodies is inefficient.

We hereby describe a new method of determining when two convex polyhedra intersect and of evaluating a measure of the amount of penetration, when it exists. Our method is much more efficient than the classic computation of the penetration depth since it can be shown that its complexity grows only linearly with the size of the problem.

We use our method to construct a signed distance function and implement it for use with a method for achieving geometrical constraint stabilization for a linear-complementarity-based time-stepping scheme for rigid multibody dynamics with joints, contact, and friction which, before now, was not equipped to handle polyhedral bodies. During our analysis, we describe how to compute normal vectors at contact, despite the cases when the classic derivative fails to exist.

We put this analysis into a time-stepping procedure that uses a convex relaxation of a mixed linear complementarity problem with a resulting fixed point iteration that is guaranteed to converge if the friction is not too large, the time step is not too large, and the initial solution is feasible. Finally, we construct an algorithm that achieves constraint stabilization with quadratic convergence.

The numerical results proved to be quite satisfactory, implying that the constraint stabilization holds, and that quadratic convergence exists.

TABLE OF CONTENTS

LIST OF FIGURES

PREFACE

Dedicated to my family, especially my mother Juanita G. Hart

Thanks to my principal advisor Dr. Mihai Anitescu for all of his hard work and dedication, and to co-advisor Dr. William J. Layton, committee members Dr. Beatrice M. Riviere, Dr. Andrew J. Schaefer, and Dr. Ivan P. Yotov, and to the Department of Mathematics at the University of Pittsburgh.

1.0 INTRODUCTION

Man has always cultivated the desire or need to predict the future, and has expended much time, energy, and capital for the pursuit of that knowledge. Numerous examples can be seen from the plethora of predictions of the weather, stock market, athletic competitions, and even political races. Some natural phenomena can be modeled by a mathematical equation, the solution of which may produce a satisfactory predictor of future behavior.

1.1 APPLICATION OF RIGID MULTI BODY DYNAMICS

Simulating the dynamics of a system with several rigid bodies and with joint, contact (noninterpenetration), and friction constraints is an important part of many areas, e.g. rock dynamics [45] and human motion [38]. Often mathematical models will ignore friction because friction makes simulation particularly difficult because there might be no acceleration solution (Painleve Paradox) even when the velocity solution exists. Hence, attempting to predict of the position of bodies using any good numerical method requires extra care, since the classical solution may not even exist [47].

However, dynamical friction and contact analysis is also part of many other research areas, such as virtual reality [41] and robotic simulations [7]. It is thus expected that progress in simulating such phenomena will have a positive impact upon many other areas.

A virtual reality driving simulator is currently being developed with the hope of helping patients, for example soldiers or car accident victims, recover from post-traumatic stress disorder (PTSD). Moreover, virtual reality exposure (VRE) therapy is used to cure fears of heights, flying, public speaking, and thunderstorms [30, 43, 44]. In some cases of PTSD

related to the World Trade Center attacks of September 11, 2001 there are documented cases when VRE therapy helped when the standard treatment of imaginal exposure therapy failed [23].

Minimally invasive surgery is usually preferred by both patients and surgeons, and a Karlsruhe Endoscopic Surgery Trainer uses a surgical training system which is based on virtual reality and the simulation software KISMET [34]. A Virtual Reality Anatomic tool models the flexion-extension movement of the human knee joint whose accuracy depends highly on its collision detection [14].

The U.S. military has extreme interest in robotic simulation for use on the battlefield. One particular need is the use of self-driving vehicles so as to comply with a congressional mandate to move towards a large unmanned ground force [52], while another predicted use in the Pentagon's Future Combat System as a significant part of this country's military fighting force [51]. The medical operating rooms have been invaded by robots that work with surgeons to save lives. According to the United Nations Economic Commision for Europe's World Robotics 2004 survey, in 2003 the demand for robots increased by 19 per cent, and in the first half of 2004, the demand increased over same period in 2003 by 18 per cent which, at the time, was the highest growth ever recorded [53].

1.2 PREVIOUS APPROACHES

The mathematical modeling of rigid multibody dynamic systems is extensive and various methods have been proposed to overcome particular difficulties. Because the equations of motion involve differential equations, it would seem natural to try an integrate-detect-restart simulation method. The possibility of several bodies in near collision might cause too many small stepsizes to be used. Other items that make the problem more difficult to solve include the presence of joint constraints, the presence of friction, and the modeling of nonsmooth bodies.

When there are joint constraints in the system, then the problem reduces to solving a system of differential algebraic equations (DAE) [13, 29]. But then specialized techniques

must be used because of the non-smooth nature of the noninterpenetration and friction constraints. Historical approaches for simulating rigid multi-body dynamics with contact and friction have included piecewise DAE methods [29],acceleration-force linear complementarity problem (LCP) methods [15, 25, 50], penalty (or regularization) methods [24, 46], and velocity-impulse LCP-based time-stepping methods [8, 10, 48, 49]. Actually, the LCP of the velocity-impulse method is identical to the one used in the compression phase of multiple collision resolution [26] when the value of the time step is set to 0.

Milenkovic and Schmidl [36] solve a quadratic program at each step for their optimization based animation technique in the attempt to avoid the extremely small stepsize that can occur in the traditional classical integrate-detect-restart simulation methods. Unfortunately, this method must still fall prey to the small stepsizes that are inevitable when many bodies collide almost simultaneously.

1.2.1 Penalty Methods

Considering all of these various methods, one very often encounters the penalty (barrier) function approach to constrained optimization in the literature [19, 20, 31]. One reason is that the non-smooth nature of contact and friction is more easily treated by smooth mathematical modeling. This approach has a nice advantage in that it is fairly easy to set up and it also results in a DAE, for which we have numerous very well developed analytic theory and software tools. Unfortunately, this approach has disadvantages, such as the creation of stiff problems even for moderate time steps, and also obtaining the *a priori* appropriate values for the needed smoothing parameters can be difficult.

1.2.2 Methods With Hard Constraints

The mathematical model of the LCP method produces inequality constraints from both contact and friction, and then treats them computationally as hard constraints. One immediate advantage of using this approach is the elimination of artificially induced stiffness. Moreover, since the user no longer needs as much input, such as extra fine-tuning *a priori* parameters, we might expect this approach to work more efficiently. On the other hand, now

the subproblems are constrained by inequalities, and so separate analysis and software tools must now be developed for this approach to be successful.

The velocity impulse LCP based approach that is used here has the advantage that it does not suffer from the lack of a solution that can appear in the piecewise DAE and acceleration-force LCP approach [15, 48], nor does it suffer from the artificial stiffness that is introduced by the penalty approach.

1.3 CURRENT NEEDS OF HARD CONSTRAINT APPROACHES

If we wish to avoid the possibility of infinitely small time steps, which can result from collisions, then a minimum size of the time step must be given. For numerical methods with a minimum time step, interpenetration of the bodies may be unavoidable. Thus for such methods, which includes fixed-step methods, an allowance must be made for interpenetrations.

When interpenetration is allowed, there is no need for collision detection, and thus the order of the numerical scheme cannot exceed 1 [27]. Because of this, it is reasonable to employ a first-order integration technique.

1.3.1 Depth of Penetration

In these cases, the need for computing a distance between objects and the extent of interpenetration, when it exists, becomes vital. In physical simulations, for example, collisions and interpenetration among objects must be detected. The minimum Euclidean distance is usually used to compute the distance between separated objects. But when penetration exists, we cannot use this minimal Euclidean distance to describe the extent of the penetration. Hence we will need to develop a useful measure of distance if we want to determine the depth of penetration, and we need to do this while maintaining constraint stabilization.

Of particular interest is choosing a method for the computation of the distance between two objects which is efficient and feasible. Recently, many have proposed using a natural

extension of the Euclidean distance in the particular case of convex polyhedra, as in [2, 32, 33]. These analyses for the penetration depth often involve the Minkowski sum and involve specialized algorithms. Unfortunately, the computational price of a method that calculates the Minkowski sums is too high because of its complexity.

1.3.2 Constraint Stabilization

In addition to the analysis of dynamic systems, the numerical solution of subproblems resulting from such simulations often results in constraint drift, especially when solving an algebraic-differential equation, which is due to the index reduction process [13]. Our method must adjust for this problem.

The constraint stabilization issue in a complementarity setting has been tackled by using nonlinear complementarity problems [49], an LCP followed by a nonlinear projection approach that includes nonlinear inequality constraints [9], and a post-processing method [18] that uses one potentially non-convex LCP based on the stiff method developed in [9] followed by one convex LCP for constraint stabilization. When applied to joint-only systems, the method from [18] belongs to the set of post-processing methods defined in [11, 12]. In order to achieve constraint stabilization, however, all of these methods need additional computation after the basic LCP subproblem has been solved. This stands in contrast with our approach which will need no additional computational effort to achieve constraint stabilization.

1.3.3 Improving Complexity

As a part of my thesis research I have developed a method [5] that achieves geometrical (noninterpenetration and joint) constraint stabilization for complementarity-based time-stepping methods for rigid multi-body dynamics with contact, joints, and friction without the need of additional postprocessing. A variant of the scheme presented here is currently used for the dynamical simulation of dynamical robotic grasps [7, 37]. This scheme needs no computational effort other than that for solving the basic LCP subproblem, though the free term of the LCP is modified compared with other time-stepping LCP approaches [8, 9, 49].

One of the goals of this thesis is to ultimately define a new measure that easily detects collision and penetration of two convex bodies, is computationally efficient by involving only solving a linear programming problem, is computationally fast because of complexity of $O(n + m)$, compared to best algorithms known for calculating penetration depth, and is metrically equivalent to the signed Euclidean distance when close to a contact. Another goal is to develop an algorithm which efficiently models the system and solves the resulting LCP while achieving constraint stabilization. Our last goal is implementation of the algorithm to simulate polyhedral multibody contact problems with friction.

2.0 RATIO METRIC: A NEW PENETRATION DEPTH MEASURE

Virtual reality is very prominent on television and movie theaters. In many episodes of the television series *Star Trek*, for example, the crew members are often seen in the holodeck, a virtual reality room where humans could interact with a computer simulated environment. Many people can not imagine the pervasive impact of virtual reality in our everyday lives.

Currently, there are some virtual environment simulations which provide force feedback to the user. Haptic technology uses this tactile information to apply forces or motion, and this can allow the user to experience a more sensory interface. Virtual reality with haptic technology has great potential for teaching, and has been used in the gaming and medical industry.

An example of these advances In the medical industry is robotic surgery, which is instrumental for some minimally invasive surgery techniques [1] or the 3D modeling of the coronary artery for angiograms [39]. It would seem logical that not only would the detection of contact be important, but the calculation of the depth of any penetration be vital as well.

The conventional method of computing the Euclidean depth of penetration is convenient for smooth bodies, but not efficient for piecewise smooth bodies. In the cases of polyhedra, one typically finds methods that compute the Minkowski sums [33]. For computational efficiency, however, we require a different procedure.

Our goal in this Chapter is to define a new measure that defines the distance between convex bodies, as opposed to only between smooth surfaces. We start by introducing and analyzing a new measure between two convex bodies. Finally, we extend the analysis to produce our new measure of penetration depth and after we have this measure defined properly, we will see that it is metrically equivalent to the Euclidean Penetration Depth measure. However, we will see that this new measure has lower computational complexity.

2.1 COMPLEXITY OF PAST APPROACHES

When the bodies are modeled by spheres, then detecting contact and calculating the depth of penetration, when it exists, is trivial because it involves only the radii and locations of the spheres. For nonsmooth bodies, however, the situation is quite different and complicated. There are several problems with computing Minkowski sums to calculate the depth of penetration when the bodies are polyhedra [33].

The worst case deterministic scenario in computing the depth of penetration using Minkowski sums has complexity $O(m^2 + n^2)$. On the other hand, Agarwal et. al. [2] have an produced a stochastic method for approximating the depth of penetration with complexity of about $O(m^{3/4+\epsilon}n^{3/4+\epsilon})$ for any $\epsilon > 0$. Thus leads us to ask the question: Is there a faster deterministic method using some metric which is similar (at least in the limit) to the penetration depth?

We can now answer in the affirmative, since it is known [35] that we can solve a linear programming problem in linear time. We will now present an efficient algorithm that calculates the depth of penetration using linear programming instead of Minkowski sums. The obvious advantage is that the complexity of linear programming problems is computationally faster for polyhedral bodies.

2.2 POLYHEDRA AND EXPANSION/CONTRACTION MAPS

We begin by using the defining inequalities to provide us with a compact way to describe a convex polyhedron. Then we define the expansion (or contraction) of that polyhedron with respect to a given interior point. We find that there exists a mapping associated with this expansion/contraction, which we also define.

Definition 2.1. We define CP(A, b, x_o) to be the convex polyhedron P defined by the linear inequalities $Ax \leq b$ with an interior point x_o. We will often just write P = CP(A, b, x_o).

Definition 2.2. Let P = CP(A, b, x_o). Then for any nonnegative real number t, the

expansion (contraction) of P with respect to the point x_o is defined to be

$$P(x_o, t) = \{x | Ax \leq tb + (1-t)Ax_o\}$$

and has an associated mapping

$$\Gamma(x, x_o, t) = tx + (1-t)x_o.$$

Notice that the mapping is component-wise affine. That is, its restriction with respect to any individual variable, is an affine transformation:

$$\begin{aligned} \Gamma(x, x_o, t) - \Gamma(y, x_o, t) &= t(x-y) \\ \Gamma(x, x_o, t) - \Gamma(x, y_o, t) &= (1-t)(x_o - y_o) \\ \Gamma(x, x_o, t_1) - \Gamma(x, x_o, t_2) &= (t_1 - t_2)(x - x_o). \end{aligned} \tag{2.1}$$

We plan to exploit other properties of this mapping. Under modest conditions, we see that one of the restricted mappings actually is invertible.

Proposition 2.3. *For any x, we have $\Gamma(x, x_o, 0) = x_o$. Also, let $t > 0$, and define G to be the restriction of $\Gamma(x, x_o, t)$ in its first component, that is,*

$$G_{x_o,t}(.) = \Gamma(., x_o, t).$$

Then G has an inverse map that satisfies

$$G^{-1}_{x_o,t}(x) = G_{x_o,\frac{1}{t}}(x).$$

Proof. That $\Gamma(x, x_o, 0) = x_o$ should be obvious. Now, for any $t > 0$, we have already established in equation (2.1) the fact that G is affine. It is also clear that G is nonconstant. Hence this nonconstant affine map must have an inverse map, say G^{-1}. In particular, if we let x $= G_{x_o,t}(z)$, then z $= G^{-1}_{x_o,t}(x)$ and it follows that

$$\begin{aligned}
G^{-1}_{x_o,t}(x) &= z \\
&= \frac{1}{t}t(z - x_o) + x_o \\
&= \frac{1}{t}t(z - x_o) + \frac{1}{t}x_o + (1 - \frac{1}{t})x_o \\
&= \frac{1}{t}\left[t(z - x_o) + x_o\right] + (1 - \frac{1}{t})x_o \\
&= \frac{1}{t}\left[tz + (1 - t)x_o\right] + (1 - \frac{1}{t})x_o \\
&= \frac{1}{t}x + (1 - \frac{1}{t})x_o \\
&= \Gamma(x, x_o, \frac{1}{t}) \\
&= G_{x_o,\frac{1}{t}}(x).
\end{aligned}$$

■

Our interests are mainly for nonnegative values of the real number t, so we examine the image of our polyhedron under this map.

Proposition 2.4. *Let P = CP(A, b, x_o). Then for any nonnegative real number t, P(x_o, t) is the image of P under the map $\Gamma(x, x_o, t)$. That is,*

$$\Gamma(P, x_o, t) = P(x_o, t)$$

Proof. Every point $x \in P$, must satisfy $Ax \leq b$, and therefore

$$\begin{aligned}
A\Gamma(x, x_o, t) &= A\left(tx + (1 - t)x_o\right) \\
&= tAx + (1 - t)Ax_o \\
&\leq tb + (1 - t)Ax_o.
\end{aligned}$$

Thus $\Gamma(P, x_o, t) \subseteq P(x_o, t)$. On the other hand, for any z $= \Gamma(x, x_o, t)$,we also have

$$\begin{aligned} Az &= A\Gamma(x, x_o, t) \\ &= A(tx + (1-t)x_o) \\ &= tAx + (1-t)Ax_o) \\ &\leq tb + (1-t)Ax_o. \end{aligned}$$

Thus $P(x_o, t) \subseteq \Gamma(P, x_o, t)$. This establishes equality, and thus completes the proof. ■

If the interior point x_o is obvious or assumed to be known, we will often simply write P(t), for simplicity of notation. Next, notice that the image of a hyperplane under our mapping is another hyperplane parallel to the original.

Proposition 2.5. *Let H be a hyperplane. Then $\Gamma(H, x_o, t)$ is a hyperplane parallel to H.*

Proof. Let the hyperplane H be given by

$$H = \left\{x | c^T x = \alpha\right\}.$$

Then define $\beta = t\alpha + (1-t)c^T x_o$. This implies that if z is any point on H and x the image of z, then

$$\begin{aligned} c^T x &= c^T \Gamma(z, x_o, t) \\ &= c^T \left(tz + (1-t)x_o\right) \\ &= tc^T z + (1-t)c^T x_o \\ &= t\alpha + (1-t)c^T x_o \\ &= \beta, \end{aligned}$$

which is in the hyperplane $H' = \left\{x | c^T x = \beta\right\}$ which is parallel to H. Now, since $t > 0$, there is a one-one relationship between α and β, thus the image of H is H'. ■

From now on, whenever we write a hyperplane $H = \left\{x | c^T x = \alpha\right\}$, we may assume, without loss of generality, that the associated vector c is a unit vector. One advantage is because the matrix form of the associated projection mapping has a simple form $P = cc^T$, and because the projection of a vector v will always satisfy $||P(v)|| \leq ||v||$.

The characteristic we described in Proposition 2.5 of mapping hyperplanes to parallel hyperplanes is useful when considering a separating hyperplane. We know that two non-intersecting convex bodies can be separated by a hyperplane. We discover that our map preserves separation.

Lemma 2.6. *Let H be a hyperplane. Then $\Gamma(H, x_o, t)$ is a hyperplane H' parallel to H which is closer to x_o when $0 < t < 1$, and more distant from x_o when $t > 1$. Moreover, if H separates two bodies, then their images under Γ is separated by H'.*

Proof. That $\Gamma(H, x_o, t)$ is a hyperplane parallel to H follows directly from Proposition 2.5. Notice that the collection of hyperplanes parallel to H forms an ordered set with $H_o = \Gamma(H, x_o, 0)$ being the hyperplane parallel to H that passes through x_o, and $\Gamma(H, x_o, 1)$ the hyperplane H itself. Further computation shows that

$$\begin{aligned} \beta &= t\alpha + (1-t)c^T x_o \\ &= tc^T x + (1-t)c^T x_o \\ &= tc^T x + c^T x_o - tc^T x_o \\ &= c^T x_o + tc^T(x - x_o), \end{aligned}$$

which, because of the order relation of the hyperplanes parallel to H, shows that if $0 < t < 1$ then hyperplane H' is between H and H_o and when $t > 1$, H is between H' and H_o.

Finally we note that Γ maps the half plane $\{x | c^T x < \alpha\}$ to $\{x | c^T x < \beta\}$, and so if H separates two bodies, then their images under Γ must be separated by H'. ■

Corollary 2.7. *Let H be a hyperplane and $t > 0$. Then the preimage of H under $\Gamma(H, x_o, t)$ is $\Gamma(H, x_o, \frac{1}{t})$, a hyperplane parallel to H.*

Proof. Since we have $\Gamma(H, x_o, t) = G_{x_o,t}(H)$, it follows from Proposition 2.3 that $G^{-1}_{x_o,t}(H) = G_{x_o,\frac{1}{t}}(H) = \Gamma(H, x_o, \frac{1}{t})$. This means that the preimage of H under $\Gamma(., x_o, t)$ is exactly $\Gamma(H, x_o, \frac{1}{t})$. We now can invoke Lemma (2.6) to obtain the desired result. ■

In addition to preserving separation of bodies, notice that our map has other interesting features.

Proposition 2.8. *Let z be a point and $t > 0$. Then $\Gamma(z, x_o, t)$ is a point z on the ray from x_o through z, which is closer to x_o when $t < 1$, and more distant from x_o when $t > 1$.*

Proof. Direct calculation shows that

$$\begin{aligned} \Gamma(z, x_o, t) - x_o &= tz + (1-t)x_o - x_o \\ &= t(z - x_o), \end{aligned}$$

and so $\Gamma(z, x_o, t)$ is indeed a point z on the ray from x_o through z. From Lemma (2.6) we get the order result. ■

Proposition 2.9. *Let $P = CP(A, b, x_o)$ have a nonempty interior. Then $P(x_o, s) \subseteq P(x_o, t)$ if and only if $s \leq t$.*

Proof. Let $s \leq t$. Recall from Definition 2.1 that we have $Ax \leq b$. Then it follows that

$$\begin{aligned} x \in P(x_o, s) &\Rightarrow Ax \leq sb + (1-s)Ax_o \\ &\Rightarrow Ax \leq s(b - Ax_o) + Ax_o \\ &\Rightarrow Ax \leq t(b - Ax_o) + Ax_o \\ &\Rightarrow Ax \leq tb + (1-t)Ax_o \\ &\Rightarrow x \in P(x_o, t). \end{aligned}$$

That is, $P(x_o, s) \subseteq P(x_o, t)$.

Now suppose that $P(x_o, s) \subseteq P(x_o, t)$. Note that the nonempty interior criterion insures us that we can choose any point x_t in $P(x_o, t)$ different from x_o. The point defined by

$$x = x_o + \alpha(x_t - x_o)$$

must reside, by convexity, within $P(x_o, t)$ if $0 \leq \alpha \leq 1$, and also satisfy

$$\begin{aligned} Ax &= A\left(x_o + \alpha(x_t - x_o)\right) \\ &= Ax_o + \alpha(Ax_t - Ax_o) \\ &\leq Ax_o + \alpha\left(tb + (1-t)Ax_o - Ax_o\right) \\ &= \alpha tb + (1 - \alpha t)Ax_o \\ &= sb + (1-s)Ax_o, \end{aligned}$$

as long as $s = \alpha t$. Therefore, we have $x \in P(x_o, s)$. Recall that $0 \leq \alpha \leq 1$, hence it must be true that $s < t$. ■

This inclusion relation is important when we use this map to expand or contract our convex polyhedra. In particular, we now show that from the way we defined it, $P(x_o, t)$ must be convex.

Proposition 2.10. *Let P = CP(A, b, x_o). Then $P(x_o, t)$ is convex.*

Proof. Let x, y ∈ P. Then

$$Ax \leq tb + (1-t)Ax_o$$

and

$$Ay \leq tb + (1-t)Ax_o.$$

It follows that for any convex combination z = α x + β y,where $\alpha + \beta = 1$, we have

$$\begin{aligned} Az &= A(\alpha x + \beta y) \\ &= \alpha Ax + \beta Ay \\ &\leq \alpha(tb + (1-t)Ax_o) + \beta(tb + (1-t)Ax_o) \\ &= (\alpha + \beta)(tb + (\alpha + \beta)(1-t)Ax_o \\ &= tb + (1-t)Ax_o, \end{aligned}$$

and thus z ∈ $P(x_o, t)$. That is, $P(x_o, t)$ is convex. ■

For any value of $t > 0$, $P(x_o, t)$ is a polyhedron similar to P. The faces of $P(x_o, t)$ are parallel to the corresponding faces of P. Also the expansion (contraction) of P(t) as t increases (decreases) is linear in every radial direction centered at x_o. In particular, every point on the boundary of $P(x_o, 2)$ is exactly twice as far as the corresponding point of P is from x_o. See Figure 1.

The family of polyhedra $\{P(x_o, t) | t \geq 0\}$ are often described as a concentric family with center x_o. Notice that we always have P(x_o, 1) = P. Notice also that for any value of t ≥ 0, we get $x_o \in P(x_o, t)$. Moreover, P = CP(A, b, x_o) is already closed, thus if P is bounded, then P(x_o, 0) = x_o.

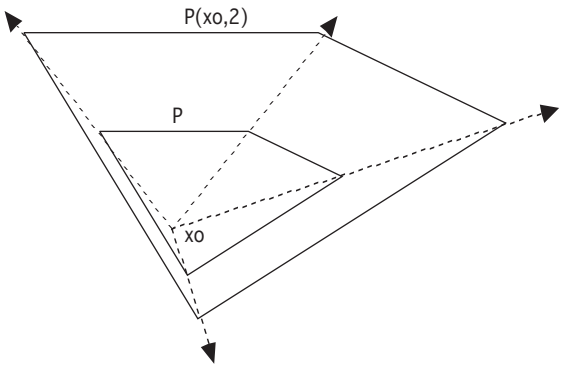

Figure 1: Demonstration of growth

2.3 POLYHEDRAL RATIO METRIC

At this point, we are finally ready to define the depth of penetration measure we plan to use. This measure will be based on a ratio metric penetration depth. Our goal is to show that we can produce a penetration depth measure which is equivalent to the Minkowski penetration depth [2], which is a standard metric for computing the distance between two convex bodies. The *Minkowski Penetration Depth* (MPD) is the natural extension of the Euclidean minimum distance function and is defined as follows:

Definition 2.11. Let $P_i = CP(A_i, b_i, x_i)$ be a convex polyhedron for i = 1,2. The Minkowski Penetration Depth between the two bodies P_1 and P_2 is defined formally as

$$PD(P_1, P_2) = \min\{||d|| \, | interior(P_1 + d) \bigcap P_2 = \emptyset\}. \tag{2.2}$$

Let P_i be the convex polyhedron given by $A_i x \leq b_i$, for i = 1,2. Then the Minkowski penetration depth between the two bodies will be obtained at two points p_1 and p_2 such that $p_i \in P_i$ and $||p_1 - p_2|| = PD(P_1, P_2)$.

We would now like to define a ratio metric corresponding to simultaneous expansion (contraction) of two convex polyhedra. The idea is that two nonintersecting convex polyhedra will simultaneously expand until they reach perfect contact. Likewise, two interpenetrating

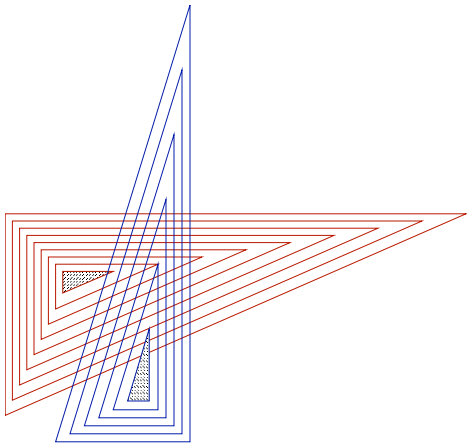

Figure 2: Visual representation of double expansion or contraction

convex polyhedra will simultaneously contract until they reach perfect contact. In brief, the ratio metric penetration depth captures the amount of expansion or contraction that is needed to achieve perfect contact.

See Figure 2 for a graphical demonstration. The two innermost triangles will simultaneously expand until they touch and the two outer triangles will simultaneously contract until they touch. We now give the formal definition.

Definition 2.12. Let $P_i = CP(A_i, b_i, x_i)$ be a convex polyhedron for i = 1,2. Then the ratio metric between the two sets is given by

$$r(P_1, P_2) = \min\{t | P_1(x_1, t) \bigcap P_2(x_2, t) \neq \emptyset\}, \tag{2.3}$$

and the corresponding *Ratio Metric Penetration Depth* (RPM) is given by

$$\rho(P_1, P_2, r) = \frac{r(P_1, P_2) - 1}{r(P_1, P_2)}. \tag{2.4}$$

Notice that if we let $P_i = CP(A_i, b_i, x_i)$ be a convex polyhedron for i = 1,2, then

- $P_i(x_i, 0)$ is always equal to $\{x_i\}$,
- $P_i(x_i, t)$ is always closed, and
- given any point z, we can find a nonnegative real number t_i such that $z \in P_i(x_i, t_i)$.

It immediately follows that as long as x_1 and x_2 are distinct, the ratio metric between the two sets is well defined, and thus so is the ratio metric penetration depth.

Proposition 2.13. *Let $P_i = CP(A_i, b_i, x_i)$ be a convex polyhedron for i = 1,2, then $r(P_1, P_2) = r(P_2, P_1)$.*

Proof. The proof follows trivially from Definition 2.3 because we have

$$\begin{aligned} r(P_1, P_2) &= \min\{t | P_1(x_1, t) \bigcap P_2(x_2, t) \neq \emptyset\}, \\ &= \min\{t | P_2(x_2, t) \bigcap P_1(x_1, t) \neq \emptyset\}, \\ &= r(P_2, P_1). \end{aligned}$$

■

This shows that the our polyhedral ratio metric is symmetric. We can see that this measure additionally satisfies a trichotomy relation, which we can express in terms of the interpenetration of the two bodies.

Proposition 2.14. *Let $P_i = CP(A_i, b_i, x_i)$ be a convex polyhedron for i = 1,2. Then*

1. *P_1 and P_2 interpenetrate if and only if $r(P_1, P_2) < 1$,*
2. *P_1 and P_2 do not intersect if and only if $r(P_1, P_2) > 1$,*
3. *P_1 and P_2 intersect but do not interpenetrate if and only if $r(P_1, P_2) = 1$.*

Proof. From the definition we use equation (2.3) and convexity to find a point $q \in P_2(x_2, r(P_1, P_2))$ which must lie on the boundary of $P_1(x_1, r(P_1, P_2))$. Finally, recall that $P_1 = P(x_1, 1)$ and $P_2 = P(x_2, 1)$, and so the results follow directly from Proposition 2.9. ■

The value returned by the ratio metric is nonnegative. Therefore, it is impossible for two of our convex polyhedra to have a ratio metric of 0 if their corresponding given interior points are distinct.

Corollary 2.15. *Let $P_i = CP(A_i, b_i, x_i)$ be a convex polyhedron for i = 1,2. Then $r(P_1, P_2) = 0$ if and only if $x_1 = x_2$.*

Proof. This follows immediately from the fact that $P_i(x_i, 0)$ is always equal to $\{x_i\}$, and thus $P_1(x_1, 0) \cap P_2(x_2, 0)$ is nonempty if and only if $\{x_1\} \cap \{x_2\}$ is nonempty. ■

The final major idea for this chapter is showing that the ratio metric penetration depth is equivalent to the Euclidean distance/MPD. To show that, we must have usable bounds for this RPM. To get our bounds, we will need to enforce slight restrictions during the construction of the convex polyhdra P_i.

In our simulations, we will allow some small penetration between bodies, but we do not allow too much penetration. To model this restriction we will choose a parameter $\epsilon \geq 0$ which represents the maximum allowable penetration between any two bodies. With this restriction, we can now state our *Metric Equivalence Theorem*.

Theorem 2.16. *Let $P_i = CP(A_i, b_i, x_i)$ be a convex polyhedron for i = 1,2, s be the Minkowski Penetration Depth between the two bodies, D be the distance between x_1 and x_2, ϵ be the maximum allowable Minkowski penetration between any two bodies. Then the ratio metric penetration depth between the two sets satisfies the relationship*

$$\frac{s}{D} \leq \rho(P_1, P_2, r) \leq \frac{s}{\epsilon}, \tag{2.5}$$

if P_1 and P_2 have disjoint interiors, and

$$-\frac{s}{\epsilon} \leq \rho(P_1, P_2, r) \leq -\frac{s}{D} \tag{2.6}$$

if the interiors of P_1 and P_2 are not disjoint.

Proof. When the bodies are in perfect contact, then we get all quantities to be zero in equations (2.5) and (2.6) and the conclusion follows trivially. Thus, we separate the proof into two additional cases, one where the bodies do not interpenetrate, and one where interpenetration exists.

In both cases, let $t = r(P_1, P_2)$, and recall that $P_1(x_2, t)$ and $P_2(x_2, t)$ are compact, convex polyhedra that intersect, but with an empty interior, and so they can be separated by a hyperplane H^*. Let p_i^* be a point on P_i which intersects $H_i^* = \Gamma(H, x_i, \frac{1}{t})$, which is the preimage of H^* from Corollary 2.7. The point p_i^* is optimal for P_i with respect to the hyperplane H^*.

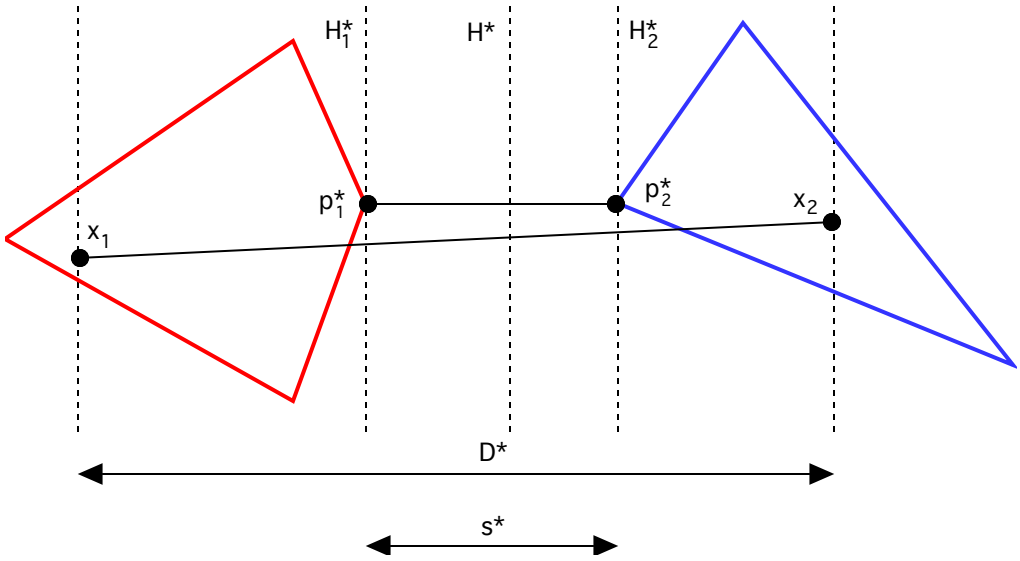

Figure 3: Ratio Metric Bounds: Exterior Case

Strict exterior case: We define $D^* = \left|c^{*T}(x_2 - x_1)\right|$ and $s^* = \left|c^{*T}(p_2^* - p_1^*)\right|$. See Figure 3. When we expand both polyhedra, their intersection can be separated by a hyperplane H^*, and upon computation of the required ratio metric, we get

$$r(P_1, P_2) = \frac{D^*}{D^* - s^*}.$$

Using this, we can calculate the ratio metric penetration depth:

$$\rho(P_1, P_2, r) = \frac{s^*}{D^*}. \tag{2.7}$$

Notice that the minimum translation necessary for the two bodies to intersect cannot have modulus less than s^*. Moreover, ϵ is easily a lower bound for the value of D^*, since the ball of radius ϵ centered at x_i is contained in P_i. Fortunately this means we can find an upper bound for this ratio metric penetration depth in this case:

$$\rho(P_1, P_2, r) \leq \frac{s}{\epsilon}. \tag{2.8}$$

Now, instead of first choosing the hyperplane in order to calculate the extremal points, let us choose the extremal points in order to calculate the hyperplane. We denote the endpoints

of the minimal translation segment, say $p_i^* \in P_i$. Our goal is to use this segment to define the separating hyperplane. Then the analysis might continue much as before.

We must show that these points can define separating hyperplanes H_1^* and H_2^*. Suppose that there were two points $p_{1,1}^*, p_{1,2}^* \in P_1$ satisfying the minimum distance requirement from, say, p_2^*. That is,

$$\big|\big|p_{1,1}^* - p_2\big|\big| = \big|\big|p_{1,2}^* - p_2\big|\big| = s > 0.$$

Then by convexity, P_1 must also contain the point $\mathrm{p} = \frac{1}{2}(p_{1,1}^* + p_{1,2}^*)$. However, we see that

$$\begin{aligned} ||p - p_2|| &= \big|\big|\tfrac{1}{2}(p_{1,1}^* + p_{1,2}^*) - p_2\big|\big| \\ &= \big|\big|\tfrac{1}{2}(p_{1,1}^* - p_2) + \tfrac{1}{2}(p_{1,2}^* - p_2)\big|\big| \\ &\leq \tfrac{1}{2}\big|\big|p_{1,1}^* - p_2\big|\big| + \tfrac{1}{2}\big|\big|p_{1,2}^* - p_2\big|\big| \\ &= s. \end{aligned}$$

But strict inequality will hold unless $p_{1,1}^* = p_{1,2}^*$. Thus, for the point p_2^*, there can only be one corresponding minimizer from P_1, namely p_1^*. Hence given the point p_2^*, there is only one point which intersects P_1 and the sphere centered at p_2^* with radius s, which we call B.

Now define H_1^* to be the hyperplane through p_1^* orthogonal to the segment $\overline{p_1^* p_2^*}$. If there is a point q outside of B, not on H, but in the same half-space as P_2, then the line segment $\overline{p_1^* q}$ will intersect the sphere B at some point q_o different from p_1^*. If $\mathrm{q} \in P_1$, then every point of the segment $\overline{p_1^* q}$, including q_o would necessarily belong to P_1. This yields a contradiction, and thus our choice of $H_!^*$ is indeed a separating hyperplane and contains p_1 orthogonal to $\overline{p_1 p_2}$. In the same way, we can define the hyperplane H_2^* through p_2^* orthogonal to the segment $\overline{p_1^* p_2^*}$, and it will be a separating hyperplane.

Our analysis now proceeds much as before. The first time that the image of both H_1^* and H_2^* coincide, we call H^*. Then the ratio factor for which $H^* = \Gamma(H_1^*, x_1, r) = \Gamma(H*_2, x_2, r)$ is precisely

$$r = \frac{D^*}{D^* - s^*}.$$

However, since we are not guaranteed that the bodies have yet intersected, we must also have $r \leq r(P_1, P_2)$. Therefore, we get $s^*/D^* \leq \rho(P_1, P_2, r)$. Also in this case we have $s^* = s$ and $D^* \leq D$, and so

$$\frac{s}{D} \leq \rho(P_1, P_2, r). \tag{2.9}$$

Strict Interior case: Similarly to the external case, we first define a hyperplane H^* that separates the bodies at simultaneous contracting contact and then get the extremal points p_1^* and p_2^*. So define $D^* = \left|c^{*T}(x_2 - x_1)\right|$ and $s^* = \left|c^{*T}(p_2^* - p_1^*)\right|$. Our construction is as in Figure 4, and the relation with the separating hyperplane at contact can be visualized using Figure 5. Then when we contract both polyhedra, their intersection can be separated by a hyperplane H^*, and upon computation of the required ratio metric, we get

$$r(P_1, P_2) = \frac{D^*}{D^* + s^*}.$$

We then calculate the ratio metric penetration depth, and since we notice that $s \leq s^*$ and $D \geq D^*$, we get that:

$$\rho(P_1, P_2, r) = -\frac{s^*}{D^*} \leq -\frac{s}{D}. \tag{2.10}$$

Now we will once again use the minimum translation segment to get the maximal points p_1^* and p_2^* as in the external case. Define H_i^* to be the hyperplane through p_i^* orthogonal to the segment $\overline{p_1^* p_2^*}$. The analysis of the previous case can show that the hyperplanes H_i^* are, in a sense, separating. Upon simultaneous contraction, the first time that the image of both H_1^* and H_2^* coincide, we call H^*. Then the ratio factor for which $H^* = \Gamma(H_1^*, x_1, r) = \Gamma(H*_2, x_2, r)$ is precisely

$$r = \frac{D^*}{D^* + s^*}.$$

Again, we cannot guaranteed that the bodies have nonempty intersection, we must also have $r \leq r(P_1, P_2)$. Therefore, we get $-s^*/D^* \leq \rho(P_1, P_2, r)$. However in this situation we know used the minimum translation segment, and so $s^* = s$. Finally, we use, ϵ as a lower bound for the value of D^*. Then we can write.

$$-\frac{s}{\epsilon} \leq \rho(P_1, P_2, r). \tag{2.11}$$

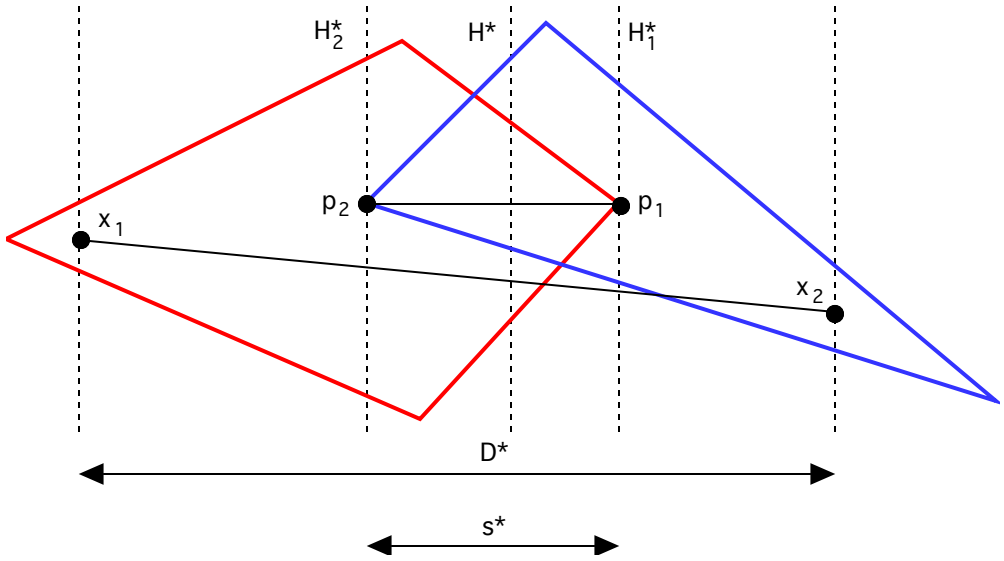

Figure 4: Ratio Metric Bounds: Interior Case

We have finished the proof of the theorem when we consider the bounds (2.8) and (2.9) for the exterior case, and bounds (2.10) and (2.11) for the interior case.

■

We have shown that the RPD is equivalent to the MPD. In particular, because we have Let $P_i = CP(A_i, b_i, x_i)$, we notice that the equation (2.3) of Definition 2.12 can be written as

$$r(P_1, P_2) = \min\{t \geq 0 \mid A_i x \leq t b_i + (1-t) A_i x_i, i = 1, 2\}. \tag{2.12}$$

Clearly this metric should handle convex polyhedral bodies and provide us with an elegant, yet simple way to detect collision and penetration of two bodies. If the "distance" between the polyhedra is less than one, then the bodies interpenetrate.

Recall the problems with computing PD. The complexity for computing PD by using the Minkowski sums is $O(m^2+n^2)$. This complexity result can be improved when stochastic methods is used to get a fast approximation to the PD. In some cases, the complexity can be reduced to $O(m^{3/4+\epsilon}n^{3/4+\epsilon})$ for any $\epsilon > 0$ [2].

One of the truly remarkable aspects of the use of this metric is its simplicity, in that

it only involves solving a linear programming problem, which is well known and has complexity of $O(n+m)$, Therefore, our *formulation (2.12) has substantially lower complexity of computation than MPD*.

Our ratio metric penetration depth does have a physical relation to the hyperplane that separates the bodies at perfect contact. It is not necessarily the same hyperplane that the Penetration Depth uses when calculating the minimal translation. See Figure 5.

Remark 2.17. Let h be the step size. The importance of the Metric Equivalence Theorem (2.16) is that, if RPD $= O(h^p)$, then MPD is also $O(h^p)$. Therefore, not only will the MPD noninterpenetration constraints be satisfied by time-stepping schemes based on RPD, but with the *same asymptotic order with lower computational complexity.*

Remark 2.18. Because we also have to deal with the boundary, or some other fixed object, we could easily expand our definition of the ratio metric (and hence ratio metric penetration depth) to handle such special situations, where only the one body will expand or contract.

For example, for any convex polyhedron $P = CP(A_i, b_i, x_o)$ and for any nonempty closed convex body Q, the ratio metric between Q and P is given by

$$\hat{r}(P,Q) = \min\{t | P(x_o, t) \bigcap Q \neq \emptyset\}, \tag{2.13}$$

and the corresponding ratio metric penetration depth ρ is defined by

$$\rho(P,Q,\hat{r}) = \frac{\hat{r}(P,Q)-1}{\hat{r}(P,Q)}.$$

This formulation is computationally friendly to handle any fixed convex body which could conceivably be considered part of the boundary. Moreover, it can be shown that this formulation of the metric also satisfies the conclusions of Theorem 2.16.

Remark 2.19. It is important to note that our ratio metric r is not a metric, but for an appropriate choice of the function f, $f(r)$ can be a metric. Indeed, we used

$$f_1(t) = \frac{t-1}{t}$$

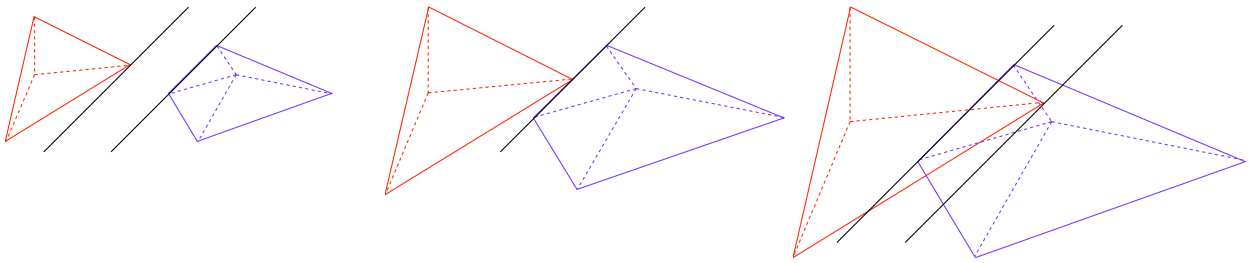

Figure 5: Separating hyperplanes and direction of minimal translation

to define our metric. That is $\rho = f_1(r)$. The reader can show that by using the simpler function $f_2(t) = t - 1$, we can also define a true metric. This should illustrate the important nature of the ratio metric r, whose properties are used to produce a feasible metric.

Remark 2.20. It was suggested for me to use $f_2(t) = t-1$ for the metric to be equivalent to the MPD, but the Metric Equivalence Theorem (2.16) was more easily proved by considering the rational expression

$$\rho(P_1, P_2, r) = \frac{r(P_1, P_2) - 1}{r(P_1, P_2)},$$

and this led to the name "Ratio Metric".

Here is a crucial observation. We can always expand/contract the bodies using $r(P_1, P_2)$, and we can let p be any point of intersection. Then we can always find a hyperplane H which separates the two convex bodies $P(x_1, r(P_1, P_2))$ and $P(x_2, r(P_1, P_2))$ and passes through the point p. Now, for i = 1,2 let H_i be the pre-image of H and p_i be the pre-image of p under $\Gamma(H, x_i, t)$. Notice that H_i passes through p_i. Recall that H_1 and H_2 are parallel.

Often, there is only one choice for a separating hyperplane H. If there are multiple possibilities, then we choose the one that makes the smallest angle with respect to the segment passing through the optimal points p_1 and p_2.

One conjecture is that for small penetration, the motion of the bodies produced by contraction is close to being a translation. Thus, we expect the distance and direction vector associated with the depth of penetration to be asymptotically equal to the distance between the hyperplanes H_1 and H_2, or the length of the segment from p_1 to p_2.

3.0 DIFFERENTIABILITY

Previously, we defined a measure of the depth of penetration which quantifies the signed distance between two convex polyhedra. Having such a measure is invaluable to our method, but we need to know if it meets all of our needs.

We anticipate that in the model of polyhedral contact dynamics problems, we will need to calculate normal vectors, which necessitates the computation of the derivative of the penetration depth. Anitescu, Cremer, and Potra [3] describe the mechanics of such formulations. This means that in addition to having the ability to determine the depth of penetration, our measure must also be reduced to differentiable functions. It is not trivial to assume that distance measures be differentiable. In one dimension, we know that the function $f(x) = |x|$ fails to be differentiable at the origin.

Our goal in this chapter, is to discuss the concept of a Basic Contact Unit, which we will define for two polyhedra in noninterpenetrational contact. Then we will examine the differentiability of our new measure when restricted with respect to a Basic Contact Unit. We will then show that our measure is piecewise differentiable, which we will find to be sufficient for our purposes.

3.1 PERFECT CONTACT

We begin our discussion by defining what it means for two convex polyhedra to be in perfect contact. We first mentioned this concept in the previous chapter but did not formally define it. Next, we will describe the basic contact unit and the various types of contact that can occur. Finally, we define an event, and the restriction of a contact to an event.

Definition 3.1. Two convex polyhedra are in **perfect contact** when there is a nonempty intersection without interpenetration.

It should be clear that when two bodies are in perfect contact, the region of contact must lie on the boundary of both bodies. Next, we define a basic contact unit.

Definition 3.2. In n-dimensional space, a **Basic Contact Unit (BCU)** is any contact that occurs when

- two convex polyhedra are in perfect contact,
- the contact region attached to a BCU is a point, and
- exactly n+1 facets are involved at the contact.

The point where the contact occurs is called an **event point**, or more simply, an **event**.

Remark 3.3. A Corner-on-Face contact is always a BCU, regardless of the dimension. In two-dimensions, the Corner-on-Face contact is the only type of basic contact unit. When we closely examine the contacts in three dimensions there are, in fact, exactly two types of BCUs, namely the Corner-on-Face (CoF) contacts, and (nonparallel) Edge-on-Edge (EoE) contacts.

Consider an n-dimensional space. If we let i be the number of facets from the first body involved for a BCU, then (n + 1 - i) must be the number of facets involved from the second body. It seems likely, therefore, that there are exactly $\left[\frac{n+1}{2}\right]$ distinct types of basic contact units.

Regardless of the dimension, when there is perfect contact, the intersection is the convex hull of the event points. We prove this in three dimensions. The two-dimensional case is similar, much simpler, and left to the reader.

Theorem 3.4. *The intersection of two convex polyhedra in perfect contact is the convex hull of the event points.*

Proof. Let P_1 and P_2 be two convex polyhedra in perfect contact. Perfect contact implies that the intersection $P_1 \bigcap P_2$, which itself is convex, belongs to the boundary of both P_1 and P_2. Recall the fact that every edge is the intersection of two faces and every point is the intersection of three faces. Now, we proceed to list all possible configurations and group

them according to the type of contact. There are exactly three distinct types of intersection, based on the region of contact.

Contact Region Is Point: It suffices to show that the point of contact is an event. There are four cases to consider.

Nonparallel Edge-on-Edge: This is already a BCU, thus the intersection is an event.

Corner-on-Face: This is also already a BCU, so the intersection is an event..

Corner-on-Corner: Every face involved with intersecting at the corner for one body constitutes a basic contact unit with the corner point of the other body. Hence the intersection is an event.

Corner-on-Edge: Every face involved with intersecting at the edge for one body constitutes a basic contact unit with the corner point of the other body. Hence the intersection is an event.

Contact Region is Line Segment: The line segment is the convex hull of its terminal points, so it suffices to show that each terminal point is an event. There are two cases to consider.

Parallel Edge-on-Edge: Each terminal point results from a Corner-on-Edge, hence is an event.

Edge-on-Face: Each terminal point results from either a Corner-on-Face or a nonparallel Edge-on-Edge, hence is an event.

Contact Region Is Polygon: Here, the polygon is a convex hull of its extreme points. It suffices to show that each extreme point is an event. There is one last case to consider.

Face-on-Face: Each extreme point must be either a Corner-on-Face, Corner-on-Edge, or a nonparallel Edge-on-Edge, hence is an event.

We have shown that every possible configuration during perfect contact results in an intersection which is the convex hull of points, and each of these points is, in fact, an event point. This completes the proof. ■

See Figure 6 and Figure 7 for visual examples of these two basic contacts in three dimensions. Observe Figure 8 as an example of Face-on-Face contact, where the two-dimensional

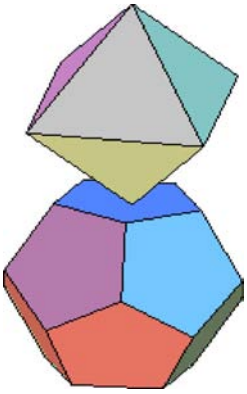

Figure 6: Corner-on-Face

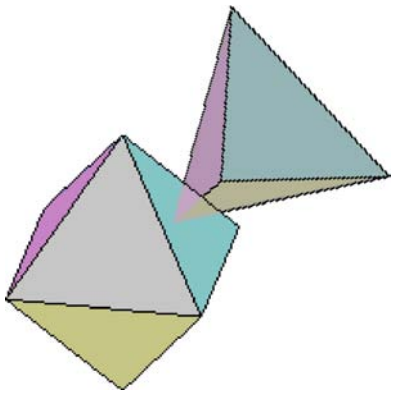

Figure 7: Edge-on-Edge

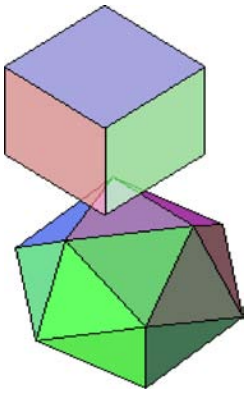

Figure 8: Face-on-Face

convex region of contact is a convex hull of four events, in this case, the events are the result of two CoF contacts and two EoE contacts.

In Figure 9, for instance, the contact region is a line segment, which is the convex hull of the two events shown. Although our distance function fails to be differentiable for this contact, *we will prove differentiability of the ratio metric when restricted to an event.* That will allow us to use a normal vector which is a convex combination of the normal vectors we get from each restriction.

Our goal is to eventually produce a normal vector at a BCU when contact occurs. Therefore, it leads us to turn our attention to the differentiability at a BCU.

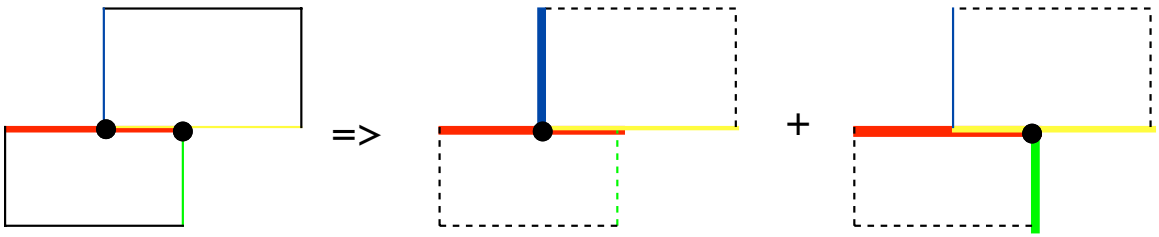

Figure 9: 2D Example: Contact Region Is Convex Hull of BCUs.

3.2 DIFFERENTIABILITY AT AN EVENT

In Calculus, we learn that it is unreasonable to expect a real valued function of a real variable to be differentiable when its graph has a corner. One explanation is because there would not exist a unique normal line to the graph. In much the same way, it is also unreasonable to expect the ratio metric to be differentiable at a point of contact that is not a BCU. Again, a unique normal vector would not exist.

A simple two dimensional example of this can be seen in Figure 10. In this example we have a triangle with vertices P_1, P_2, and P_3 which is above the fixed boundary given by $\{(x, y) \in \mathbb{R}^2 \mid y \leq 0\}$. The coordinates of vertex P_i are (x_i, y_i). The Euclidean distance d from the triangle to the boundary is given by $d = \max\{|y_1|, |y_2|, |y_3|\}$. The distance d, as a function of y_1, y_2, and y_3 is not differentiable for all $y_i \geq 0$.

To specifically illustrate the lack of differentiability, suppose that the triangle is defined so that $y_2 = y_1 + a\sin\theta$ and $y_3 = y_1 - a\sin(\theta)$ for some positive constant a, and where θ is a parameter. Then the Euclidean distance between the triangle and the boundary is

$$d(y_1, \theta) = \min\{y_1 + a\sin\theta, y_1 - \sin\theta\},$$

which is singular when $\theta = 0$. Notice that the distance could be expressed as the minimum of two functions, each of which could be interpreted as some measure of distance. That is, we have

$$d_2(x_2, y_2, \theta) = y_1 + a\sin\theta$$

and

$$d_3(x_3, y_3, \theta) = y_1 - a\sin\theta,$$

and basically we have $d = \min\{d_2, d_3\}$.

Notice that the Euclidean distance function can actually be considered to be piecewise smoothly defined. The concept of a piecewise smoothly defined distance function, which this example illustrates, is extremely important and is a recurring theme throughout this thesis. Moreover, it is possible to exploit this piecewise differentiability to enable the calculation of a normal vector (or a set of normal vectors), despite the nonexistence of the derivative. We

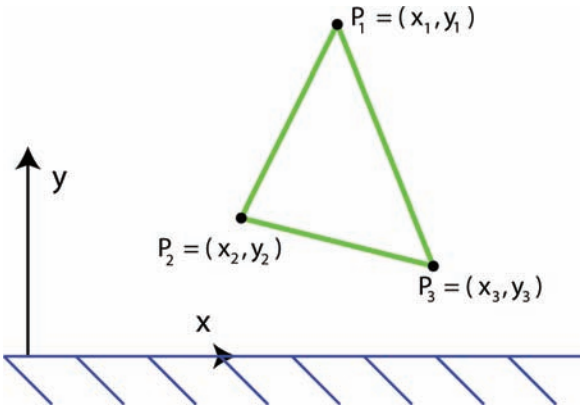

Figure 10: Nondifferentiability of Euclidean distance function

calculate a normal vector by using a convex combination of differentiable functions. This is accomplished by breaking up the contact region as a convex combination of BCUs.

To get some of our differentiability results, we prove a small lemma that shows that under suitable conditions, we can get differentiability of a solution of a system of linear equations.

Lemma 3.5. *Let m be the order of the square matrix $A(\alpha)$ and the vector $b(\alpha)$, which are differentiable with respect to the real parameter α. Suppose further, that*

$$x(\alpha^*) = A(\alpha^*)^{-1} b(\alpha^*).$$

Then

$$x'(\alpha^*) = A(\alpha^*)^{-1} \left[b(\alpha^*) - A'(\alpha^*) A(\alpha^*)^{-1} b(\alpha^*) \right].$$

Proof. This follows directly from the fact that

$$\begin{aligned} x(\alpha^*) = A(\alpha^*)^{-1} b(\alpha^*) &\implies A(\alpha^*) x(\alpha^*) = b(\alpha^*) \\ &\implies A'(\alpha^*) x(\alpha^*) + A(\alpha^*) x'(\alpha^*) = b'(\alpha^*) \\ &\implies x'(\alpha^*) = A(\alpha^*)^{-1} \left[b(\alpha^*) - A'(\alpha^*) x(\alpha^*) \right]. \end{aligned}$$

■

This tells us that if the coefficient matrix and the right hand side of a system of linear equations is continuously differentiable, then so is the solution when the coefficient matrix is nonsingular. We will exploit this property very soon to get the desired differentiability we seek.

Corollary 3.6. *Let m be the order of the square matrix $A(\alpha)$ and the vector $b(\alpha)$, which are differentiable with respect to the real parameter α. Suppose further, that*

$$x(\alpha^*) = A(\alpha^*)^{-1}b(\alpha^*).$$

1. *If $A(\alpha)$ and $b(\alpha)$ are differentiable to order n, then so is $x(\alpha^*)$.*
2. *If $A(\alpha)$ and $b(\alpha)$ are infinitely differentiable, then so is $x(\alpha^*)$.*

Occasionally, at a point of perfect contact, we will simply say that an event occurs. Now, to get our needed differentiability, we must consider restricting the polyhedron to only the convex body facets involved at an event.

Definition 3.7. Let $P_i = CP(A_i, b_i, x_i)$ be a convex polyhedron for i = 1,2. Let $t^* = r(CP(A_1, b_1, x_1), CP(A_2, b_2, x_2))$. Then $P_1(x_1, t^*)$ and $P_2(x_2, t^*)$ are in perfect contact. Let E be any event of this perfect contact. For any i = 1,2, we define the restrictions of $P_i(x_i, t)$ to E, which we denote as $P_E(x_i, t)$, to be the convex body defined by the facets of $P(x_i, t)$ which involve E.

Suppose that we have $P_{L_i} = CP(A_{L_i}, b_{L_i}, 0)$ as the local representation for a convex polyhedron for i = 1, 2. The transformation from local coordinates x_{L_i} to world coordinates x is given by

$$x = x_i + R_i x_{L_i},$$

which can be rewritten into the form

$$x_{L_i} = R_i^T(x - x_i).$$

Here the matrices R_1 and R_2 are typical rotation matrices. We assume the use of Euler rotation matrices, or anything comparable, so that the matrices are differentiable with respect

to their arguments. For example, we can use the classical Fick ZYX implementation of the Euler angles, since it does not suffer from singularities at the identity orientation [40].

We find that

$$\begin{aligned} A_{L_i} x_{L_i} \leq b_{L_i} &\iff A_{L_i} R_i^T (x - x_i) \leq b_{L_i} \\ &\iff A_{L_i} R_i^T x \leq b_{L_i} + A_{L_i} R_i^T x_i. \end{aligned} \tag{3.1}$$

It then follows that the local formulation of $P_i = CP(A_{L_i}, b_{L_i}, 0)$ is equivalent to the global formulation of $P_i = CP(A_{L_i} R_i^T, b_{L_i} + A_{L_i} R_i^T x_i, x_i)$. This means that our ratio metrics globally becomes the computation of

$$\begin{aligned} r(P_1, P_2) &= \min_{t \geq 0} \begin{cases} A_{L_1} R_1^T x \leq t(b_{L_1} + A_{L_1} R_1^T x_1) + (1-t) A_{L_1} R_1^T x_1 \\ A_{L_2} R_2^T x \leq t(b_{L_2} + A_{L_2} R_2^T x_2) + (1-t) A_{L_2} R_2^T x_2 \end{cases} \\ &= \min_{t \geq 0} \begin{cases} A_{L_1} R_1^T x - b_1 t \leq A_{L_1} R_1^T x_1 \\ A_{L_2} R_2^T x - b_2 t \leq A_{L_2} R_2^T x_2 \end{cases}. \end{aligned} \tag{3.2}$$

Suppose that we have two convex polyhedra in perfect contact. When we restrict ourselves to any event that occurs because of this perfect contact, the ratio metric (and thus the ratio metric penetration depth) is, in fact, differentiable. This result we now prove.

Theorem 3.8. *Let $P_i = CP(A_{L_i} R_i^T, b_{L_i} + A_{L_i} R_i^T x_i, x_i)$ be a convex polyhedron (in world coordinates) for i = 1,2. Moreover, let $t^* = r(P_1, P_2)$. Then, at any event of perfect contact E, $r(P_E(x_1, t), P_E(x_2, t))$ is infinitely differentiable with respect to the translation vectors and rotation angles.*

Proof. We are required to compute the ratio metric in (3.2). This computation yields

$$\begin{aligned} r(P_1, P_2) &= \min_{t \geq 0} \begin{cases} A_{L_1} R_1^T x \leq t(b_{L_1} + A_{L_1} R_1^T x_1) + (1-t) A_{L_1} R_1^T x_1 \\ A_{L_2} R_2^T x \leq t(b_{L_2} + A_{L_2} R_2^T x_2) + (1-t) A_{L_2} R_2^T x_2 \end{cases} \\ &= \min_{t \geq 0} \begin{cases} A_{L_1} R_1^T x - b_1 t \leq A_{L_1} R_1^T x_1 \\ A_{L_2} R_2^T x - b_2 t \leq A_{L_2} R_2^T x_2 \end{cases}, \end{aligned}$$

which allows us to expand (or contract) the polyhedra until we get perfect contact.

With $t^* = r(P_1, P_2)$, we let E be any event at the perfect contact with event point, say x^*. We want to consider the restrictions $P_E(x_i, t)$ for i = 1,2 which can be written as

$$\hat{A}_{L_i} R_i^T x - \hat{b}_i t \leq \hat{A}_{L_i} R_i^T x_i,$$

where $\hat{A}_i = Q_i A_i$ and $\hat{b}_i = Q_i b_i$ and Q_i is the projection matrix that chooses the inequalities that define the facets of $P(x_i, t)$ that involve E. Therefore we know that

$$r(P_E(x_1, t), P_E(x_2, t)) \quad = \quad \min_{t \geq 0} \begin{cases} \hat{A}_{L_1} R_1^T x - \hat{b}_1 t \leq \hat{A}_{L_1} R_1^T x_1 \\ \hat{A}_{L_2} R_2^T x - \hat{b}_2 t \leq \hat{A}_{L_2} R_2^T x_2 \end{cases} \tag{3.3}$$

where the sum of the rows of $\hat{A}_{L_1}$ and $\hat{A}_{L_2}$ totals n+1.

Notice that (x^*, t^*) an optimal solution. Suppose that $(x^\dagger, t^\dagger)$ is any other solution of (3.3). Then we clearly have $t^\dagger = t^*$. Moreover, since E is an event at the perfect contact with event point x^*, which is a BCU, we can conclude that $x^\dagger = x^*$.

This means (x^*, t^*) is the unique solution of (3.3) and thus to the reduced system

$$\begin{array}{l} \hat{A}_{L_1} R_1^T x - \hat{b}_1 t = \hat{A}_{L_1} R_1^T x_1 \\ \hat{A}_{L_2} R_2^T x - \hat{b}_2 t = \hat{A}_{L_2} R_2^T x_2 \end{array}, \tag{3.4}$$

which is square of order $n + 1$ and can be rewritten into matrix form:

$$\begin{bmatrix} \hat{A}_{L_1} R_1^T & -\hat{b}_1 \\ \hat{A}_{L_2} R_2^T & -\hat{b}_2 \end{bmatrix} \begin{bmatrix} x \\ t \end{bmatrix} = \begin{bmatrix} \hat{A}_{L_1} R_1^T x_1 \\ \hat{A}_{L_2} R_2^T x_2 \end{bmatrix}. \tag{3.5}$$

Of importance is the fact that we know, because of our assumption that the contact region attached to any BCU must be a point, that the *coefficient matrix in (3.4) is nonsingular.*

Now, it is clear that both the coefficient matrix and the right hand side of equation (3.5) are infinitely differentiable with respect to the components of the translation vectors x_1 and x_2, and also infinitely differentiable with respect to the rotation angles in R_1 and R_2.

Finally, recall that the t component of the solution is $t^* = r(P_E(x_1, t), P_E(x_2, t))$. Upon application of Corollary 3.6, this completes the proof. ■

We have shown in Theorem 3.4 that every region of perfect contact between two convex polyhedra is the convex hull of event points. At an event point of perfect contact, we are actually guaranteed a solution to equation (3.5), which in turn guarantees the existence of the derivative. We wish to describe mathematical and physical constraints for this. Let us examine properties of two specific types of event points, namely Corner-on-Face and nonparallel Edge-on-Edge contacts. Recall from our discussion in Remark 3.3 that these cover all possible types in two or three dimensional space.

The CoF contact is characterized by the interaction of a corner of one polyhedron with a face of the other polyhedron. Let us consider the case where a corner point p_1 of P_1 and a face F_2 of P_2 produce a CoF contact at the optimal value of t.

Recall that our reduced system is equation (3.5). For convenience, let us write $A = \hat{A}_{L_1}$, $b = \hat{b}_1$, $c = \hat{A}^T_{L_2}$, and $\delta = \hat{b}_2$. Then we can rewrite (3.5) as

$$\begin{bmatrix} AR_1^T & -b \\ c^T R_2^T & -\delta \end{bmatrix} \begin{bmatrix} x \\ t \end{bmatrix} = \begin{bmatrix} AR_1^T x_1 \\ c^T R_2^T x_2 \end{bmatrix}. \tag{3.6}$$

We are interested in the conditions that will ensure that the system of equations in (3.6) has a solution.

Lemma 3.9. *If A, R_1, and R_2 are any nonsingular matrices of size n and b and c are any vectors of length n and δ is an arbitrary scalar, then the matrix*

$$\begin{bmatrix} AR_1^T & -b \\ c^T R_2^T & -\delta \end{bmatrix}$$

is nonsingular if and only if $c^T R_2^T R_1^{-T} A^{-1} b \neq \delta$. Furthermore, we have

$$\det \begin{bmatrix} AR_1^T & -b \\ c^T R_2^T & -\delta \end{bmatrix} = \left(c^T R_2^T R_1^{-T} A^{-1} b - \delta\right) \det A \ \det R_1.$$

Proof. The proof follows directly from the factorization

$$\begin{bmatrix} AR_1^T & -b \\ c^T R_2^T & -\delta \end{bmatrix} = \begin{bmatrix} I & 0 \\ c^T R_2^T R_1^{-T} A^{-1} & c^T R_2^T R_1^{-T} A^{-1} b - \delta \end{bmatrix} \begin{bmatrix} AR_1^T & -b \\ 0 & 1 \end{bmatrix}.$$

■

Remark 3.10. Notice that the solution (x^*, t^*) of (3.6) must satisfy

$$x^* = x_1 + R_1^{-T} A^{-1} b t^*$$

and, since $t^* \neq 0$, it follows that

$$c^T R_2^T x_1 + c^T R_2^T R_1^{-T} A^{-1} b t^* - \delta t^* = c^T R_2^T x_2.$$

Rewritten as

$$c^T R_2^T x_1 - c^T R_2^T x_2 = (\delta - c^T R_2^T R_1^{-T} A^{-1} b) t^*, \tag{3.7}$$

it means equation (3.6) has a unique solution if and only if $c^T R_2^T x_1 \neq c^T R_2^T x_2$, that is, the centers x_1 and x_2 can be separated by the hyperplane determined by $c^T R_2^T$. Observe that we get

$$t^* = \frac{c^T R_2^T x_2 - c^T R_2^T x_1}{c^T R_2^T R_1^{-T} A^{-1} b - \delta}.$$

We can now explicitly compute the derivative. Doing so, we have

$$\bigtriangledown_{x_1} t^* = \bigtriangledown_{x_1} r(P_E(x_1, t), P_E(x_2, t)) = -\frac{1}{c^T R_2^T R_1^{-T} A^{-1} b - \delta} \, c^T R_2^T \tag{3.8}$$

and

$$\bigtriangledown_{x_2} t^* = \bigtriangledown_{x_2} r(P_E(x_1, t), P_E(x_2, t)) = \frac{1}{c^T R_2^T R_1^{-T} A^{-1} b - \delta} \, c^T R_2^T.$$

Remark 3.11. Upon close inspection of our formulation of the reduced problem for a CoF contact, we can see that the results depend on the two interior points and the hyperplane. It becomes clearly evident that the gradient we compute depends purely on the hyperplane, and thus the number of facets that make up the corner point is irrelevant.

Therefore, another amazing result of our computations is that for a CoF contact, any combination of facets that produce the corner will give the same results. It follows directly that although there might be many formulations that give the CoF contact, there is truly only one event taking place.

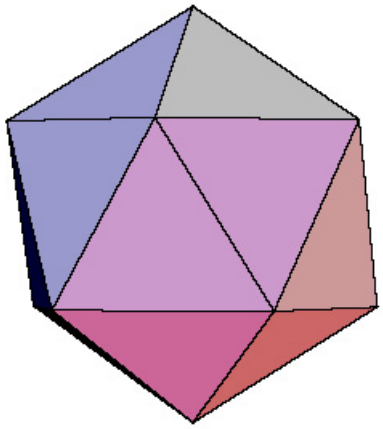

Figure 11: Icosahedron With 20 Faces

We can easily notice that if the corner of an icosahedron (as shown in Figure 11) determines the corner point of a CoF contact, then there are five possible facets from the icosahedron that would intersect at the point. There are 10 combinations of facets that could uniquely determine the point, but the result would be the same, since it depends on the point, but not the facets.

Remark 3.12. In the three dimensional case with nonparallel EoE contact, we would have to consider the system in equation (3.5) where there are two rows each in the matrices $\hat{A}_{L_1}$ and $\hat{A}_{L_2}$. Since the edges are nonparallel, there is at least one face associated with $\hat{A}_{L_2}$ which is globally linearly independent from the set of global face of $\hat{A}_{L_1}$.

Hence, we can find vectors c and d such that

$$\hat{A}_{L_2} = \begin{bmatrix} d \\ c \end{bmatrix}$$

and the matrix

$$\mathbb{A} = \begin{bmatrix} \hat{A}_{L_1} R_1^T \\ d^T R_2^T \end{bmatrix}$$

is nonsingular. Then we can write our system

$$\begin{aligned} \hat{A}_{L_1} R_1^T x - b_1 t &= \hat{A}_{L_1} R_1^T x_1 \\ d^T R_2^T x - \epsilon t &= d^T R_2^T x_2 \\ c^T R_2^T x - \delta t &= c^T R_2^T x_2 \end{aligned} \tag{3.9}$$

in the form

$$\begin{aligned} \mathbb{A}x - \mathbb{B}t &= \mathbb{A}x_1 + \Delta \\ c^T R_2^T x - \delta t &= c^T R_2^T x_2 \end{aligned}, \tag{3.10}$$

where we define

$$\mathbb{B} = \begin{bmatrix} b_1 \\ \epsilon \end{bmatrix} \tag{3.11}$$

and

$$\Delta = \begin{bmatrix} 0 \\ d^T R_2^T (x_2 - x_1) \end{bmatrix}. \tag{3.12}$$

If we have $c^T R_2^T \mathbb{A}^{-1} \mathbb{B} \neq \delta$, we can solve to get

$$t^* = -\frac{c^T R_2^T x_2 - c^T R_2^T x_1 - c^T R_2^T \mathbb{A}^{-1} \Delta}{c^T R_2^T \mathbb{A}^{-1} \mathbb{B} - \delta}, \tag{3.13}$$

and conclude that the gradients $\bigtriangledown_{x_1} t^*$ and $\bigtriangledown_{x_2} t^*$ will again exist.

The gradient is used to produce the normal vectors at contact between two bodies. It is important, though, to give more details concerning the choice of normal vectors. In our computation model, we consider any event E at the perfect contact, and we use the restrictions $P_E(x_i, t)$ for i = 1,2. As before, we obtain

$$r(P_E(x_1,t), P_E(x_2,t)) = \min_{t \geq 0} \begin{cases} \hat{A}_{L_1} R_1^T x - b_1 t \leq \hat{A}_{L_1} R_1^T x_1 \\ \hat{A}_{L_2} R_2^T x - b_2 t \leq \hat{A}_{L_2} R_2^T x_2 \end{cases}.$$

The restriction that $t \geq 0$ is not superfluous, since it is possible to define

$$\min_t \begin{cases} \hat{A}_{L_1} R_1^T x - b_1 t \leq \hat{A}_{L_1} R_1^T x_1 \\ \hat{A}_{L_2} R_2^T x - b_2 t \leq \hat{A}_{L_2} R_2^T x_2 \end{cases},$$

which might not exist if we consider some other potential event E_{pot}. Our goal is not to consider allowing negative values of t, but rather, to consider all potential events.

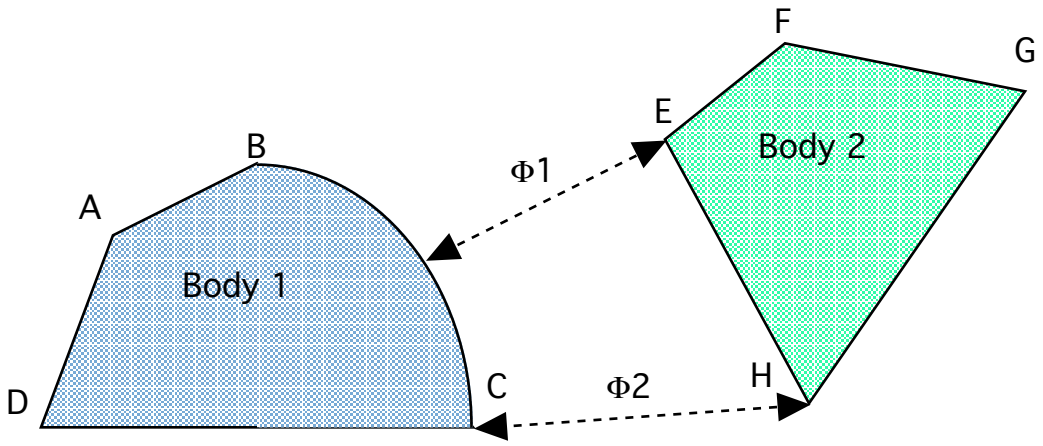

Figure 12: Example of Two Component Signed Distance Functions

For example, consider the two-dimensional case with two convex bodies P_1 and P_2. Each body P_i has f_i flat facets, n_i non-flat facets, and p_i corner points, respectively. We can produce $n_1n_2 + n_1f_2 + f_1p_2 + f_1n_2 + p_1f_2$ different potential events, one for each pairing of a non-flat facet from one body to a flat or non-flat facet of the other body, and each pairing of a flat facet of one body with a corner point of the other body. We associate a component function with each event.

In Figure 12, there would be 32 potential events, hence 32 component functions: 4 from the one non-flat facet from P_1 paired with the four flat facets of P_2, 12 from the three flat facets of P_1 paired with the four corner points of P_2 and 16 from the four flat facets of P_2 paired with the four corner points of P_1. Two particular functions are $\widehat{\Phi}^{(1)}$ which calculated the distance between the non-flat facet $\widehat{BC}$ with the flat facet $\overline{EH}$, and $\widehat{\Phi}^{(2)}$ which calculated the distance between the flat facet $\overline{CD}$ with the point H.

It is unfortunate, however, that computationally, we must consider whole hyperplanes instead of partial ones. For example, when we consider the function $\widehat{\Phi}^{(2)}$ from Figure 12, which would ideally give the distance between the point H and the facet $\overline{CD}$, we would require more than just the typical number of equations associated with a CoF event. Indeed, for a typical CoF event, we would be measuring the distance between the point H and the whole

hyperplane that contains facet $\overline{CD}$, and not just the facet itself.

For the global formulation of $P_i = CP(A_{L_i}R_i^T, b_{L_i} + A_{L_i}R_i^T x_i, x_i)$ for $i = 1, 2$, it is possible for us to list all of the potential events. Suppose that there are $n_{1,2}$ such potential events. We will use the component functions that correspond to each potential event.

Therefore, we can always associate with the m^{th} potential event $E^{(m)}$, a component function $\widehat{\Phi}^{(m)}$. Following the procedures we earlier followed, we use the restrictions $P_{E^{(m)}}(x_1, t)$ and $P_{E^{(m)}}(x_2, t)$. Then we can write $\widehat{\Phi}^{(m)}$ in the form $\widehat{\Phi}^{(m)} = f(r_m)$, where $f(t) = (t-1)/t$ and

$$r_m = \min_{t \geq 0} \begin{cases} \hat{A}_{m_1} R_1^T x - b_{m_1} t \leq \hat{A}_{m_1} R_1^T x_1 \\ \hat{A}_{m_2} R_2^T x - b_{m_2} t \leq \hat{A}_{m_2} R_2^T x_2 \end{cases} \tag{3.14}$$

where the sum of the numbers of rows of $\hat{A}_{m_1}$ and $\hat{A}_{m_2}$ is n+1.

Notice that $\widehat{\Phi}^{(m)}$ depends on the translation and rotation variables. Also note that $\widehat{\Phi}^{(m)}$ might not be defined. Indeed, we expect $\widehat{\Phi}^{(m)}$ to be defined for some configurations of the global position variables, and not defined for others, in which cases we consider $\widehat{\Phi}^{(m)}$ to have the value of $-\infty$ for convenience. This leads us to the following result, which tells us that the ratio metric penetration depth is the maximum of component distance functions.

Theorem 3.13. *Suppose $x_1 \neq x_2$ and let $P_i = CP(A_{L_i}R_i^T, b_{L_i} + A_{L_i}R_i^T x_i, x_i)$ be convex polyhedra for $i = 1, 2$ and let $\left\{E^{(1)}, E^{(2)}, \cdots, E^{(N)}\right\}$ be the list of all possible events with corresponding component distance functions $\left\{\widehat{\Phi}^{(1)}, \widehat{\Phi}^{(2)}, \cdots, \widehat{\Phi}^{(N)}\right\}$. Then*

$$\rho(P_1, P_2, r) = \max\left\{\widehat{\Phi}^{(1)}, \widehat{\Phi}^{(2)}, \cdots, \widehat{\Phi}^{(N)}\right\},$$

where $\rho(P_1, P_2, r)$ is defined by (2.4).

Proof. We begin by noting that $r(P_1, P_2)$ is a nonnegative real number. Since $x_1 \neq x_2$, then by Corollary 2.15 we know that $r(P_1, P_2) > 0$. Let $t^* = r(P_1, P_2)$. Then there exists an event E_k at the perfect contact. Let us denote the corresponding component function as $\widehat{\Phi}_k$.

Proceeding exactly as before, we can write

$$r(P_{E^{(k)}}(x_1, t), P_{E^{(k)}}(x_2, t)) = \min_{t \geq 0} \begin{cases} \hat{A}_{k_1} R_1^T x - b_1 t \leq \hat{A}_{k_1} R_1^T x_1 \\ \hat{A}_{k_2} R_2^T x - b_2 t \leq \hat{A}_{k_2} R_2^T x_2 \end{cases},$$

where the sum of the rows of $\hat{A}_{k_1}$ and $\hat{A}_{k_2}$ totals n+1. Now,

$$\begin{aligned}
t^* &= r(P_1, P_2) \\
&= \min_{t\geq 0} \begin{cases} A_1 x + (A_1 x_1 - b_1)t \leq A_1 x_1 \\ A_2 x + (A_2 x_2 - b_2)t \leq A_2 x_2 \end{cases} \\
&\geq \min_{t\geq 0} \begin{cases} \hat{A}_{k_1} R_1^T x - b_1 t \leq \hat{A}_{k_1} R_1^T x_1 \\ \hat{A}_{k_2} R_2^T x - b_2 t \leq \hat{A}_{k_2} R_2^T x_2 \end{cases} \\
&= r_k \\
&= r(P_{E_k}(x_1, t), P_{E_k}(x_2, t)) \\
&= t^*,
\end{aligned}$$

which shows that $r(P_1, P_2) = r_k$. Next, if we choose any other index m for possible event and component function pair $(E_m, \widehat{\Phi}^{(m)})$, we find that

$$\begin{aligned}
r_k &= \min_{t\geq 0} \begin{cases} A_1 x + (A_1 x_1 - b_1)t \leq A_1 x_1 \\ A_2 x + (A_2 x_2 - b_2)t \leq A_2 x_2 \end{cases} \\
&\geq \min_{t\geq 0} \begin{cases} \hat{A}_{m_1} R_1^T x - b_1 t \leq \hat{A}_{m_1} R_1^T x_1 \\ \hat{A}_{m_2} R_2^T x - b_2 t \leq \hat{A}_{m_2} R_2^T x_2 \end{cases} \\
&= r_m.
\end{aligned}$$

Since m was arbitrary, we have $r_k = \max\{r_1, r_2, \cdots, r_N\}$. Now we exploit the strict monotonicity of $f(t)$ and the fact that $\widehat{\Phi}^{(m)} = f(r_m)$ to conclude that $\widehat{\Phi}^{(k)} = \max\left\{\widehat{\Phi}_1, \widehat{\Phi}_2, \cdots, \widehat{\Phi}_N\right\}$. This completes the proof. ■

3.3 ACTIVE AND NEARLY ACTIVE EVENTS

Up until now, we have produced an innovative computationally convenient method for finding a signed distance between two convex polyhedra. In particular, we know when the two bodies are in perfect contact. When that happens, we need to obtain a list of active events.

If we were planning to use a classical integrate-detect-restart simulation method, then our analysis is sufficient to this point, and we would compute the normal vector at any active event. We plan, however, to allow some small interpenetration to exist, and this makes it necessary for us calculate, at any given step, a list of normal vectors for all events that are close enough to being active.

In this section we will discuss how such a list can be determined. Our discussion for this section will deal with three dimensional problems, and can be generalized or extended to include other cases.

Recall that our computation of the ratio metric (3.2) has the form

$$r(P_1, P_2) \quad = \quad \min_t \begin{cases} A_{L_1} R_1^T x - b_1 t \leq A_{L_1} R_1^T x_1 \\ A_{L_2} R_2^T x - b_2 t \leq A_{L_2} R_2^T x_2 \end{cases} . \tag{3.15}$$

If any point (x^o, t^o) belongs to the region of perfect contact, then it must simultaneously solve the system

$$\begin{aligned} A_{L_1} R_1^T x - b_1 t &= A_{L_1} R_1^T x_1, \\ A_{L_2} R_2^T x - b_2 t &= A_{L_2} R_2^T x_2. \end{aligned} \tag{3.16}$$

Recall that we can always associate with the m^{th} potential event $E^{(m)}$, a component function $\widehat{\Phi}^{(m)}$, and point $(x^{(m)}, t^{(m)})$,when it exists. If we want to indicate that the point $(x^{(m)}, t^{(m)})$ is the solution of the system of equations associated with the potential event $E^{(m)}$, we will write

$$\begin{aligned} x^{(m)} &= E_x^{(m)} \\ t^{(m)} &= E_t^{(m)} \end{aligned} \tag{3.17}$$

and if we want to indicate the two bodies j_1 and j_2 used to describe the contact $E^{(m)}$, we will write

$$(j_1, j_2) = Bod(E^{(m)}).$$

Also, given any event potential $E^{(m)}$, there are precisely two distinct indices j_1 and j_2, $1 \leq j_1, j_2 \leq n_B$ which give us the two particular bodies whose distance is being computed. Then $E^{(m)}$ is actually an event if

- The two bodies j_1 and j_2 are in contact, where $(j_1, j_2) = Bod(E^{(m)})$,
- $E_t^{(m)} = r(P_{j_1}, P_{j_2}) = 1$,
- $E_x^{(m)} \in CP(A_{L_{j_1}} R_{j_i}^T, b_{L_{j_1}} + A_{L_{j_1}} R_{j_1}^T x_{j_1}, x_{j_1})$, and
- $E_x^{(m)} \in CP(A_{L_{j_2}} R_{j_2}^T, b_{L_{j_2}} + A_{L_{j_2}} R_{j_2}^T x_{j_2}, x_{j_2})$.

We don't even consider the event $E^{(m)}$ to be active if the bodies j_1 and j_2 are not in contact. We require the ratio metric calculated with the reduced system of inequalities to be identical with the ratio metric calculated with the full system of inequalities. Likewise, the solution of the reduced system of linear equations must yield a point on the intersection of the two bodies. We define the set of indices m for which these conditions are satisfied as the Active Events.

Because we will allow small interpenetration at each step, we must discuss what happens when the bodies are not necessarily in perfect contact, but are close. In particular, what happens when we have slight interpenetration or if the bodies are almost but not quite in contact?

For computational efficiency, we need to determine the list of events that are imminently active. In order to determine this list, we need to amend our criteria. Therefore, given the potential event $E^{(m)}$, we know that m belongs to the set of *nearly active events* if:

- The distance between bodies j_1 and j_2 is small enough, where $(j_1, j_2) = Bod(E^{(m)})$,
- $E_t^{(m)} = r(P_{j_1}, P_{j_2})$ is close enough to 1,
- $E_x^{(m)}$ is close to being an element of $CP(A_{L_{j_1}} R_{j_i}^T, b_{L_{j_1}} + A_{L_{j_1}} R_{j_1}^T x_{j_1}, x_{j_1})$, and
- $E_x^{(m)}$ is close to being an element of $CP(A_{L_{j_2}} R_{j_2}^T, b_{L_{j_2}} + A_{L_{j_2}} R_{j_2}^T x_{j_2}, x_{j_2})$.

Assume for now that we have $t^* = r(P_1, P_2)$, which ideally should be some value close to 1, of course, because it indicates that the two bodies are almost in contact, in perfect contact, or have a little interpenetration. Notice that our analysis can continue even if t^* is not close to 1.

Now, when we need to solve a system like (3.16), we have a potential event, say (x^o, t^o). The compatibility check has the condition that the value of t^o must be close to the value of t^* instead of 1. This assures us that the potential event is close to being optimal.

This condition is exactly what we need for a suffiect check for potential events. We thus outline our algorithm for the compatibility check:

Algorithm 3.14. Compatibility Check

Check for potential CoF and EoE events.

1. The solution (x^o, t^o) must exist.
2. $$\begin{cases} b_1 t^o - \hat{A}_{L_1} R_1^T (x^o - x_1) \leq \epsilon_x \\ b_2 t^o - \hat{A}_{L_2} R_2^T (x^o - x_2) \leq \epsilon_x \end{cases}$$
3. $|t^o - t^*| \leq \epsilon_t$

where the parameters $\epsilon_x > 0$ and $\epsilon_t > 0$ are given.

When the bodies are in perfect contact, we become aware that when there are some potential events that are, in some sense, "close enough", we need to include them. Notice that Condition 2 insures us that the point is physically close to the intersection of the two bodies, and Condition 3 insures us that we choose events close to being maximal.

If we want to list the active events only, we choose the parameters ϵ_x and ϵ_t close to zero. However, if we wish to include the nearly active events, we merely choose larger values of our parameters ϵ_x and ϵ_t.

Recall that when two bodies are in perfect contact, the region of perfect contact is itself a convex region. If the region of perfect contact is two dimensional, then there can only be one active hyperplane from each body.

Again, the solution of the dual problem will indicate which hyperplanes are active. When a nonzero component occurs, then the corresponding hyperplane is in contact, and thus is active. Unfortunately, the converse in not true, and so if we want to determine all of the active events, we need a procedure that will obtain that information for us.

A good procedure will check all of the possible Corner-on-Face events by testing each active face of one body with the possibly active corners of the other body. Then the procedure

would check all of the possible Edge-on-Edge events by testing each possibly active edge of one body with each possibly active edge of the other body.

With this is mind, we can produce a good procedure which will systematically determine all of the nearly active events:

Algorithm 3.15. Good Algorithm

Good Algorithm for choosing the nearly active events.

Step 1: Solve the dual problem.

Step 2: List the active hyperplanes $H_{1i}, i = 1, \ldots, n_1$ and $H_{2j}, j = 1, \ldots, n_2$.

Step 3: Choose appropriate parameters $\epsilon_x > 0$ and $\epsilon_t > 0$,

Step 4a: Check (general) compatibility of H_{1i} with the list of adjacent points of H_{2j}.

Step 4b: Check (general) compatibility of H_{2j} with the list of adjacent points of H_{1i} .

Step 4c: Check (general) compatibility of adjacent edges of H_{1i} with adjacent edges of H_{2j}.

Finally, we just note that when we consider two bodies in perfect contact in a three dimensional space, it is possible for the convex hull of the nearly active events to be three dimensional, although the convex hull of the active events is at most two dimensional.

4.0 CONSTRAINTS AND MODEL

Perhaps it is true that science is man's attempt to explain what God had done. It is important for us to explain some of the details of our mathematical model of the kinematics of rigid convex polyhedral bodies with joints, contact, and friction constraints. Moreover, our explanation cannot be purely theoretical, but computational as well.

Our goal in this chapter is to provide a description of our approach and show how we arrive at the prevailing equations for our model. We begin by discussing the major physical constraints, including the inequality constraints that define the convex bodies, the generalized position coordinates, noninterpenetration constraints, and our model of the Coulomb friction. Next, we elaborate our choice of the active set, discuss differentiability which permits the computation of the contact normal vector, then we produce linear complementary model.

Throughout this paper, we will often use complementarity notation which we now define.

Definition 4.1. Let a and b be Real numbers satisfying:

1. $a \geq 0$
2. $b \geq 0$
3. $ab = 0$

then a and b are complementary to each other. We say that a and b satisfy a complementarity condition and we write

$$a \geq 0 \perp b \geq 0.$$

The vectors u and v of length k satisfy a complementarity condition if $u^{(i)}$ is complementary to $v^{(i)}$ for $i = 1, 2, \cdots, k$. We denote it by

$$u \geq 0 \perp v \geq 0.$$

4.1 PHYSICAL CONSTRAINTS

As we model the motion, we have to observe constraints, whether implicit or explicit, if our model is to be realistic. Geometrical constraints involve only the position variable and depend on the shape of the bodies and the type of constraints involved. Friction, as a kinematic constraints, should not be ignored simply because of the mathematical difficulties that accompany it.

Thus, we will focus our attention on two geometrical constraints, namely joint constraints and noninterpenetration constraints, and on the kinematic friction constraint. It is common to group the translational and angular components of body into one vector, which we call the composite position [29]. In what follows, we use a vector q to represent the composite position of a body.

Polyhedral Bodies. Notice that any nonconvex body can be approximated by a union of convex bodies. Thus, our model will assume that all of the bodies are convex and polyhedral.

For the ${j_i}^{th}$ body, we define $P_{j_i} = CP(A_{j_j}, b_{j_i}, 0)$ to be the polyhedron defined by the linear inequalities

$$A_{j_i} x \leq b_{j_i}$$

which contains the origin. By convention, and without loss of generality, we can normalize this system such that all entries of vector b_{j_i} are equal to 1. Then the position of the body is described by specifying its center x_{j_i} and its rotation angles θ_{j_i} with respect to the center.

Rotation Matrix. Suppose that the position of the body B_{j_i} has center at x_{j_i} and rotation angles θ_{j_i}. Recall that using world coordinates, we get $P_{j_i} = CP(A_{j_i} R^T_{j_i}(\theta_{j_i}), b_{j_i} + A_{j_i} R^T_{j_i}(\theta_{j_i}) x_{j_i} x_{j_i})$.

Here R_{j_i} is a rotation matrix. We will use an Euler angle parameterization of the rotation matrix. In three dimensions, for instance, the angle θ_{j_i} will have three components, say

$\theta_{j_i} = [\alpha_{j_i}, \beta_{j_i}, \gamma_{j_i}]^T$. Then for the rotation matrix we could use

$$R_{j_i}(\theta_{j_i}) = \begin{pmatrix} \cos\gamma_{j_i} & -\sin\gamma_{j_i} & 0 \\ \sin\gamma_{j_i} & \cos\gamma_{j_i} & 0 \\ 0 & 0 & 1 \end{pmatrix} \begin{pmatrix} \cos\beta_{j_i} & 0 & \sin\beta_{j_i} \\ 0 & 1 & 0 \\ -\sin\beta_{j_i} & 0 & \cos\beta_{j_i} \end{pmatrix} \begin{pmatrix} 1 & 0 & 0 \\ 0 & \cos\alpha_{j_i} & -\sin\alpha_{j_i} \\ 0 & \sin\alpha_{j_i} & \cos\alpha_{j_i} \end{pmatrix}$$

which is the classical Fick ZYX implementation of the Euler angles (sometimes referred as the yaw, pitch and roll angles), and does not have a singularity at the identity orientation.

Position Coordinates. Let the space Q_j contain the generalized coordinates for the bodies B_{j_1} and B_{j_2}. This is accomplished if the bodies B_{j_1} and B_{j_2} have centers at x_{j_1} and x_{j_2}, respectively, and respective rotation angles θ_{j_1} and θ_{j_2}. Then the generalized position vector in Q_j is

$$q_j = \begin{bmatrix} x_{j_1} \\ \theta_{j_1} \\ x_{j_2} \\ \theta_{j_2} \end{bmatrix}.$$

Now suppose that we have n_B rigid bodies in the system. Denote by $Q_1, Q_2, \cdots, Q_{n_B}$ the spaces that contain generalized coordinates of the bodies $B_1, B_2, \cdots B_{n_B}$, whose generalized coordinates we denote by $q_1, q_2, \cdots, q_{n_B}$. These spaces are locally homeomorphic with some bounded open set of R^s [29]. The aggregate generalized position (from here on, the generalized position) becomes $q = (q_1^T, q_2^T, \cdots, q_{n_B}^T)^T$. We denote $Q = Q_1 \times Q_2 \times \cdots Q_{n_B}$.

Noninterpenetration Constraints. Physically, it is necessary to constrain the bodies from penetrating one another if they are not to occupy the same space. It is typical for mathematical models of the constraints of noninterpenetration be defined in terms of a continuous signed distance function between the two bodies $\Phi^{(j)}(q)$ [3]. We will write the collection of these noninterpenetration constraints as

$$\Phi^{(j)}(q) \geq 0, \quad j = 1, 2, \cdots, p. \tag{4.1}$$

Our model computes the ratio metric penetration depth as the signed distance functions between the piecewise smooth polyhedra P_{j_1} and P_{j_2} using Definition (2.12). If the bodies

B_{j_1} and B_{j_2} have centers at x_{j_1} and x_{j_2}, respectively, and respective rotation angles θ_{j_1} and θ_{j_2}, then at the generalized position q we have

$$\Phi^{(j)}(q) = \rho(P_{j_1}, P_{j_2}, r) = \frac{r(P_{j_1}, P_{j_2}) - 1}{r(P_{j_1}, P_{j_2})},$$

where

$$r(P_{j_1}, P_{j_2}) = \min\{t | P_{j_1}(x_{j_1}, t) \bigcap P_{j_2}(x_{j_2}, t) \neq \emptyset\}.$$

We will just refer to the $\Phi^{(j)}(q)$ simply as the *(signed) distance functions*. It should be clear that these distance functions are mappings that depend continuously on q and on the shape of the bodies, but we consider the latter dependency only implicitly.

Sufficient conditions for local differentiability of $\Phi^{(j)}(q)$ have been discussed in [5]. However for our polyhedral bodies, the function $\Phi^{(j)}(q)$ cannot be differentiable everywhere. We have earlier discussed the fact that our distance function is piecewise differentiable. We need to take advantage of this piecewise differentiability.

Suppose that the j^{th}signed distance function $\Phi^{(j)}(q)$ will have k_j component signed distance functions.

$$\Phi_1^{(j)}(q), \Phi_2^{(j)}(q), \cdots, \Phi_{k_m}^{(j)}(q), \quad j = 1, 2, \cdots, p.$$

Then by Theorem 3.13 we have

$$\Phi^{(j)}(q) = \max_{j=1,2,\cdots,p} \left\{ \Phi_1^{(j)}(q), \Phi_2^{(j)}(q), \cdots, \Phi_{k_m}^{(j)}(q) \right\}. \tag{4.2}$$

For convenience, we can consider the collection of component functions and rename them. When we do that, we write them as

$$\widehat{\Phi}^{(m)}(q), \quad m = 1, 2, \cdots, p_o,$$

where $p_o = k_1 + k_2 + \cdots + k_p$. We can use (4.2) to prove that $\Phi^{(j)}(q)$ is continuous.

At any event E at the perfect contact, our model uses the restrictions $P_E(x_{j_i}, t)$ for i = 1, 2 to compute $r(P_E(x_{j_1}, t), P_E(x_{j_2}, t))$, with which we define the component function

$$\widehat{\Phi}^{(m)}(q) = \frac{r(P_E(x_{j_1}, t), P_E(x_{j_2}, t))) - 1}{r(P_E(x_{j_1}, t), P_E(x_{j_2}, t))}.$$

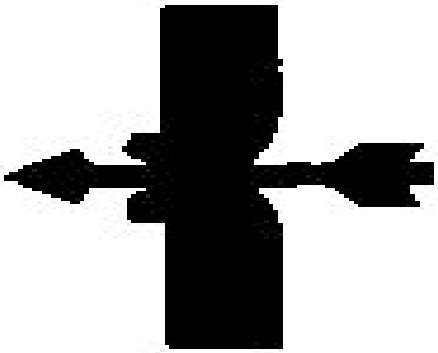

Figure 13: Noninterpenetration Constraint: Constraint not enforced

In Figure 13, we see what may happen when a noninterpenetration constraint is not enforced.

Joint Constraints. In biomechanics and robotics, there are five types of joints: hinge, fixed, ball and socket, gliding, and pivot joints. In mathematical modeling, joint constraints are typically described by the equations

$$\Theta^{(i)}(q) = 0,\ i = 1, 2, \cdots, n_J\,. \tag{4.3}$$

Here, $\Theta^{(i)}(q)$ are sufficiently smooth functions. If the gradients $\nabla_q \Theta^{(i)}(q), \quad i = 1, 2, \cdots, m$ exist, then we define $\nu^{(i)}(q)$ by

$$\nu^{(i)}(q) = \nabla_q \Theta^{(i)}(q), \quad i = 1, 2, \cdots, n_J. \tag{4.4}$$

The impulse exerted by a joint on the system is $c_\nu^{(i)} \nu^{(i)}(q)$, where $c_\nu^{(i)}$ is a scalar related to the Lagrange multiplier of classical constrained dynamics [29]. The requirement that the distance between two bodies remain fixed is one example of a joint constraint. This is illustrated in Figure 14, where the car works best if the wheels of the car have a fixed distance between them.

Friction Constraints. Frictional constraints are expressed by means of a discretiza-

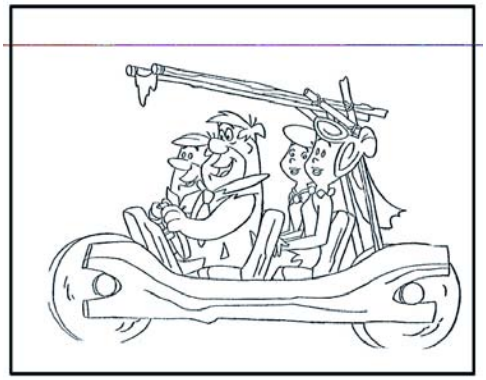

Figure 14: Joint Constraint: Fixed distance between wheels

tion of the Coulomb friction cone [8, 9, 49]. For a contact $m \in \{1, 2, \cdots, p_o\}$, we take a collection of coplanar vectors $d_i^{(m)}(q)$, $i = 1, 2, \cdots, M_C^{(m)}$, which span the plane tangent at the contact (though the plane may cease to be tangent to the contact normal when mapped in generalized coordinates [3]). The convex cover of the vectors $d_i^{(m)}(q)$ should approximate the transversal shape of the friction cone. In two-dimensional mechanics, the tangent plane is one dimensional, its transversal shape is a segment, and only two such vectors $d_1^{(m)}(q)$ and $d_2^{(m)}(q)$ are needed in this formulation.

Denote by $D^{(m)}(q)$ a matrix whose columns are $d_i^{(m)}(q) \neq 0$, $i = 1, 2, \cdots, M_C^{(m)}$, that is, $D^{(m)}(q) = \left[d_1^{(m)}(q), d_2^{(m)}(q), \cdots, d_{M_C^{(m)}}^{(m)}(q) \right]$. A tangential impulse is $\sum_{i=1}^{M_C^{(m)}} \beta_i^{(m)} d_i^{(m)}(q)$, where $\beta_i^{(m)} \geq 0$, $i = 1, 2, \cdots, M_C^{(m)}$. Assume that the tangential contact description is balanced, that is,

$$\forall i,\ 1 \leq i \leq M_C^{(m)},\ \exists k,\ 1 \leq k \leq M_C^{(m)} \text{ such that } d_i^{(m)}(q) = -d_k^{(m)}(q). \tag{4.5}$$

The friction model requires maximum dissipation for given normal impulse $c_n^{(m)}$ and velocity v and guarantees that the total contact force is inside the discretized cone. This model can be expressed as

$$\begin{aligned} D^{(m)^T}(q)v + \lambda^{(m)} e^{(m)} &\geq 0 \quad \perp \quad \beta^{(m)} \geq 0, \\ \mu c_n^{(m)} - e^{(m)^T} \beta^{(m)} &\geq 0 \quad \perp \quad \lambda^{(m)} \geq 0. \end{aligned} \tag{4.6}$$

Here we define $e^{(m)}$ to be a vector of ones of dimension $M_C^{(m)}$, $e^{(m)} = (1, 1, \cdots, 1)^T$, $\mu^{(m)} \geq 0$ is the Coulomb friction parameter, and $\beta^{(m)}$ is the vector of tangential impulses $\beta^{(m)} = \left(\beta_1^{(m)}, \beta_2^{(m)}, \cdots, \beta_{M_C^{(m)}}^{(m)}\right)^T$. The additional variable $\lambda^{(m)} \geq 0$ is approximately equal to the norm of the tangential velocity at the contact, if there is relative motion at the contact, or $\left|\left|D(q)^{(m)^T} v\right|\right| \neq 0$ [8, 49].

Notation. Let $M(q)$ be the symmetric, positive definite mass matrix of the system in the generalized coordinates q and by $k(t, q, v)$ the external force. All quantities described in this associated with contact m are denoted by the superscript $^{(m)}$. When we use a vector or matrix norm whose index is not specified, it is the 2 norm.

4.2 MODEL

Active Set. Given the position q, two bodies are in physical contact if and only if one of the distance functions is zero, that is, we have $\Phi^{(j)}(q) = 0$ for some j, $1 \leq j \leq p$. That is, we define the physically active set as

$$\left\{j \mid \Phi^{(j)}(q) = 0, j = 1, \cdots, p\right\}. \tag{4.7}$$

Because of the components of $\Phi^{(j)}(q)$, this is equivalent to having $\Phi_k^{(j)}(q) = 0$, for some j, $1 \leq j \leq p$ and for some k, $1 \leq k \leq k_p$. Since we renamed and reordered the functions, we know that if two bodies are in physical contact, then for some index m, $1 \leq m \leq p_o$, we have $\widehat{\Phi}^{(m)}(q) = 0$.

We need a way to identify where the contact occurs, so in the following, when we refer to *contact j*, we are saying that the two bodies whose (piecewise) distance is determined by $\Phi_k^{(j)}$ are in contact and, because of renaming, we have $\widehat{\Phi}^{(m)} = \Phi_k^{(j)}$. If two bodies are in contact at position q, then $\Phi^{(j)}(q) = \Phi_k^{(j)}(q) = 0$ and hence $\widehat{\Phi}^{(m)}(q) = 0$ for some m. On the other hand, it is conceivable that $\widehat{\Phi}^{(m)}(q) = 0$ for some j without any the occurrence of contact. That is to say, at the same time we can have $\Phi_k^{(j)}(q) \neq 0$ for all j and k. The problem is dictated by several factors, including the piecewise definition of $\Phi^{(j)}(q)$.

For computational efficiency, only the contacts that are imminently active are included in the dynamical resolution and linearized, and their set is denoted by $\mathcal{E}$. One practical way of determining $\mathcal{E}$ is by choosing sufficiently small parameters $\hat{\epsilon}_t$ and $\hat{\epsilon}_x$, and the definition becomes

$$\begin{aligned}
\mathcal{E}_1(q) &= \left\{m \mid \Phi^{(j)} \leq \hat{\epsilon}_t,\ j = Bod(E^{(m)}),\ 1 \leq m \leq p_o\right\} \\
\mathcal{E}_2(q) &= \left\{m \mid 0 \leq \widehat{\Phi}^{(m)} - \Phi^{(j)} \leq \hat{\epsilon}_t,\ j = Bod(E^{(m)}),\ 1 \leq m \leq p_o\right\} \\
\mathcal{E}_3(q) &= \left\{m \mid E_x^{(m)} \in CP(A_{L_{m_1}} R_{m_2}^T, b_{L_{m_1}} + A_{L_{m_1}} R_{m_1}^T x_{m_1}, x_{m_1}) + \hat{\epsilon}_x,\ 1 \leq m \leq p_o\right\} \\
\mathcal{E}_4(q) &= \left\{m \mid E_x^{(m)} \in CP(A_{L_{m_2}} R_{m_2}^T, b_{L_{m_2}} + A_{L_{m_2}} R_{m_2}^T x_{m_2}, x_{m_2}) + \hat{\epsilon}_x,\ 1 \leq m \leq p_o\right\}
\end{aligned} \tag{4.8}$$

and

$$\mathcal{E}(q) = \mathcal{E}_1(q) \bigcap \mathcal{E}_2(q) \bigcap \mathcal{E}_3(q) \bigcap \mathcal{E}_4(q). \tag{4.9}$$

This defines the nearly active (or computationally active) set, but we will just call it the active set, since we are interested in numerical results. Our Good Algorithm 3.15 will produce precisely this set of active events.

Determining when a quantity is equal to zero, as in our definition of the physically Active Set in (4.7), is often numerically disastrous. To accommodate our needs, we formally define the computationally active set (or nearly active set) by

$$\mathcal{A}(q) = \left\{j \mid \Phi^{(j)}(q) \leq \epsilon_t, j = 1, \cdots, p\right\}, \tag{4.10}$$

where $\epsilon_t > 0$ is a given parameter. Since this is the only set of use to us, we shall simply call it the active set.

Notice that $m \in \mathcal{E}_1(q)$ if the bodies are active. Also, $m \in \mathcal{E}_2(q)$ if the measured event distance is close enough to without exceeding the measured distance between the bodies. Finally, we see that $m \in \mathcal{E}_3(q)$ or $m \in \mathcal{E}_4(q)$ if the event m is physically active if at least one of the bodies is allowed to slightly expand.

Let a position q be given. If $\mathcal{A}(q)$ is empty, then by definition $\mathcal{E}(q)$ must be empty. On the other hand, if $\mathcal{A}(q)$ is not empty, then there must be at least one event which is active, and so $\mathcal{E}(q)$ cannot be empty. In other words, we have shown that

$$\mathcal{A}(q) = \emptyset \quad \Longleftrightarrow \quad \mathcal{E}(q) = \emptyset.$$

In fact, when $\mathcal{A}(q)$ is not empty, there is some event m such that $\Phi^{(j)}(q) = \widehat{\Phi}^{(m)}(q)$. We cannot have an m such that $\widehat{\Phi}^{(m)}(q) < \Phi^{(j)}(q)$, because then $m \notin \mathcal{E}_2(q)$. The consequences of this is that we find that

$$\min_{j \in \mathcal{A}} \Phi^{(j)}(q) = \min_{m \in \mathcal{E}} \widehat{\Phi}^{(m)}(q). \tag{4.11}$$

Differentiability properties. The mappings $\Theta^{(i)}(q)$ that define the joint constraints are differentiable [29]. Unfortunately, the situation is different, however, for the mapping defining the noninterpenetration constraints. If the bodies are smooth and relatively strictly convex, then the mapping $\Phi^{(j)}(q)$ is differentiable as long as the amount of interpenetration not large [3].

The mappings $\Phi^{(j)}(q)$ are obviously not differentiable for bodies with non-smooth shapes, such as convex polyhedra. Fortunately, we only need piecewise continuity of $\Phi^{(j)}(q)$ and sufficient differentiability of $\widehat{\Phi}^{(m)}(q)$ in order to get the results we desire.

Therefore, to simplify the analysis, assume that the mappings that define the joint constraints $\Theta^{(i)}(q)$ are differentiable. Assume, further, that the noninterpenetration constraints $\Phi^{(j)}(q)$ are continuously defined with component functions $\widehat{\Phi}^{(m)}(q)$ which are differentiable, which is true for our ratio metric penetration depth.

Contact Normal Vector. Now, denote the normal at an event (m) by

$$n^{(m)}(q) = \nabla_q \widehat{\Phi}^{(m)}(q), \quad m \in \mathcal{E}. \tag{4.12}$$

When the contact is active, it can exert a compressive normal impulse, $c_n^{(m)} n^{(m)}(q)$, on the system, which is modeled mathematically by requiring $c_n^{(m)} \geq 0$. The fact that the contact must be active before a nonzero compression impulse can act is expressed by the complementarity constraint

$$\widehat{\Phi}^{(m)}(q) \geq 0 \perp c_n^{(m)} \geq 0, \quad m \in \mathcal{E}. \tag{4.13}$$

See Figure 15 for an illustration.

Linear Complementarity Model. Let $h_l > 0$ be the time step at time $t^{(l)}$, when the system is at position $q^{(l)}$ and velocity $v^{(l)}$. We have that $h_l = t^{(l+1)} - t^{(l)}$. Choose the new

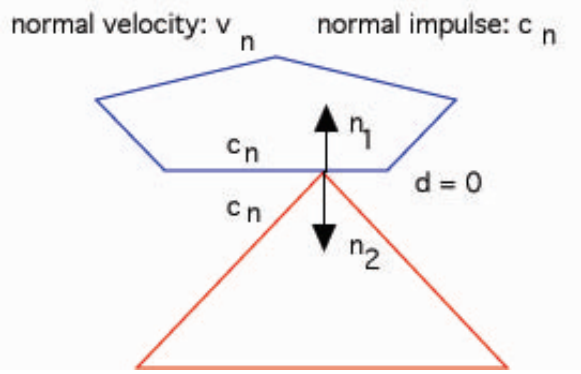

Figure 15: Contact Model

position to be $q^{(l+1)} = q^{(l)} + h_l v^{(l+1)}$, where $v^{(l+1)}$ is determined by enforcing the simulation constraints.

The geometrical constraints are enforced at the velocity level by modified linearization of the mappings $\Theta^{(i)}$ and $\widehat{\Phi}^{(m)}$. For joint constraints the modified linearization leads to

$$\begin{aligned} \gamma\Theta^{(i)}(q^{(l)}) + h_l \nabla_q \Theta^{(i)^T}(q^{(l)}) v^{(l+1)} &= \\ \gamma\Theta^{(i)}(q^{(l)}) + h_l \nu^{(i)^T}(q^{(l)}) v^{(l+1)} &= 0, \quad i = 1, 2, \cdots, n_J, \end{aligned} \tag{4.14}$$

where γ is a user-defined parameter. If $\gamma = 1$, then we would achieve proper linearization, which is the case treated in [5].

For a noninterpenetration constraint of index j, we have $\Phi^{(j)}(q) \geq 0$, and so modified linearization at $q^{(l)}$ for one time step amounts to $\gamma\Phi^{(j)}(q^{(l)}) + h_l \nabla_q \Phi^{(j)^T}(q^{(l)}) v^{(l+1)} \geq 0$.

Since our noninterpenetration constraints are piecewise defined as we discussed earlier, we modify the linearization we obtained earlier. Recall that we need to have $\widehat{\Phi}^{(m)}(q^{(l)}) \leq \Phi^{(j)}(q^{(l)})$. Thus our linearization becomes $\gamma\Phi^{(j)}(q^{(l)}) + h_l \nabla_q \widehat{\Phi}^{(m)^T}(q^{(l)}) v^{(l+1)} \geq 0$; that is, after including the complementarity constraints (4.13) and using the definition of $n^{(m)}(q^{(l)}) = \nabla_q \widehat{\Phi}^{(m)}(q^{(l)})$, we have

$$n^{(m)^T}(q^{(l)}) v^{(l+1)} + \frac{\gamma}{h_l} \Phi^{(j)}(q^{(l)}) \geq 0 \perp c_n^{(m)} \geq 0. \tag{4.15}$$

The choice of $\gamma \neq 0$ is of interest to consider for the following reason. If we analyze the linearization of the joint constraint, we see that, to be included in a system whose unknown is

$v^{(l+1)}$, it must be rewritten as $\gamma\frac{\Theta^{(i)}(q^{(l)})}{h_l}+\nu^{(i)^T}(q^{(l)})v^{(l+1)}=0, \quad i=1,2,\cdots,n_J,$. Clearly, if h_l needs to be small and $\Theta^{(i)}$ is large, this may cause a problem. So the effect of h_l being small is compensated by a suitably chosen γ. Obviously $\gamma=0$ would result in the constraint drift not being compensated at all, so some lower bound on γ is, practically speaking, necessary. As is the case with other parameter-dependent schemes, its choice in the end will be problem specific.

Now we completely define the prevailing system that describes our model. We first use an Euler discretization of the equations of motion, that is, of Newton's law. This results in the following equation [6]:

$$\begin{aligned} M(q^{(l)})\left(v^{(l+1)}-v^{(l)}\right) &= h_l k\left(t^{(l)},q^{(l)},v^{(l)}\right)+\textstyle\sum_{i=1}^{n_J} c_\nu^{(i)}\nu^{(i)}(q^{(l)}) \\ &+ \sum_{m\in\mathcal{E}}\left(c_n^{(m)}n^{(m)}(q^{(l)})+\sum_{i=1}^{M_C^{(m)}}\beta_i^{(m)}d_i^{(m)}(q^{(l)})\right). \end{aligned} \tag{4.16}$$

Next, we use the modified linearization of the geometrical constraints (4.14) and noninterpenetration constraints (4.15) to get

$$\begin{aligned} \gamma\Theta^{(i)}(q^{(l)})+h_l\nu^{(i)^T}(q^{(l)})v^{(l+1)} &= 0, && i=1,2,\cdots,n_J, \\ n^{(m)^T}(q^{(l)})v^{(l+1)}+\tfrac{\gamma}{h_l}\widehat{\Phi}^{(m)}(q^{(l)}) &\geq 0 \quad \perp c_n^{(m)}\geq 0, && m\in\mathcal{E}. \end{aligned} \tag{4.17}$$

Finally, we include the conditions for model of friction (4.6).

$$\begin{aligned} D^{(m)^T}(q)v+\lambda^{(m)}e^{(m)} &\geq 0 \quad \perp \quad \beta^{(m)}\geq 0 \quad m\in\mathcal{E}, \\ \mu c_n^{(m)}-e^{(m)^T}\beta^{(m)} &\geq 0 \quad \perp \quad \lambda^{(m)}\geq 0 \quad m\in\mathcal{E}. \end{aligned} \tag{4.18}$$

5.0 ISSUES IN SOLVING THE LCP

Now that we have the prevailing mathematical system that describes our model, there are a few unanswered questions. We need to determine if there a solution, and if so, a method that will compute the solution.

In this chapter, we will produce a linear complementarity problem from the prevailing system (4.16), (4.17), and (4.18), after which we will consider a convex relaxation thereof. That will allow us to produce a fixed-point iteration that will converge, for small values of the friction coefficient, to a solution of the LCP.

To simplify the notation, we replace the superscript $(l+1)$ of the velocity solution of (5.1–5.2) by the superscript $*$, and there will be no superscripts for the complementarity problems. After collecting all the constraints introduced previously, with the geometrical constraints replaced by their linearized versions (4.14) and (4.15), we got the prevailing system which includes (4.16), (4.17), and (4.18).

We can rewrite the system to obtain the following mixed LCP:

$$\begin{bmatrix} M^{(l)} & -\widetilde{\nu} & -\widetilde{n} & -\widetilde{D} & 0 \\ \widetilde{\nu}^T & 0 & 0 & 0 & 0 \\ \widetilde{n}^T & 0 & 0 & 0 & 0 \\ \widetilde{D}^T & 0 & 0 & 0 & \widetilde{E} \\ 0 & 0 & \widetilde{\mu} & -\widetilde{E}^T & 0 \end{bmatrix} \begin{bmatrix} v^{(l+1)} \\ c_\nu \\ c_n \\ \widetilde{\beta} \\ \lambda \end{bmatrix} + \begin{bmatrix} -Mv^{(l)} - h_l k^{(l)} \\ \Upsilon \\ \Delta \\ 0 \\ 0 \end{bmatrix} = \begin{bmatrix} 0 \\ 0 \\ \rho \\ \widetilde{\sigma} \\ \zeta \end{bmatrix} \tag{5.1}$$

$$\begin{bmatrix} c_n \\ \widetilde{\beta} \\ \lambda \end{bmatrix}^T \begin{bmatrix} \rho \\ \widetilde{\sigma} \\ \zeta \end{bmatrix} = 0, \qquad \begin{bmatrix} c_n \\ \widetilde{\beta} \\ \lambda \end{bmatrix} \geq 0, \qquad \begin{bmatrix} \rho \\ \widetilde{\sigma} \\ \zeta \end{bmatrix} \geq 0\,. \tag{5.2}$$

Here

$$
\begin{aligned}
\widetilde{\nu} &= [\nu^{(1)}, \nu^{(2)}, \cdots, \nu^{(n_J)}], \\
c_\nu &= [c_\nu^{(1)}, c_\nu^{(2)}, \cdots, c_\nu^{(n_J)}]^T, \\
\widetilde{n} &= [n^{(m_1)}, n^{(m_1)}, \cdots, n^{(m_s)}], \\
c_n &= [c_n^{(m_1)}, c_n^{(m_2)}, \cdots, c_n^{(m_s)}]^T, \\
\widetilde{\beta} &= [\beta^{(m_1)T}, \beta^{(m_2)T}, \cdots, \beta^{(m_s)T}]^T, \\
\widetilde{D} &= [D^{(m_1)}, D^{(m_2)}, \cdots, D^{(m_s)}], \\
\lambda &= [\lambda^{(m_1)}, \lambda^{(m_2)}, \cdots, \lambda^{(m_s)}]^T, \\
\widetilde{\mu} &= diag(\mu^{(m_1)}, \mu^{(m_2)}, \cdots, \mu^{(m_s)})^T, \\
\Upsilon &= \gamma \tfrac{1}{h} \left(\Theta^{(1)}, \Theta^{(2)}, \cdots, \Theta^{(m)}\right)^T, \\
\Delta &= \gamma \tfrac{1}{h} \left(\Phi^{(Bod(E^{(m_1)}))}, \Phi^{(Bod(E^{(m_2)}))}, \cdots, \Phi^{(Bod(E^{(m_s)}))}\right)^T,
\end{aligned}
$$

and

$$
\widetilde{E} = \begin{bmatrix}
e^{(m_1)} & 0 & 0 & \cdots & 0 \\
0 & e^{(m_2)} & 0 & \cdots & 0 \\
\vdots & \vdots & \vdots & \vdots & \vdots \\
0 & 0 & 0 & \cdots & e^{(m_s)}
\end{bmatrix}
$$

are the lumped LCP data, and $\mathcal{E} = \{m_1, m_2, \cdots, m_s\}$ are the active events constraints. Here $e^{(j)}$ is a vector of ones of dimension $m_C^{(j)}$, that is, $e^{(j)} = (1, 1, \ldots, 1)^T$. The vector inequalities in (5.2) are to be understood componentwise.

To simplify the presentation, the dependence of the parameters in (5.1–5.2) on $q^{(l)}$ is not explicitly included. Also, $M^{(l)} = M(q^{(l)})$ is the value of the mass matrix at time $t^{(l)}$, and $k^{(l)} = k(t^{(l)}, q^{(l)}, v^{(l)})$ represents the external force at time $t^{(l)}$.

Consider a perturbation to this mixed linear complementarity problem by introducing the parameters Δ and Υ and defining $\Gamma = \left(\Gamma^{(m_1)}, \Gamma^{(m_2)}, \cdots, \Gamma^{(m_s)}\right)^T$ to be a nonnegative vector that has as many components as active constraints. In reality, Δ and Υ are used to maintain the full generality of our results, and we will use the fact that $\Delta \geq 0$ and $\Upsilon = 0$ only when needed.

The perturbation of our mixed LCP (5.1–5.2) we will consider is

$$\begin{bmatrix} M^{(l)} & -\widetilde{\nu} & -\widetilde{n} & -\widetilde{D} & 0 \\ \widetilde{\nu}^T & 0 & 0 & 0 & 0 \\ \widetilde{n}^T & 0 & 0 & 0 & -\widetilde{\mu} \\ \widetilde{D}^T & 0 & 0 & 0 & \widetilde{E} \\ 0 & 0 & \widetilde{\mu} & -\widetilde{E}^T & 0 \end{bmatrix} \begin{bmatrix} v \\ c_\nu \\ c_n \\ \widetilde{\beta} \\ \lambda \end{bmatrix} + \begin{bmatrix} -Mv^{(l)} - hk^{(l)} \\ \Upsilon \\ \Gamma + \Delta \\ 0 \\ 0 \end{bmatrix} = \begin{bmatrix} 0 \\ 0 \\ \rho \\ \widetilde{\sigma} \\ \zeta \end{bmatrix} \tag{5.3}$$

$$\begin{bmatrix} c_n \\ \widetilde{\beta} \\ \lambda \end{bmatrix}^T \begin{bmatrix} \rho \\ \widetilde{\sigma} \\ \zeta \end{bmatrix} = 0, \qquad \begin{bmatrix} c_n \\ \widetilde{\beta} \\ \lambda \end{bmatrix} \geq 0, \qquad \begin{bmatrix} \rho \\ \widetilde{\sigma} \\ \zeta \end{bmatrix} \geq 0\,. \tag{5.4}$$

Notice that the matrix of this linear complementarity problem is clearly positive semidefinite. This fact will allow us to get some very useful results by simply interpreting (5.3–5.4) as a a quadratic program. To simplify the notation, let $q^{(l)} = -Mv^{(l)} - hk^{(l)}$.

We now can rewrite the mixed complementarity problem (5.3–5.4) into the form

$$\begin{array}{llllll} M^{(l)}v & -\widetilde{n}\widetilde{c_n} & -\widetilde{D}\widetilde{\beta} & & = -q^{(l)} & \\ \widetilde{\nu}^T v & & & & = -\Upsilon & \\ \widetilde{n}^T v & & & -\tilde{\mu}\lambda & \geq -\Gamma - \Delta & \perp \quad c_n \geq 0 \\ \widetilde{D}^T v & & & +\widetilde{E}\lambda & \geq 0 & \perp \quad \widetilde{\beta} \geq 0 \\ & \tilde{\mu}c_n & -\widetilde{E}^T\widetilde{\beta} & & \geq 0 & \perp \quad \lambda \geq 0 \end{array} \tag{5.5}$$

and from this we can show a relation between the velocity solutions of (5.1–5.2) and (5.3–5.4) under suitable conditions.

Lemma 5.1. *Let $\Upsilon = 0$. If for a solution $\left(v^*, c_\nu, c_n, \tilde{\beta}, \lambda\right)$ of (5.5) we have that $\Gamma = \tilde{\mu}\lambda$, then that solution of (5.5) is a solution of (5.1–5.2). Conversely, any solution $\left(v^*, c_\nu, c_n, \tilde{\beta}, \lambda\right)$ of (5.1–5.2) is a solution of (5.3–5.4) with $\Gamma = \tilde{\mu}\lambda$.*

Proof. The proposed substitution makes the two LCPs identical. ■

Observe that (5.5) can be seen as constituting the first-order optimality conditions of

the quadratic program

$$\begin{array}{rlcll} \min_{v,\lambda} & \frac{1}{2} v^T M^{(l)} v + q^{(l)^T} v & & & \\ \text{subject to} & n^{(m)^T} v - \mu^{(m)} \lambda^{(m)} & \geq & -\Gamma^{(m)} - \Delta^{(m)}, & m \in \mathcal{E} \\ & D^{(m)^T} v + \lambda^{(m)} e^{(m)} & \geq & 0, & m \in \mathcal{E} \\ & \nu_i^T v & = & -\Upsilon_i, & i = 1, 2, \cdots, n_J \\ & \lambda^{(m)} & \geq & 0 & m \in \mathcal{E} \end{array} \tag{5.6}$$

and that allows us to relate the solutions of (5.3–5.4) and (5.2).

Lemma 5.2. *Any solution (v, λ) of (5.6), together with its Lagrange multipliers, is a solution of the linear complementarity problem (5.3–5.4). Conversely, the v, λ components of any solution of (5.3–5.4) are a solution of (5.6).*

Proof. The proof follows directly from the property of first-order optimality conditions and by the convexity of the quadratic program (5.6), once we write out the first-order optimality conditions for (5.6) to get (5.5). ■

Even though the quadratic program (5.6) is not strictly convex with respect to (v, λ), it is strictly convex with respect to v. It then follows that v is the unique solution of the following strictly convex quadratic program:

$$\begin{array}{rlcll} \min_{v} & \frac{1}{2} v^T M^{(l)} v + q^{(l)^T} v & & & \\ \text{subject to} & e^{(m)} n^{(m)^T} v + \mu^{(m)} D^{(m)^T} v & \geq & -\left(\Gamma^{(m)} + \Delta^{(m)}\right) e^{(m)}, & m \in \mathcal{E} \\ & \nu_i^T v & = & -\Upsilon_i, & i = 1, 2, \cdots, n_J. \end{array} \tag{5.7}$$

If $\Gamma \geq 0$, $\Delta \geq 0$ and $\Upsilon_i = 0$, then $v = 0$ is a feasible point of the quadratic program. Moreover, our previous assumption that $M^{(l)}$ be positive definite means that whenever (5.7) is feasible, it has a unique solution $v^*(\Gamma)$. Now, it follows that the mapping

$$P_1(\Gamma) = v^*(\Gamma) \tag{5.8}$$

is well-defined for any Γ for which (5.7) is feasible.

Let v be a velocity vector. For the given active events $\mathcal{E}$, we can define

$$\Lambda(v) = \lambda, \tag{5.9}$$

where

$$\lambda^{(m)} = \max_{i=1,2,\cdots,M_C^{(m)}} \left\{ d_i^{(m)^T}(v) \right\}, \quad m \in \mathcal{E}.$$

Because of the way $D^{(m)}$ is balanced for a given contact m, for any fixed v, $\Lambda(v) \geq 0$.and, $\Lambda(v)$ produces the smallest possible λ that satisfies

$$\widetilde{D}^T v + \widetilde{E}\lambda \geq 0.$$

After $v^*(\Gamma)$ is found, then a λ^*, that, together with $v^*(\Gamma)$, is a solution of (5.6) can be found by choosing

$$\lambda^* = \Lambda(v^*). \tag{5.10}$$

Therefore, all the properties of the velocity solution of (5.3–5.4) can be inferred by working with (5.7), once we show that the two problems have the same v-solution. The quantity λ^* is implicitly a function of Γ, but, for defining its properties, we prefer to regard λ^* as a function of v^*, or $\lambda^*(v^*)$.

Theorem 5.3. *Whenever (5.6) is feasible, the v-solution of (5.6) is unique and is, in fact, a solution of (5.7). Conversely, if v is a solution of (5.7), then $(v, \Lambda(v))$ is a solution of (5.6).*

Proof. Let (v_2, λ_2) be a solution to (5.6). Therefore, we have

$$n^{(m)^T} v_2 - \mu^{(m)} \lambda_2^{(m)} \geq -\Gamma^{(m)} - \Delta^{(m)}, \quad m \in \mathcal{E}$$

and

$$D^{(m)^T} v_2 + e^{(m)} \lambda_2^{(m)} \geq 0, \quad m \in \mathcal{E},$$

from which it follows, by multiplying the second inequality by $\mu^{(m)}$ and adding it componentwise to the first inequality, that

$$e^{(m)} n^{(m)^T} v_2 + \mu^{(m)} D^{(m)^T} v_2 \geq -e^{(m)} \left(\Gamma^{(m)} + \Delta^{(m)} \right), \quad m \in \mathcal{E}.$$

Hence, v_2 is feasible for (5.7), which must now have an optimal solution v_1 that satisfies

$$\frac{1}{2}{v_1}^T M^{(l)} v_1 + q^T v_1 \leq \frac{1}{2}{v_2}^T M^{(l)} v_2 + q^T v_2.$$

On the other hand, the solution of (5.7) satisfies

$$e^{(m)} n^{(m)^T} v_1 + \mu^{(m)} D^{(m)^T} v_1 \geq -e^{(m)} \left(\Gamma^{(m)} + \Delta^{(m)}\right), \quad m \in \mathcal{E}. \tag{5.11}$$

Define $\lambda_1 = \Lambda(v_1)$, so, by (5.9), we have that

$$D^{(m)^T} v_1 + e^{(m)} \lambda_1^{(m)} \geq 0, \; m \in \mathcal{E}. \tag{5.12}$$

Also, from (5.9) and the fact that the columns of $D^{(m)}$ form a balanced set, we must have that $d_i^{(m)^T} v_1 + \lambda_1^{(m)} = 0$ for some i among $1, 2, \cdots, M_C^{(m)}$. Since from (5.11) we must have that $n^{(m)^T} v_1 + \mu^{(m)} d_i^{(j)^T} v_1 \geq -\left(\Gamma^{(m)} + \Delta^{(m)}\right)$, the last equality implies

$$n^{(m)^T} v_1 - \mu^{(m)} \lambda_1^{(m)} \geq -\left(\Gamma^{(m)} + \Delta^{(m)}\right), m \in \mathcal{E}$$

and thus from (5.12) we obtain that (v_1, λ_1) is feasible for (5.6). Hence

$$\frac{1}{2}{v_2}^T M^{(l)} v_2 + q^T v_2 \leq \frac{1}{2}{v_1}^T M^{(l)} v_1 + q^T v_1.$$

Therefore, the objective functions of (5.6) and (5.7) must be equal to each other. That means $(v_1, \Lambda(v_1))$ is optimal for (5.6) and v_2 is optimal for (5.7). The proof is complete upon recalling the uniqueness of the solution of (5.7). ■

Consider now another related linear complementarity problem.

$$\begin{bmatrix} M^{(l)} & -\widetilde{\nu} & -\widetilde{n} & -\widetilde{D} \\ \widetilde{\nu}^T & 0 & 0 & 0 \\ \widetilde{n}^T & 0 & 0 & 0 \\ \widetilde{D}^T & 0 & 0 & 0 \end{bmatrix} \begin{bmatrix} v \\ c_\nu \\ c_n \\ \widetilde{\beta} \end{bmatrix} + \begin{bmatrix} -Mv^{(l)} - hk^{(l)} \\ 0 \\ \Delta \\ \tilde{E}\lambda \end{bmatrix} = \begin{bmatrix} 0 \\ 0 \\ \tilde{\rho} \\ \widetilde{\sigma} \end{bmatrix} \tag{5.13}$$

$$\begin{bmatrix} c_n \\ \widetilde{\beta} \end{bmatrix}^T \begin{bmatrix} \rho \\ \widetilde{\sigma} \end{bmatrix} = 0, \qquad \begin{bmatrix} c_n \\ \widetilde{\beta} \end{bmatrix} \geq 0, \qquad \begin{bmatrix} \rho \\ \widetilde{\sigma} \end{bmatrix} \geq 0\,, \tag{5.14}$$

where λ is fixed, and thus not a variable of the problem. Clearly the LCP (5.13–5.13) represents the optimality conditions for the quadratic program

$$\begin{array}{rlrcll} \min_v & \frac{1}{2} v^T M^{(l)} v + {q^{(l)}}^T v & & & & \\ \text{subject to} & & {n^{(m)}}^T v & \geq & -\Delta^{(m)}, & m \in \mathcal{E} \\ & & {D^{(m)}}^T v & \geq & -\lambda^{(m)} e^{(m)}, & m \in \mathcal{E} \\ & & \nu_i^T v & = & 0, & i = 1, 2, \cdots, n_J, \end{array} \tag{5.15}$$

where $\lambda \geq 0$ is given. In this section we will assume that $\Delta \geq 0$, and thus that (5.15) is feasible.

Recall that $M^{(l)}$ is positive definite, hence (5.15) has a unique solution $v^*(\lambda)$, which means that the mapping

$$P_2(\lambda) = v^*(\lambda) \tag{5.16}$$

is well defined whenever (5.7) is feasible.

Lemma 5.4. *Assume that (v^*, λ^*) are components of the solution of (5.1-5.2). Then the solution of (5.15) with $\lambda = \lambda^*$ is exactly v^*, or $P_2(\lambda^*) = v^*$.*

Proof. Let $\left(v^*, c_\nu, c_n, \tilde{\beta}, \lambda^*\right)$ be a solution of (5.1–5.2). By comparing the linear complementarity problems (5.1–5.2) and (5.13–5.14), we see that if we set $\lambda = \lambda^*$, we obtain that $\left(v^*, c_\nu, c_n, \tilde{\beta}\right)$ is a solution of (5.13–5.14). The conclusion follows by our previous observation that (5.13–5.14) are the optimality conditions of (5.15), and thus v^* is the unique solution of (5.15) for $\lambda = \lambda^*$. ■

The fundamental result of this section is based on analyzing the properties of a series of aggregate maps. Recall that, following the definition of the mixed linear complementarity problem (5.1–5.2), $\tilde{\mu}$ is a diagonal matrix whose entries are the friction coefficients at the individual contacts.

Assume for now that $\Delta \geq 0$ and $\Upsilon = 0$. Then we can define three aggregate maps by

$$\begin{aligned} \chi_1(v) &= P_1(\tilde{\mu}\Lambda(v)), \\ \chi_2(\Gamma) &= \mu\Lambda \circ P_1(\Gamma), \\ \chi_3(\Gamma) &= \mu\Lambda \circ P_2 \circ \Lambda \circ P_1(\Gamma). \end{aligned} \tag{5.17}$$

It turns out under modest conditions, each of the mappings above is indeed a contraction. The results were proven in [6].

Next, we consider the so-called Mangasarian-Fromovitz Constraint Qualification (MFCQ) for quadratic programs. Consider the generic quadratic program

$$\begin{aligned} \text{minimize} \quad & q^T x + \tfrac{1}{2} x^T Q x \\ \text{subject to} \quad & A^T x + \alpha \geq 0 \\ & B^T x + \beta = 0, \end{aligned} \tag{5.18}$$

where $A \in R^{n \times m}$, $B \in R^{n \times p}$, $\alpha \in R^m$, and $\beta \in R^p$.

Definition 5.5. Consider the quadratic program (5.18). MFCQ holds at any point $x \in R^n$ if the following conditions are true:

1. B has full row rank,
2. $\exists f \in R^m$, $f < 0$, and $d \in R^n$, such that $\begin{cases} A^T d = f \\ B^T d = 0 \end{cases}$.

An important consequence of (5.18) satisfying MFCQ is the following [6].

Lemma 5.6. *If the quadratic program (5.18) satisfies MFCQ, then it is feasible for any $\alpha \in R^m$ and $\beta \in R^p$. If, in addition, the matrix Q is positive definite, then the quadratic program has a solution.*

We need to have a certain constraint regularity to hold if we want to ensure that the solution $v^{(l+1)}$ remain stable, despite the parameters Δ and Υ. In order to state sufficient conditions, we use some properties of the friction cone. We define the friction cone at a given position as follows:

$$FC(q) = \left\{ t = \tilde{\nu} c_\nu + \tilde{n} c_n + \tilde{D}\tilde{\beta} \;\middle|\; c_n \geq 0,\ \tilde{\beta} \geq 0, \quad \left|\left|\beta^{(m)}\right|\right|_1 \leq \mu^{(m)} c_n^{(m)},\ \forall m \in \mathcal{E} \right\}. \quad (5.19)$$

Simply put, the friction cone is the portion in the velocity space that can be covered by feasible constraint interaction impulses, and is clearly a convex set.

We do not wish our configuration to become disassembled, which now forces us to exploit one of the properties of the friction cone. This leads us to define when the friction cone is pointed.

Definition 5.7 (**Stewart [48]**). We say that the friction cone $FC(q)$ is pointed if for all $(c_\nu, c_n, \tilde{\beta})$ satisfying $c_n \geq 0$ and $\left|\left|\beta^{(m)}\right|\right|_1 \leq \mu^{(m)} c_n^{(m)}$, $\forall m \in \mathcal{E}$, then $\tilde{\nu} c_\nu + \tilde{n} c_n + \tilde{D}\tilde{\beta} \neq 0$.

We will assume that from now on, all of the configurations that we encounter have a *uniformly* pointed friction cone. This assumption is essential if we want to be certain that our time-stepping scheme (5.1)–(5.2) converges in the limit to a weak solution of the continuous problem [48].

Pang and Stewart [42] use the pointed friction cone to show the existence of a solution to the mixed LCP (5.1)–(5.2).

Theorem 5.8. *Assume that the friction cone $FC(q)$ is pointed. Then the mixed LCP (5.1)–(5.2) has a solution.*

Proof. The proof follows directly from the results in [42]. ■

Suppose now that the friction cone is pointed, therefore we know that the mixed LCP (5.1)–(5.2) has a solution. Then determining a method for solving the mixed LCP is simple, because if the mass matrix $M^{(l)}$ is constant, we can find the solution by using Lemke's algorithm [21].

Theorem 5.9 (**Anitescu and Hart [6]**).

i) Assume that, for $\tilde{\mu} = 0$, the friction cone $FC(q)$ is pointed. Then there exists $\mu^\circ > 0$ such that, whenever $||\tilde{\mu}|| \leq \mu^\circ$ the mapping $\chi_1(v)$ is a contraction with parameter $\frac{1}{2}$, and therefore has a unique fixed point.

ii) Let $K_\Gamma > 0$ and $K_\mu > 0$ such that the friction cone $FC(q)$ is pointed whenever $||\hat{\mu}||_\infty \leq K_\mu$, $\forall m \in \mathcal{E}$. Then there exists μ° such that for $0 \leq ||\mu|| \leq \mu^\circ$, the mapping χ_2 is a contraction.

iii) Let $K_\Gamma > 0$ and $K_\mu > 0$ such that the friction cone $FC(q)$ is pointed whenever $||\hat{\mu}||_\infty \leq K_\mu$, $\forall m \in \mathcal{E}$. Then there exists μ° such that for $0 \leq \mu \leq \mu^\circ$, the mapping χ_3 is a contraction.

Our assumption that the friction cone be pointed plays an important key to the proof. This is because the friction cone being pointed implies that the quadratic program (5.7) will satisfy MFCQ. It would then follow that Lemma 5.6 applies, and thus not only does the solution of (5.7) exist, but it is Lipschitz continuous with respect to Δ and Υ.

In [6] we also show that, for sufficiently small friction, we can use the aggregate mappings above to get a fixed point iteration that converges globally and linearly to the velocity solution while solving convex subproblems, provided that the friction cone is pointed. Moreover, an energy bound is found for the solution for the quadratic program (5.7).

Anitescu and Hart [5] show that the velocity solution of the mixed LCP (5.1)–(5.2) has an upper bound:

$$\begin{aligned} v^{(l+1)^T} M^{(l)} v^{(l+1)} \quad \leq \quad & v^{(l)} M^{(l)} v^{(l)} + h_l^2 k^{(l)} M^{(l)-1} k^{(l)} \\ & + 2h_l v^{(l)^T} k^{(l)} + c(q^{(l)}, \tilde{\mu}, M^{(l)})^2 \left|\left| \Delta_-^{(l)}, \Upsilon^{(l)} \right|\right|_\infty^2 . \end{aligned} \tag{5.20}$$

They then use the uniformly pointed friction cone assumption to obtain uniformly upper boundedness of the quantity $c(q^{(l)}, \tilde{\mu}, M^{(l)})$, with upper bound c_U, during simulation. When we rewrite inequality 5.20 using this uniform bound, we get

$$v^{(l+1)^T} M^{(l)} v^{(l+1)} \leq v^{(l)} M^{(l)} v^{(l)} + h_l^2 k^{(l)} M^{(l)-1} k^{(l)} + 2h_l v^{(l)^T} k^{(l)} + c_U^2 \left|\left| \Delta_-^{(l)}, \Upsilon^{(l)} \right|\right|_\infty^2 . \tag{5.21}$$

We can summarize their results.

Proposition 5.10. *Suppose that the quadratic program (5.7) satisfies MFCQ. Let* $A(q^{(l)}, \tilde{\mu})$ *be the matrix of inequality constraints and* $B(q^{(l)})$ *the matrix of equality constraints in (5.7). Also, assume that* $\Gamma^{(m)} \geq 0$, $m \in \mathcal{E}$. *Then there exists* $c = c(A(q^{(l)}, \tilde{\mu}), B(q^{(l)}), M^{(l)})$ *such that the solution* $v^{(l+1)}$ *of (5.7) satisfies*

$$v^{(l+1)^T} M^{(l)} v^{(l+1)} \leq v^{(l)} M^{(l)} v^{(l)} + h_l^2 k^{(l)} M^{(l)-1} k^{(l)} + 2h_l v^{(l)^T} k^{(l)} + c^2 \left|\left| \Delta_-^{(l)}, \Upsilon^{(l)} \right|\right|_\infty^2 .$$

The various bounds are used to show that constraint stabilization can be achieved as we construct our constant step time-stepping algorithm, which we do in the next chapter.

6.0 CONSTRAINT STABILIZATION

As we discussed, rigid multibody dynamics is an important area of mathematical modeling and attempts to predict the position and velocity of a system of rigid bodies. Noninterpenetration constraints, joint constraints, and friction forces serve to make the task more difficult. The predicted position and velocity is accomplished by some numerical integration technique.

The problem is that in order to solve the prevailing equations and constraints, an integration technique must be used. However, all integration time-stepping schemes will introduce a discretization error, which means that for successive steps, the bodies may drift apart from each other without solving the necerssary constraints. When the geometrical constraints are not satisfied, this constraint drift becomes visible,and then the simulation may be useless. Baumgarte was one of the earliest pioneers dealing with constraint stabilization [16].

What we are proposing here is a method that achieves geometrical (noninterpenetration and joint) constraint stabilization for complementarity-based time-stepping methods for rigid multi-body dynamics with contact, joints, and friction. A variant of the scheme presented here is currently used for the dynamical simulation of dynamical robotic grasps [7, 37]. This scheme needs no computational effort other than that for solving the basic LCP subproblem, though the free term of the LCP is modified compared with other time-stepping LCP approaches [8, 9, 49].

The constraint stabilization issue in a complementarity setting has been tackled by using nonlinear complementarity problems [49], an LCP followed by a nonlinear projection approach that includes nonlinear inequality constraints [9], and a post-processing method [18] that uses one potentially non-convex LCP based on the stiff method developed in [9] followed by one convex LCP for constraint stabilization. When applied to joint-only systems,

the method from [18] belongs to the set of post-processing methods defined in [11, 12]. In order to achieve constraint stabilization, however, all of these methods need additional computation after the basic LCP subproblem has been solved. They stands in contrast with our approach that needs no additional computational effort to achieve constraint stabilization.

In this chapter, we will prove a generalized theorem on constraint stability and state the conditions that are needed therein. We next give details about the general algorithm we use that achieves constraint stability. *Two major contributions of this thesis are the introduction of an efficient metric which can calculate the depth of penetration for convex polyhedral bodies and its implementation within an algorithm which achieves constraint stabilization.*

One big advantage of our time-stepping scheme is that for an appropriately choice of the step size h_l and parameter $\hat{\epsilon}$, at the end of each step our algorithm, while allowing small interpenetrations, guarantees that the physically actives set will be contained in $\mathcal{E}$, and hence *there will never be a need to stop the simulation.*

6.1 GENERALIZED STABILITY RESULTS USING RPD

For the generalized position vector q, we denote by $\delta_{j_1 j_2}(q)$ the signed distance between the bodies B_{j_1} and B_{j_2}. Recall that there is a j such that $\Phi^{(j)}(q) = \delta_{j_1 j_2}(q)$. The feasible set of all noninterpenetration and joint constraints is then defined by

$$\delta_{j_1 j_2}(q) \geq 0,\ 1 \leq j_1 < j_2 \leq n_B, \quad \Theta^{(i)}(q) = 0,\ i = 1, 2, \cdots, n_J. \tag{6.1}$$

We next rewrite the noninterpenetration constraints and associate a pair (j_1, j_2) with an index $j \in \{1, 2, \cdots, p\}$ and define $\Phi^{(j)}(q) = \delta_{j_1 j_2}(q)$. Here $p = \frac{1}{2} n_B(n_B + 1)$. Next, we see that the feasible set defined in (6.1) is equivalent to the set defined by

$$\Phi^{(j)}(q) \geq 0,\ 1 \leq j \leq p, \quad \Theta^{(i)}(q) = 0,\ i = 1, 2, \cdots, m. \tag{6.2}$$

In proving that our method provides constraint stabilization, we need to have continuity and piecewise differentiability of $\Phi^{(j)}(q)$, $1 \leq j \leq p$, over a sufficiently large subset of Q.

Unfortunately, it is unreasonable to expect differentiability over all of Q. Anitescu and Hart [5] give an example of nondifferentiability even for a simple two-dimensional problem.

We note that the signed distance function is defined for any two bodies. In that respect the relations of (6.2) quantifies the geometrical constraints between any two bodies. For this analysis, however, it is not sufficient to have the feasible set defined by continuous functions; here we need piecewise differentiability of the involved mappings at least over the feasible set and an open neighborhood of it.

While such a property holds if all the bodies involved are smooth and strictly convex [3], we are particularly interested in using bodies with planar facets for which a representation like the one in equation (6.2) that uses differentiable mappings is available only locally.

A downside of our approach in the bodies-with-facets case, however, is that the linear complementarity problem from our approach will involve more constraints than the integrate-detect-restart procedure. Nonetheless, we expect that it will solve fewer problems per time step.

Recall that we are interested in achieving feasibility as the time step goes to 0 and keeping infeasibility under control for finite time step. To accommodate this, we need to define the set of allowable positions. An allowable position is not necessarily physically feasible, but will allow our analysis to proceed relatively smoothly when small penetration exists. Thus, define now, for some $\epsilon > 0$, the sets

$$\Omega_\epsilon^\Phi = \{q \in Q \mid \Phi^{(j)}(q) \geq -\epsilon, 1 \leq m \leq p\},$$

$$\Omega_\epsilon^\Theta = \{q \in Q \mid \left|\Theta^{(i)}(q)\right| \geq -\epsilon, i = 1, 2, \cdots, n_J\},$$

$$\Omega_\epsilon = \Omega_\epsilon^\Phi \cap \Omega_\epsilon^\Theta.$$

Also, in order to describe the behavior of the infeasibility of the non-interpenetration and joint constraints, we define

$$I(q) = \max_{1 \leq j \leq p, 1 \leq i \leq n_J} \left\{ \Phi_-^{(j)}(q), \left|\Theta^{(i)}(q)\right| \right\}, \tag{6.3}$$

which we will use to measure the extent of infeasibility of the non-interpenetration and joint constraints. Here we use the notation f_- to denote the negative part of the real valued function f. That is,

$$\begin{aligned} f_-(x) &= \max\{-f(x), 0\} \\ &= \tfrac{1}{2}\left(|f(x)| - f(x)\right). \end{aligned}$$

Let us now prove a small Lemma concerning the representation of our piecewise functions on a line segment.

Lemma 6.1. *Let the functions $\Phi^{(j)}$ be piecewise continuously differentiable. Also, let the position q, the vector w, and real number $t > 0$ be given such that the line segment from q to $q + tv$ is feasible. Then we can find a sequence $\{t_1, t_2, \ldots, t_{k_j}\}$ of increasing positive real numbers and a sequence of component functions $\left\{\hat{\Phi}^{(m_1)}, \hat{\Phi}^{(m_2)}, \ldots, \hat{\Phi}^{(m_{k_j})}\right\}$ such that*

$$\Phi^{(j)}(q + tv) - \Phi^{(j)}(q) = \sum_{i=1}^{k_j} \left[\hat{\Phi}^{(m_i)}(q + t_i v) - \hat{\Phi}^{(m_i)}(q + t_{i-1} v)\right]. \tag{6.4}$$

Proof. Since we know that the segment from q to $q+tv$ is in the domain of $\Phi^{(j)}$, we consider that very segment which we will subdivide into finitely many subsegments.

Let $t_o = 0$. At the point p, there is an active event, m_1. We can then find t_1 which is the largest value of t for which m_1 is active. If $q + t_1 v$ is not equal to $q + tv$, then we repeat the process, finding an active event m_2 at $q + t_1 v$ and the largest value of t,say t_2 with $t_2 > t_1$, for which m_2 is active.

Because of the unique way $\Phi^{(j)}$ is defined, the way we defined the t_i and the fact that there exist only finitely many events, we can use Theorem (3.13) to enumerate a finite number of values $t_1, t_2, \ldots, t_{k_j}$ and associated events $m_1, m_2, \ldots, m_{k_j}$ such that on the i^{th} segment, we get

$$\Phi^{(j)}(q + tv) = \hat{\Phi}^{(m_i)}(q + tv) \quad \forall t \in [t_{i-1}, t_i].$$

Notice that we can then write

$$\begin{aligned} \Phi^{(j)}(q + tv) - \Phi^{(j)}(q) &= \sum_{i=1}^{k_j} \left[\Phi^{(j)}(q + t_i v) - \Phi^{(j)}(q + t_{i-1} v)\right] \\ &= \sum_{i=1}^{k_j} \left[\hat{\Phi}^{(m_i)}(q + t_i v) - \hat{\Phi}^{(m_i)}(q + t_{i-1} v)\right] \end{aligned} \tag{6.5}$$

and that completes the proof. ■

Proposition 6.2. *Let the functions $\Phi^{(i)}$ be piecewise continuously differentiable. If the component functions $\widehat{\Phi}^{(m)}$ are locally differentiable and have uniformly bounded derivatives with bound C_1, then for any position q and vector w and real number $t > 0$,*

$$\left|\Phi^{(j)}(q + tw) - \Phi^{(j)}(q)\right| \leq t\,||w||\,C_1. \tag{6.6}$$

Proof. We can immediately invoke Lemma 6.1 so that from q to $q + \tau w$ for $0 \leq \tau \leq t$, we can find an increasing sequence of values $0 = t_o < t_1 < \cdots < t_n = t$ and its corresponding restriction $\hat{\Phi}^{(m_i)}$. Then using Taylor's Theorem and the uniform bound C, we get

$$\begin{aligned}
\Phi^{(j)}(q + tw) - \Phi^{(j)}(q) &= \sum_{k=1}^{n} \left(\hat{\Phi}^{(m_i)}(q + t_k w) - \hat{\Phi}^{(m_i)}(q + t_{k-1} w)\right) \\
&\leq \sum_{k=1}^{n} ||t_k w - t_{k-1} w||\,C_1 \\
&= \sum_{k=1}^{n} (t_k - t_{k-1})\,||w||\,C_1 \\
&= (t_n - t_o)\,||w||\,C_1 \\
&= t\,||w||\,C_1,
\end{aligned}$$

and

$$\begin{aligned}
-\left(\Phi^{(j)}(q + tw) - \Phi^{(j)}(q)\right) &= -\sum_{k=1}^{n} \left(\hat{\Phi}^{(m_i)}(q + t_k w) - \hat{\Phi}^{(m_i)}(q + t_{k-1} w)\right) \\
&\leq \sum_{k=1}^{n} ||t_k w - t_{k-1} w||\,C_1 \\
&= \sum_{k=1}^{n} (t_k - t_{k-1})\,||w||\,C_1 \\
&= (t_n - t_o)\,||w||\,C_1 \\
&= t\,||w||\,C_1,
\end{aligned}$$

which completes the proof. ■

We now list one of the assumptions about the kinematic description of the non-interpenetration constraints.

Assumption A1: There exists $\epsilon_o > 0$, $C_1^d > 0$, and $C_2^d > 0$ such that

- $\Phi^{(j)}$ for $1 \leq j \leq n_B$ are piecewise continuous on their domains Ω_ϵ, with piecewise components $\widehat{\Phi}^{(m)}(q)$ which are twice continuously differentiable in their respective open domains with first and second derivatives uniformly bounded by $C_1^d > 0$ and $C_2^d > 0$, respectively, and
- $\Theta^{(i)}(q)$ for $i = 1, 2, \cdots, m$ are twice continuously differentiable in Ω_ϵ with first and second derivatives uniformly bounded by $C_1^d > 0$ and $C_2^d > 0$, respectively.

Lemma 6.3. *If Assumption A1 holds, then for any j such that $1 \leq j \leq n_B$, we have $\Phi^{(j)}$ is everywhere directionally differentiable. Moreover, the generalized gradient of $\Phi^{(j)}$ is contained in the convex cover of the gradients of its component functions which are active at q and evaluated at q.*

Proof. Let q be any point in the domain of $\Phi^{(j)}$. We need to consider the generalized directional derivative of $\Phi^{(j)}$ at q in the direction v is defined, see [17], by

$$\Phi^{(j)^o}(q; v) = \limsup_{p \to q, t \downarrow 0} \frac{\Phi^{(j)}(p + tv) - \Phi^{(j)}(p)}{t}.$$

So we consider the segment from q to $q + tv$ which we will subdivide into finitely many subsegments.

Once again, we invoke Lemma 6.1 so that from p to $p + \tau w$ for $0 \leq \tau \leq t$, we can find an increasing sequence of values $0 = t_o < t_1 < \cdots < t_n = t$ and corresponding restrictions $\hat{\Phi}^{(m_i)}$.

Next we can use differentiability of the component functions and the mean value theorem to calculate

$$\begin{aligned} \tfrac{1}{t}\left[\Phi^{(j)}(p + tv) - \Phi^{(j)}(p)\right] &= \frac{1}{t}\sum_{i=1}^{k}\left[\hat{\Phi}^{(m_i)}(p + t_i v) - \Phi^{(j)}(p + t_{i-1}v)\right] \\ &= \frac{1}{t}\sum_{i=1}^{k}\left[(t_i - t_{i-1})\nabla\hat{\Phi}^{(m_i)^T}(p + \zeta_{i-1}v)v\right]. \end{aligned} \tag{6.7}$$

Since we know that

$$\limsup_{p \to q, t \downarrow 0} \nabla\hat{\Phi}^{(m_i)}(p + \zeta_{i-1}v) = \nabla\hat{\Phi}^{(m_i)}(q)$$

and

$$\lim_{t\to 0}\frac{1}{t}\sum_{i=1}^{k}(t_i - t_{i-1}) = 1,$$

our initial calculation can be simplified because the calculation of $\Phi^{(j)^o}(q;v)$ always produces a convex combination of the gradients of the events which are active at q and evaluated at q. This is enough to show that the generalized gradient $\partial\Phi^{(j)}(q)$ must be contained within the convex cover of the gradients of the component functions which are active at q and evaluated at q. ■

Lemma 6.4. *If Assumption A1 holds, then for any j such that $1 \leq j \leq n_B$, then $\Phi^{(j)}$ satisfies a Lipschitz condition.*

Proof. By Lebourg's Mean Value Theorem [17], given q_1 and q_2 in the domain of $\Phi^{(j)}$, there exists q_o on the line segment between q_1 and q_2 that satisfies

$$\Phi^{(j)}(q_1) - \Phi^{(j)}(q_2) \in \left\langle \partial\Phi^{(j)}(q_o), q_1 - q_2 \right\rangle.$$

This means that there is some $\Gamma \in \partial\Phi^{(j)}$ such that

$$\Phi^{(j)}(q_1) - \Phi^{(j)}(q_2) = \Gamma(q_1 - q_2).$$

However, we know, by Lemma 6.3, that Γ must be a convex combination of gradients of component functions. Notice that by Assumption A1, each of these gradients can be bounded above by C_1^d, and so we must have

$$\left|\Phi^{(j)}(q_1) - \Phi^{(j)}(q_2)\right| \leq C_1^d \left|\left|q_1 - q_2\right|\right|,$$

which concludes the proof. ■

The stability results we seek concern the behavior of the infeasibility of the constraints, noninterpenetration and joint. It is especially noteworthy that, because of the way we defined the active set (4.10), the measure of constraint infeasibility we defined as

$$I(q) = \max_{1 \leq j \leq p, 1 \leq i \leq n_J} \left\{ \Phi_-^{(j)}(q), |\Theta^{(i)}(q)| \right\} \tag{6.8}$$

has a special relation to another measure of infeasibility that is attached to a choice of the active set. That is, we can define

$$I^{\mathcal{A}}(q) = \max_{j \in \mathcal{A}, 1 \leq i \leq n_J} \left\{ \Phi_-^{(j)}(q), |\Theta^{(i)}(q)| \right\} \tag{6.9}$$

and notice that the active set, by definition (4.10), must include all of the noninterpenetration constraints that are infeasible at the current point q. It follows that

$$I(q) = I^{\mathcal{A}(q)}(q),$$

although if q_1 and q_2 are different, then we will, in general, have

$$I(q_1) \neq I^{\mathcal{A}(q_2)}(q_1).$$

Notice that we could also define a measure of infeasibility as

$$I^{\mathcal{E}}(q) = \max_{m \in \mathcal{E}, 1 \leq i \leq n_J} \left\{ \widehat{\Phi}_-^{(m)}(q), |\Theta^{(i)}(q)| \right\}, \tag{6.10}$$

and from (4.11) and our definitions of infeasibility, it is not very difficult see that we have $I^{\mathcal{A}}(q) = I^{\mathcal{E}}(q)$.

Now by the definition of Δ and Υ after (5.1)–(5.2), we know that

$$I^{\mathcal{A}}(q^{(l)}) = \frac{h_l}{\gamma} \left|\left| \Delta_-^{(l)^T}, \Upsilon^{(l)} \right|\right|_\infty. \tag{6.11}$$

There is a connection between Ω_ϵ for ϵ_0 and $I(q)$, namely that

$$q \in \Omega_\epsilon \Leftrightarrow I(q) \leq \epsilon.$$

Finally, we make the following additional assumptions about the kinematic description of the noninterpenetration constraints.

Assumption D1: The mass matrix is constant. That is, $M\left(q^{(l)}\right) = M^{(l)} = M$.

Assumption D2: The norm growth parameter $c(\cdot,\cdot,\cdot)$ used in [5] is constant. That is,

$$c\left(A(q,\widetilde{\mu}), B(q).M\right) \leq c_o \quad \forall \epsilon \in [0,\epsilon_o] \quad \forall q \in \Omega_\epsilon, \tag{6.12}$$

where $A(q,\widetilde{\mu})$ and $B(q)$ are the matrices defining the inequality constraints and equality constraints, respectively.

Assumption D3: The external force is continuous and increases at most linearly with the position and velocity, and is uniformly bounded in time. That is

$$k(t,v,q) = k_o(t,v,q) + f_c(v,q) + k_1(v) + k_2(q) \tag{6.13}$$

and there is some constant $c_K \geq 0$ such that

$$\begin{aligned} ||k_o(t,v,q)|| &\leq c_K \\ ||k_1(v)|| &\leq c_K\,||v|| \\ ||k_2(q)|| &\leq c_K\,||q||\,. \end{aligned} \tag{6.14}$$

In addition, assume that

$$v^T f_c(v,q) = 0 \quad \forall v,q. \tag{6.15}$$

Now that we have Assumptions (A1) and (D1) - (D3), we are ready to produce our time-stepping algorithm.

6.2 THE ALGORITHM

Most previous approaches have pursued a simulate-detect-restart approach [8, 15, 22, 49]. In these approaches, when a collision occurs after the velocity is determined as a solution of the LCP, the simulation does not necessarily proceed for the duration of the timestep. Usually, the simulation is stopped at the collision, the collision is resolved by using LCP techniques [8, 26], and the simulation is restarted.

For these approaches, the active set is updated as a result of collision detection. If many collisions occur per unit of simulation, then there will be many costly updates that will interfere with the performance of the solver. Moreover, for a variable timestep procedure, the timestep may easily approach zero in the face of multiple collisions.

In the approach presented here, the active set $\mathcal{A}$ (4.10) is always defined, and with the appropriately chosen parameter $\hat{\epsilon}$, we can compute the computationally active events $\mathcal{E}$ (4.10) by using the Compatibility Check from Algorithm 3.14. Our hope is that for appropriately chosen step size h_l and parameter $\hat{\epsilon}$, our time-stepping scheme may now proceed in the face of small interpenetrations and the physically actives set at the end of each step should be contained in $\mathcal{E}$.

Therefore, in this case there is no need to stop the simulation if $\hat{\epsilon}$ is appropriately chosen. A good guideline for this choice is $\hat{\epsilon} = v_{\max} h$, where h is of the order of the expected size of the timestep and v_{max} is the expected range of the velocity. Since the definitions of the active sets are different, the results of computing with our definition of the active set and the simulate-detect-restart strategy are different. However, we can formally recover the simulate-detect-restart strategy in our approach by choosing $\gamma = 0$ in (4.14) and (4.15).

Computationally, our approach is more appealing, because we solve only one LCP for fixed time-step h, and this makes it more attractive for interactive simulation. In [4] we showed for the smooth case, that this scheme achieves constraint stabilization and that infeasibility at step l is upper bounded by $O(||h_{l-1}||^2 \left|\left|v^{(l)}\right|\right|^2)$. We will show that constraint stabilization is achieved in the case for our piecewise smooth distance functions.

We have all of our necessary pieces and this leads us to formally define our method by the following algorithm.

Algorithm 6.5. Time-stepping Algorithm for Convex Polyhedra

Algorithm for piecewise smooth multibody dynamics

Step 1: Given $q^{(l)}$. $v^{(l)}$. and h_l, calculate the active set $\mathcal{A}\left(q^{(l)}\right)$ and active events $\mathcal{E}\left(q^{(l)}\right)$.

Step 2: Compute $v^{(l+1)}$. the velocity solution of the mixed LCP (5.3–5.4) by using the quadratic program (5.6) .

Step 3: Compute $q^{(l+1)} = q^{(l)} + h_l v^{(l)}$.

Step 4: IF finished, THEN stop ELSE set $l = l + 1$ and restart.

For the remainder of this section, we consider the time-stepping algorithm defined above applied over a finite time interval [0, T]. Typical assumptions are that the active set $\mathcal{A}(q)$ is defined by (4.10), the time steps $h_l > 0$ satisfy $\sum_{i=0}^{N-1} h_l = T, \quad l = 1, 2, \cdots, N-1$ and $\frac{h_{l-1}}{h_l} = c_h, \quad l = 1, 2, \cdots, N-1$.

We will use the constant mass matrix from Assumption (D3) and define the quantities

$$
\begin{aligned}
z_l &= \left|\left| M^{-\frac{1}{2}} v^{(l)} \right|\right| \\
w_l &= \left|\left| q^{(l)} \right|\right| \\
\hat{w}_l &= \max_{j=0,1,\ldots,l} w_j \\
\hat{z}_l &= \max_{j=0,1,\ldots,l} z_j \\
\hat{h}_l &= \max_{j=0,1,\ldots,l} h_j.
\end{aligned}
\tag{6.16}
$$

Also, recall that we calculate the new position by

$$
q^{(l+1)} = q^{(l)} + h_l v^{(l+1)}. \tag{6.17}
$$

Next, we use an important result.

Lemma 6.6. *If Assumptions (D1) - (D3) hold and for some $l \in \{0, 1, \cdots, N\}$ and we have $q^{(l)} \in \Omega_{\epsilon_o/2}$, that is,*

$$\theta_l = I(q^{(l)}) \leq \frac{\epsilon_o}{2}, \tag{6.18}$$

then there is a non negative continuous function $\psi_1 = \psi_1(z, w)$ such that

$$z_{l+1}^2 \leq z_l^2 + 2h_l \left(c_k \left|\left| M^{-1} \right|\right|^{\frac{1}{2}} z_l + c_k \left|\left| M^{-1} \right|\right| z_l^2 + c_k \left|\left| M^{-\frac{1}{2}} \right|\right| z_l w_l + h_l^2 \psi_1 + c_o \frac{||\theta_l||^2}{h_l^2} \right) \tag{6.19}$$

and

$$w_{l+1} \leq w_l + h_l \left|\left| M^{-\frac{1}{2}} \right|\right| z_l. \tag{6.20}$$

Proof. By Assumption (D1), definition 6.16, and our time stepping process (6.17), we use the Cauchy-Schwarz inequality to see that the condition

$$w_{l+1} \leq w_l + h_l \left|\left| M^{-\frac{1}{2}} \right|\right| z_l$$

is always satisfied.

We obtain an upper bound on the term $v^{(l)^T} k^{(l)}$, based on the assumption (D3). Using the identification (6.16) and the property of the Coriolis force (6.15), we now get

$$\begin{aligned} v^{(l)^T} k^{(l)} &= v^{(l)^T} \left(f_c(v^{(l)}, q^{(l)}) + k_0(v^{(l)}, q^{(l)}, t^{(l)}) + k_1(v^{(l)}) + k_2(q^{(l)}) \right) \\ &= v^{(l)^T} \left(k_0(v^{(l)}, q^{(l)}, t^{(l)}) + k_1(v^{(l)}) + k_2(q^{(l)}) \right) \\ &\leq c_K \left|\left| M^{-1} \right|\right|^{\frac{1}{2}} z_l + c_K \left|\left| M^{-1} \right|\right| z_l^2 + c_K \left|\left| M^{-\frac{1}{2}} \right|\right| z_l w_l. \end{aligned} \tag{6.21}$$

It follows from our assumption (D2), that there exists a constant $c_B > 0$ such that

$$v^{(l)^T} k^{(l)} \leq c_B (z_l + z_l^2 + z_l w_l).$$

Now we use the computation of infeasibility measure of the active set $\mathcal{A}$ and the definitions of Δ and Υ in (5.1)–(5.2) to get

$$I(q^{(l)}) = \frac{h_l}{\gamma} \left|\left| \Delta_-^{(l)}, \Upsilon^{(l)} \right|\right|_\infty.$$

Assume now that for some $l \in \{0, 1, \dots, N\}$ we have that $q^{(l)} \in \Omega_{\frac{\epsilon_0}{2}}$, that is,

$$\theta_l = I(q^{(l)}) \leq \frac{\epsilon_0}{2}. \tag{6.22}$$

Next we need to use Corollary 5.10, which applies because of our assumption (D2) and (6.22) to get our needed inequalities. Furthermore, we use this with (5.21) and the previous inequality, and this implies that

$$z_{l+1}^2 \leq z_l^2 + h_l^2 k^{(l)} M^{(l)-1} k^{(l)} + 2c_B h_l (z_l + z_l^2 + z_l w_l) + c_U \gamma^2 \left(\frac{I(q^{(l)})}{h_l} \right)^2. \tag{6.23}$$

If we define

$$\psi_1 = \psi_1(z, w) = \max_{t \leq T,\, ||v|| \leq z \left|\left| M^{-\frac{1}{2}} \right|\right|, ||q|| \leq w} k(q, v, t)^T M^{-1} k(q, v, t), \tag{6.24}$$

which, by assumption (D3) , must be continuous, and recall that $I(q) = I^{\mathcal{A}(q)}(q)$, we can use Corollary 5.10, Assumption (D2), (6.9), and (6.11) to conclude the proof, since $I(q) = I^{\mathcal{A}(q)}(q)$. ■

Lemma 6.7. *If Assumptions (A1), (D1) - (D3) hold and for some $l \in \{0, 1, \cdots, N\}$, and $q^{(l)} \in \Omega_{\epsilon_o/2}$, and*

$$C_1^d h_l \left|\left| M^{-\frac{1}{2}} \right|\right| z_{l+1} = C_1^d h_l \left|\left| v^{l+1} \right|\right| \leq \frac{1}{2} \min \left\{ \hat{\epsilon}, \frac{\epsilon_o}{2} \right\}, \tag{6.25}$$

then

$$I(q^{(l)} + \tau v^{(l+1)}) \leq \epsilon_o \quad \forall\ \tau \in [0, h_l]. \tag{6.26}$$

Proof. Suppose that $q^{(l)} \in \Omega_{\epsilon_o/2}$, and assume that (6.26) is not true. Then since $I(q^{(l)}) \leq \frac{\epsilon_o}{2}$, we can define

$$t^* = \min_{0 \leq t \leq h_l} \{t \mid I(q^{(l)} + \tau v^{(l+1)}) \leq \epsilon_o \quad \forall\ 0 \leq \tau \leq t\},$$

and conclude that $0 < t^* < h_l$, and, because of the way we measure infeasibility (6.3), we have $I(q^{(l)} + t^* v^{(l+1)}) = \epsilon_o$, so there are exactly two possible cases.

Case 1: Noninterpenetration Infeasibility. We can find exactly where the infeasibility exists. That is, there is some index m such that $\Phi^{(j)}(q^{(l)} + t^* v^{(l+1)}) = -\epsilon_o$. From (6.22) we must have $\delta_{i_1 i_2}(q^{(l)}) \geq -\frac{\epsilon_0}{2}$. Since, from the definition of t^*, we know $I(q^{(l)} + \tau v^{(l+1)}) \leq \epsilon_0$, $\forall \tau, 0 \leq \tau \leq t^*$, the rest follows directly from (6.18), Assumption (A1), and Proposition 6.2.

$$\begin{aligned} \tfrac{\epsilon_o}{2} &\leq \Phi^{(j)}\left(q^{(l)}\right) - \Phi^{(j)}\left(q^{(l)} + t^* v^{(l+1)}\right) \\ &\leq \left|\Phi^{(j)}\left(q^{(l)}\right) - \Phi^{(j)}\left(q^{(l)} + t^* v^{(l+1)}\right)\right| \\ &\leq t^* \left|\left|v^{(l+1)}\right|\right| C_1^d \\ &\leq \tfrac{\epsilon_o}{4}, \end{aligned} \tag{6.27}$$

which cannot be true.

Case 2: Joint Infeasibility. There is some index i such that $\left|\Theta^{(i)} q^{(l)} + t^* v^{(l+1)})\right| = \epsilon_o$. Now, using (6.18), Assumption (A1), and Taylor's Theorem, we get

$$\begin{aligned} \tfrac{\epsilon_o}{2} &\leq \Theta^{(i)}\left(q^{(l)}\right) - \Theta^{(i)}\left(q^{(l)} + t^* v^{(l+1)}\right) \\ &\leq \left|\Theta^{(i)}\left(q^{(l)}\right) - \Theta^{(i)}\left(q^{(l)} + t^* v^{(l+1)}\right)\right| \\ &\leq \left|t^* v^{(l+1)} \nabla \Theta^{(i)}(\xi)\right| \\ &\leq t^* \left|\left|v^{(l+1)}\right|\right| C_1^d \\ &\leq \tfrac{\epsilon_o}{4}, \end{aligned} \tag{6.28}$$

which cannot be true either. Since neither case can occur, then our original assumption is false, so this completes the proof. ■

Lemma 6.8. *If Assumptions (A1), (D1) - (D3) hold and for some $l \in \{0, 1, \cdots, N\}$ we have $q^{(l)} \in \Omega_{\epsilon_o/2}$ and (6.25). Moreover, if*

$$C_1^d h_l \left|\left|v^{(l+1)}\right|\right| \leq \frac{\epsilon_x}{2},$$

then

$$\Phi^{(j)}(q^{(l+1)}) \geq \frac{\hat{\epsilon}}{2} > 0 \quad \forall\ j \notin \mathcal{A}(q^{(l)}). \tag{6.29}$$

Proof. For any $j \notin \mathcal{A}(q^{(l)})$, we get, from the definition of the Active Set (4.10), that $\Phi^{(j)}(q^{(l)}) \geq \hat{\epsilon}$. It now follows from Assumption (A1) and Proposition 6.2 that

$$\begin{aligned} \Phi^{(j)}(q^{(l+1)}) &= \Phi^{(j)}(q^{(l)} + h_l v^{(l+1)}) \\ &\geq \Phi^{(j)}\left(q^{(l)}\right) - h_l \left|\left|v^{(l+1)}\right|\right| C_1^d, \end{aligned} \tag{6.30}$$

from which the result follows. ■

This Lemma shows us that if the distance function corresponding to two bodies is not on the active list, then after taking a step with our algorithm, the two bodies cannot be infeasible, because there cannot be any interpenetration between them. Next, we show that after taking a step under suitable conditions, any infeasibility that may exist remains suitably bounded. This is accomplished by considering all possible instances from which the infeasibility might occur.

Lemma 6.9. *If Assumptions (A1), (D1) - (D3) hold and for some* $l \in \{0, 1, \cdots, N\}$ *we have* $q^{(l)} \in \Omega_{\epsilon_o/2}$ *and (6.25). Moreover, if*

$$C_1^d h_l \left|\left|v^{(l+1)}\right|\right| \leq \frac{\hat{\epsilon}}{2},$$

then

$$\theta_{l+1} = I\left(q^{(l+1)}\right) \leq \frac{1}{2} C_c^d h_l^2 \left|\left|M^{-1}\right|\right| z_{l+1}^2. \tag{6.31}$$

Proof. We will use the fact that $v^{(l+1)}$ is a solution of the quadratic program (5.6). We need to consider four different cases.

Case 1: $I(q^{(l+1)}) = -\left|\Theta^{(i)}(q^{(l+1)})\right|$, for some index i, $1 \leq i \leq n_J$. Here, the infeasibility comes from one of the joint constraints. We find that

$$\begin{aligned} \left|\Theta^{(i)}\left(q^{(l+1)}\right)\right| &= \left|\Theta^{(i)}\left(q^{(l)} + h_l v^{(l+1)}\right)\right| \\ &\leq \left|\Theta^{(i)}\left(q^{(l)}\right) + h_l \nabla_q \Theta^{(i)}\left(q^{(l)}\right)^T v^{(l+1)}\right| + \tfrac{1}{2} h_l^2 C_2^d \left|\left|v^{(l+1)}\right|\right|^2 \\ &= \left|\Theta^{(i)}\left(q^{(l)}\right) + h_l \nu^{(j)^T} v^{(l+1)}\right| + \tfrac{1}{2} h_l^2 C_2^d \left|\left|v^{(l+1)}\right|\right|^2 \\ &= \left|\Theta^{(i)}\left(q^{(l)}\right) - h_l \Upsilon^{(i)}\right| + \tfrac{1}{2} h_l^2 C_2^d \left|\left|v^{(l+1)}\right|\right|^2 \\ &= \tfrac{1}{2} h_l^2 C_2^d \left|\left|v^{(l+1)}\right|\right|^2 \end{aligned} \tag{6.32}$$

and hence the result follows.

Case 2: $I(q^{(l+1)}) = \Phi_-^{(j)}(q^{(l+1)}) = -\Phi^{(j)}(q^{(l+1)}) > 0$ for some index $j \notin \mathcal{A}(q^{(l)})$. Here the infeasibility comes from two bodies which were not initially active. Note that since $j \notin \mathcal{A}(q^{(l)})$, this contradicts Lemma 6.8. Therefore, this case cannot happen.

Case 3: $I(q^{(l+1)}) = \Phi_-^{(j)}(q^{(l+1)}) = -\Phi^{(j)}(q^{(l+1)}) > 0$ for some $j \in \mathcal{A}(q^{(l)})$ and every event m that is optimal at some point in the segment $[q^{(l)}, q^{(l)} + h_l v^{(l+1)}]$ is in $\mathcal{E}(q^{(l)})$. This describes the situation when the infeasibility occurs from progressing to the $(l+1)^{st}$ step with all of the events that become active are included.

A theorem from Lebourg,[17] states there is some ξ on the line segment joining $q^{(l)}$ and $q^{(l+1)}$ such that

$$\Phi^{(j)}(q^{(l+1)}) - \Phi^{(j)}(q^{(l)}) = \partial\Phi^{(j)}(\xi)(q^{(l+1)} - q^{(l)}).$$

For some $\tau \geq 0$, we can write

$$\xi \;=\; q^{(l)} + \tau(q^{(l+1)} - q^{(l)}). \tag{6.33}$$

Moreover, by Lemma 6.3 the generalized gradient at ξ is contained in the convex cover of

$$\left\{\nabla\hat{\Phi}^{m_1}(\xi), \nabla\hat{\Phi}^{m_2}(\xi), \ldots, \nabla\hat{\Phi}^{m_k}(\xi)\right\}$$

where $\{m_1, m_2, \ldots, m_k\}$ are the active events at q. We may then write

$$\partial\Phi^{(j)}(\xi) \in \sum_{j=1}^{k} \lambda_j \nabla\hat{\Phi}^{m_j}(\xi)$$

where $\lambda_j \geq 0$ for $1 \leq j \leq k$ and $\sum_{j=1}^{k} \lambda_j = 1$. Using the differentiability of component functions, we get

$$\begin{aligned} \nabla\hat{\Phi}^{m^T}(\xi)w &= \nabla\hat{\Phi}^{m^T}(q^{(l)} + \tau(q^{(l+1)} - q^{(l)}))w \\ &\leq \nabla\hat{\Phi}^{m^T}(q^{(l)})w + \tau C_2^d \left|\left|q^{(l+1)} - q^{(l)}\right|\right| ||w|| \\ &\leq \nabla\hat{\Phi}^{m^T}(q^{(l)})w + C_2^d \left|\left|q^{(l+1)} - q^{(l)}\right|\right| ||w|| \end{aligned} \tag{6.34}$$

for any vector w.

Now from Lebourg's Mean Value Theorem [17], we know there is some ξ between $q^{(l)}$ and $q^{(l+1)}$, and $\Gamma \in \partial\Phi^{(j)}$ such that

$$\Phi^{(j)}(q^{(l+1)}) = \Phi^{(j)}(q^{(l)}) - \Gamma^T(\xi)(q^{(l+1)} - q^{(l)}).$$

Combining these results and using our assumption that $m_\nu \in \mathcal{E}(q^{(l)})$ and the fact that $\Phi^{(j)}(q^{(l)}) + h_l n^{m_\nu T} v^{(l+1)} \geq 0$ because of our linearization (4.15), we can write

$$\begin{aligned}
I(q^{(l+1)}) &= -\Phi^{(j)}(q^{(l+1)}) \\
&= -\Phi^{(j)}(q^{(l)}) - \Gamma^T(\xi)(q^{(l+1)} - q^{(l)}) \\
&= -\Phi^{(j)}(q^{(l)}) - \sum_{\nu=1}^{k} \lambda_\nu \nabla \hat{\Phi}^{m_\nu T}(\xi)(q^{(l+1)} - q^{(l)}) \\
&= -\sum_{\nu=1}^{k} \lambda_\nu \left(\Phi^{(j)}(q^{(l)}) + \nabla \hat{\Phi}^{m_\nu T}(\xi) h_l v^{(l+1)} \right) \\
&\leq -\sum_{\nu=1}^{k} \lambda_\nu \left(\Phi^{(j)}(q^{(l)}) + h_l \nabla \hat{\Phi}^{m_\nu T}(q^{(l)}) v^{(l+1)} - C_2^d \left|\left| h_l v^{(l+1)} \right|\right|^2 \right) \\
&= -\sum_{\nu=1}^{k} \lambda_\nu \left(\Phi^{(j)}(q^{(l)}) + h_l \nabla \hat{\Phi}^{m_\nu T}(q^{(l)}) v^{(l+1)} \right) + C_2^d \left|\left| h_l v^{(l+1)} \right|\right|^2 \\
&= -\sum_{\nu=1}^{k} \lambda_\nu \left(\Phi^{(j)}(q^{(l)}) + h_l n^{m_\nu T} v^{(l+1)} \right) + C_2^d \left|\left| h_l v^{(l+1)} \right|\right|^2 \\
&\leq C_2^d \left|\left| h_l v^{(l+1)} \right|\right|^2,
\end{aligned} \tag{6.35}$$

which is what we wanted to show.

Case 4: $I(q^{(l+1)}) = \Phi_-^{(j)}(q^{(l+1)}) = -\Phi^{(j)}(q^{(l+1)}) > 0$ for some index $j \in \mathcal{A}(q^{(l)})$ and $\exists m \notin \mathcal{E}(q^{(l)})$ but $\Phi^{(j)}(\hat{q}) = \widehat{\Phi}^{(m)}(\hat{q})$ at $\hat{q} = q^{(l)} + \tau v^{(l+1)}$. In this case, the infeasibility is caused by some event which was not itself initially active, but became active in motion from $q^{(l)}$ to $q^{(l+1)}$. Notice that we obviously have that $\boxed{m \in \mathcal{E}_1(q^{(l)})}$, since the bodies were initially active at the position $q^{(l)}$.

Without loss of any generality whatsoever, our analysis may assume that the first time that event m became active is at the $q^{(l)} + h_l v^{(l+1)}$. So we first note that if k were the active index for contact j at the l^{th} step, then from Theorem (3.13) we have

$$\widehat{\Phi}^{(m)}(q^{(l)}) \leq \widehat{\Phi}^{(k)}(q^{(l)}).$$

Using the Mean Value Theorem and our bounds on the first derivatives, we once again invoke Proposition 6.2 and also get

$$\begin{aligned}
\widehat{\Phi}^{(m)}(q^{(l)}) - \widehat{\Phi}^{(k)}(q^{(l)}) &= \left(\widehat{\Phi}^{(m)}(q^{(l)}) - \widehat{\Phi}^{(m)}(q^{(l+1)})\right) + \left(\widehat{\Phi}^{(m)}(q^{(l+1)}) - \widehat{\Phi}^{(k)}(q^{(l)})\right) \\
&\leq \left|\widehat{\Phi}^{(m)}(q^{(l)}) - \widehat{\Phi}^{(m)}(q^{(l+1)})\right| + \left|\Phi^{(j)}(q^{(l+1)}) - \Phi^{(j)}(q^{(l)})\right| \\
&= \left|\widehat{\Phi}^{(m)}(q^{(l)}) - \widehat{\Phi}^{(m)}(q^{(l)} + h_l v^{(l+1)})\right| \\
&\qquad + \left|\Phi^{(j)}(q^{(l)} + h_l v^{(l+1)}) - \Phi^{(j)}(q^{(l)})\right| \\
&\leq h_l \left|\left|v^{(l+1)}\right|\right| C_1 + h_l \left|\left|v^{(l+1)}\right|\right| C_1 \\
&= 2h_l \left|\left|v^{(l+1)}\right|\right| C_1 \\
&\leq \epsilon_x,
\end{aligned} \tag{6.36}$$

which shows that $\boxed{m \in \mathcal{E}_2(q^{(l)})}$.

Similar to previous analysis, we consider the restriction to the event E of index m. At each step l we get, as we did in equation (3.4), the system of equations

$$\begin{aligned}
\hat{A}_{L_1} {R_1^{(l)}}^T x - b_{L_1} t &= \hat{A}_{L_1} {R_1^{(l)}}^T x_1^{(l)} \\
\hat{A}_{L_2} {R_2^{(l)}}^T x - b_{L_2} t &= \hat{A}_{L_2} {R_2^{(l)}}^T x_2^{(l)}
\end{aligned}, \tag{6.37}$$

where the sum of the numbers of rows of $\hat{A}_{L_1}$ and $\hat{A}_{L_2}$ is n+1. We are assuming that at step $l+1$, we are at the optimal event, so that the equation

$$\begin{aligned}
\hat{A}_{L_1} {R_1^{(l+1)}}^T x - b_{L_1} t &= \hat{A}_{L_1} {R_1^{(l+1)}}^T x_1^{(l+1)} \\
\hat{A}_{L_2} {R_2^{(l+1)}}^T x - b_{L_2} t &= \hat{A}_{L_2} {R_2^{(l+1)}}^T x_2^{(l+1)}
\end{aligned} \tag{6.38}$$

has a unique solution, which we will call $(\tilde{x}^{(l+1)}, \tilde{t}^{(l+1)})$. Note that $\tilde{t}^{(l+1)}$ is used to compute the value of $\widehat{\Phi}^{(m)}(q^{(l+1)})$. If we rewrite the system (6.38) in matrix form, we get

$$\begin{bmatrix} \hat{A}_{L_1} {R_1^{(l+1)}}^T & -b_{L_1} \\ \hat{A}_{L_2} {R_2^{(l+1)}}^T & -b_{L_2} \end{bmatrix} \begin{bmatrix} x \\ t \end{bmatrix} = \begin{bmatrix} \hat{A}_{L_1} {R_1^{(l+1)}}^T x_1^{(l+1)} \\ \hat{A}_{L_2} {R_2^{(l+1)}}^T x_2^{(l+1)} \end{bmatrix}. \tag{6.39}$$

Suppose that we can produce ${R_1^{(l)}}^T$, ${R_2^{(l)}}^T$, $x_1^{(l)}$, and $x_2^{(l)}$ from respective small perturbations of ${R_1^{(l+1)}}^T$, ${R_2^{(l+1)}}^T$, $x_1^{(l+1)}$, and $x_2^{(l+1)}$. Then we could guarantee a unique solution to the system

$$\begin{bmatrix} \hat{A}_{L_1} {R_1^{(l)}}^T & -b_{L_1} \\ \hat{A}_{L_2} {R_2^{(l)}}^T & -b_{L_2} \end{bmatrix} \begin{bmatrix} x \\ t \end{bmatrix} = \begin{bmatrix} \hat{A}_{L_1} {R_1^{(l)}}^T x_1^{(l)} \\ \hat{A}_{L_2} {R_2^{(l)}}^T x_2^{(l)} \end{bmatrix}. \tag{6.40}$$

In fact, we know that the polyhedral positions and rotation matrices are all directly calculated from the step computation

$$q^{(l+1)} = q^{(l)} + h_l v^{(l+1)}.$$

Let $(\tilde{x}^{(l+1)}, \tilde{t}^{(l+1)})$ be the solution of the system (6.40). We easily see that if $h_l v^{(l)}$ is small enough, then we use differentiability of the systems (6.39) and 6.40 with perturbation analysis to find a bound C_M such that

$$\left|\left|\tilde{x}^{(l)} - \tilde{x}^{(l+1)}\right|\right| \leq C_M \left|\left|h_l v^{(l+1)}\right|\right|.$$

Next, let us define the three quantities

$$\begin{aligned} \bar{\delta} &= \tilde{x}^{(l)} - \tilde{x}^{(l+1)} \\ \bar{\bar{\delta}}_i &= x_i^{(l+1)} - x_i^{(l)} \\ \bar{\bar{\Delta}}_i &= R_i^{(l+1)} - R_i^{(l)}. \end{aligned} \tag{6.41}$$

Let C_R be the constant satisfied by the rotation matrices. If we use the constant C_M from the perturbation analysis, we can obtain the bounds

$$\begin{aligned} \left|\left|\bar{\delta}\right|\right| &\leq C_M \left|\left|h_l v^{(l+1)}\right|\right| \\ \left|\left|\bar{\bar{\delta}}_i\right|\right| &\leq \left|\left|h_l v^{(l+1)}\right|\right| \\ \left|\left|\bar{\bar{\Delta}}_i\right|\right| &\leq C_R \left|\left|h_l v^{(l+1)}\right|\right|. \end{aligned} \tag{6.42}$$

Finally we define

$$\xi_i = \hat{A}_{L_i} {R_i^{(l)}}^T (\bar{\delta} + \bar{\bar{\delta}}_i) + \hat{A}_{L_i} \bar{\bar{\Delta}}_i (\tilde{x}^{(l+1)} - x_i^{(l+1)}),$$

and d_i to be the radius of polyhedron i. Then

$$\begin{aligned} ||\xi_i|| &= \left|\left|\hat{A}_{L_i} {R_i^{(l)}}^T (\bar{\delta} + \bar{\bar{\delta}}_i) + \hat{A}_{L_i} \bar{\bar{\Delta}}_i (\tilde{x}^{(l+1)} - x_i^{(l+1)})\right|\right| \\ &\leq \left|\left|\hat{A}_{L_i}\right|\right| \left(||\bar{\delta}|| + \left|\left|\bar{\bar{\delta}}_i\right|\right| + d_i \left|\left|\bar{\bar{\Delta}}_i\right|\right|\right) \\ &\leq (1 + C_M + d_i C_R) \left|\left|\hat{A}_{L_i}\right|\right| \left|\left|h_l v^{(l+1)}\right|\right|. \end{aligned} \tag{6.43}$$

If we now choose a small enough stepsize such that

$$(1 + C_M + d_i C_R) \left|\left|\hat{A}_{L_i}\right|\right| \left|\left|h_l v^{(l+1)}\right|\right| \leq \hat{\epsilon}_x$$

then obviously $||\xi_i|| \leq \hat{\epsilon}_x$, but in addition, we now have

$$\begin{aligned}
\hat{A}_{L_i} R_i^{(l)^T}(\tilde{x}^{(l)} - x_i^{(l)}) &= \hat{A}_{L_i} R_i^{(l)^T}\left((\tilde{x}^{(l)} - \tilde{x}^{(l+1)}) + (\tilde{x}^{(l+1)} - x_i^{(l+1)}) + (x_i^{(l+1)} - x_i^{(l)})\right) \\
&= \hat{A}_{L_i} R_i^{(l)^T}\left(\bar{\delta} + (\tilde{x}^{(l+1)} - x_i^{(l+1)}) + \bar{\bar{\delta}}_i\right) \\
&= \hat{A}_{L_i} R_i^{(l)^T}(\bar{\delta} + \bar{\bar{\delta}}_i) + \hat{A}_{L_i} R_i^{(l)^T}(\tilde{x}^{(l+1)} - x_i^{(l+1)}) \\
&= \hat{A}_{L_i} R_i^{(l)^T}(\bar{\delta} + \bar{\bar{\delta}}_i) + \hat{A}_{L_i}\left(R_i^{(l+1)^T} + \bar{\bar{\Delta}}_i\right)(\tilde{x}^{(l+1)} - x_i^{(l+1)}) \\
&= \hat{A}_{L_i} R_i^{(l)^T}(\bar{\delta} + \bar{\bar{\delta}}_i) + \hat{A}_{L_i}\bar{\bar{\Delta}}_i(\tilde{x}^{(l+1)} - x_i^{(l+1)}) \\
&\qquad + \hat{A}_{L_i} R_i^{(l+1)^T}(\tilde{x}^{(l+1)} - x_i^{(l+1)}) \\
&\leq \hat{A}_{L_i} R_i^{(l)^T}(\bar{\delta} + \bar{\bar{\delta}}_i) + \hat{A}_{L_i}\bar{\bar{\Delta}}_i(\tilde{x}^{(l+1)} - x_i^{(l+1)}) + b_{L_i} \\
&\leq \xi_i + b_{L_i}
\end{aligned} \tag{6.44}$$

which show that

$$\tilde{x}^{(l)} \in CP(A_{L_i} R_i^T, b_{L_i} + A_{L_i} R_i^T x_i, x_i) + \hat{\epsilon}_x.$$

This is true for $i = 1, 2$. Hence we have shown that $\boxed{m \in \mathcal{E}_3 \bigcap \mathcal{E}_4}$.

Notice that we have shown that $m \in \mathcal{E}_1 \bigcap \mathcal{E}_2 \bigcap \mathcal{E}_3 \bigcap \mathcal{E}_4 = \mathcal{E}$, which is a contradiction. Therefore, this case can never happen. Now we have completely exhausted all possible cases, and we have thus completed the proof. ■

As we rapidly approach the finale, let us now state a Lemma and a Theorem from Anitescu and Hart which can be found in [5], where their proof is also given. They are crucial for us to obtain our ultimate result.

Lemma 6.10. *Consider the nonnegative sequences t_n and z_n, for $0 \leq n \leq N$ and h_n for $0 \leq n \leq N-1$, where $t_0 = 0$ and $t_N = T$. Here h_n satisfies $t_{n+1} - t_n = h_n$, for $0 \leq n \leq N-1$, and z_n satisfies the inequality*

$$z_{n+1}^2 \leq z_n^2 + h_n c_1(5z_n^2 + 2z_n) + c_2 h_n, \forall 0 \leq n \leq N-1,$$

where $c_1 > 0$ and $c_2 > 0$ are two real parameters. Let $y(t, y_0)$ be the solution of the scalar differential equation

$$\dot{y} = 6c_1 y + (c_1 + c_2)$$

that satisfies $y(0, y_0) = y_0$. Then,

1. $y(t)$ *satisfies*
   a. $y(t, x_1) \geq y(t, x_2)$ *whenever* $x_1 \geq x_2$,
   b. $z_{n+1}^2 \leq y(h_n, z_n^2)$.
2. $z_n^2 \leq y(t_n, z_0^2)$, *for* $0 \leq n \leq N$.

Theorem 6.11. *Consider the nonnegative sequences* t_n, z_n, w_n *and* θ_n *for* $0 \leq n \leq N$ *and* h_n *for* $0 \leq n \leq N-1$, *where* $\theta_0 = 0$, $t_0 = 0$ *and* $t_N = T$. *Here* $h_n > 0$ *satisfies* $t_{n+1} - t_n = h_n$, *for* $0 \leq n \leq N-1$. *Let* $c_i > 0$, $i = 1, 2, \ldots, 5$, *and* $\psi_1(z, w)$ *a continuous mapping of two real arguments that is nonnegative whenever* $z \geq 0$ *and* $w \geq 0$.

Assume the following:

Condition 1: *Whenever*

$$\theta_n \leq c_5, \tag{6.45}$$

for some n *satisfying* $0 \leq n \leq N-1$, *the following inequalities hold:*

$$z_{n+1}^2 \leq z_n^2 + h_n c_1 (z_n^2 + w_n z_n + w_n^2 + w_n + z_n) + \frac{c_2}{2} h_n + h_n^2 \psi_1 + c_4 \frac{\theta_n^2}{h_n^2} \tag{6.46}$$

$$w_{n+1} \leq w_n + c_1 h_n z_{n+1}, \tag{6.47}$$

where $\psi_1 = \psi_1(z_n, w_n)$.

Condition 2: *If, in addition,*

$$c_1 h_n z_{n+1} \leq c_5, \tag{6.48}$$

then the following inequality also holds for $0 \leq n \leq N-1$*:*

$$\theta_{n+1} \leq c_3 h_n^2 z_{n+1}^2. \tag{6.49}$$

Condition 3: *The time steps* h_n, $n = 1, 2, \ldots, N-1$ *are chosen such that*

$$\frac{h_{n-1}}{h_n} \leq c_h, \tag{6.50}$$

where $c_h > 0$ *is a fixed parameter.*

Then there exists an $H > 0$ *such that, whenever* $h_n < H$, $\forall 0 \leq n \leq N-1$, *we have that (6.45), (6.48) and thus (6.46), (6.47) and (6.49) hold for any* $0 \leq n \leq N-1$ *and that* $z_n^2 \leq y(t_n, \max\{z_0, w_0\}^2)$ *and* $w_n^2 \leq y(t_n, \max\{z_0, w_0\}^2)$, $\forall n, 0 < n < N$. *Here* $y(t, y_0)$ *is the function defined in Lemma 6.10.*

Now we have carefully constructed all of the preliminaries items we need for our major result. We have meticulously assembled all of the necessary parts to use Theorem 6.11. Thus, we can now state our main results on the constraint stability of our algorithm which can be summarized in the next theorem which is a direct consequence of Theorem 6.11. The crux of its proof immediately follows from fact that the Assumption 1 of Theorem 6.11 is satisfied because of Lemma 6.6. Assumption 2 is satisfied because of Lemma 6.9.

Theorem 6.12. *Consider the time-stepping algorithm defined above and applied over a finite time interval [0, T]. Assume that*

- *The active set $\mathcal{A}(q)$ is defined by (4.10).*
- *The active events $\mathcal{E}(q)$ are defined by (4.9).*
- *The time steps $h_l > 0$ satisfy*
  $\sum_{l=0}^{N-1} h_l = T, \quad l = 1, 2, \cdots, N-1,$
  $\frac{h_{l-1}}{h_l} = c_h, \quad l = 1, 2, \cdots, N-1 \ .$
- *The system satisfies Assumtions (A1) and (D1) - (D3) .*
- *The system is initially feasible. That is, $I(q^{(0)}) = 0$.*

Then, there exist $H > 0$, $V > 0$, and $C_c > 0$ such that

1. $\left|\left|v^{(l)}\right|\right| \leq V \ \forall l, 1 \leq l \leq N$ *and*
2. $I\left(q(l)\right) \leq C_c \left|\left|v^{(l)}\right|\right|^2 h_{l-1}^2, \forall l, 1 \leq l \leq N.$

Proof. Define $t_0 = 0$ and $t_{n+1} = t_n + h_n$ for $0 \leq n \leq N-1$, and let z_n, w_n, $\hat{w}_n$, $\hat{z}_n$, and $\hat{h}_n$ be the quantities that we defined in (6.16), and define $\theta_n = I(q^{(n)})$. Then we have nonnegative sequences t_n, z_n, w_n and θ_n for $0 \leq n \leq N$ and h_n for $0 \leq n \leq N-1$, where $t_0 = 0$ and $t_N = T$, and $\theta_0 = 0$ because the system is initially feasible. Notice that $h_n > 0$ satisfies $t_{n+1} - t_n = h_n$, for $0 \leq n \leq N-1$.

Notice that Lemma (6.6) is precisely a statement that Condition 1 is satisfied. Likewise, Condition 2 is satisfies immediately from the application of Lemma 6.9. Finally, Condition 3 is satisfied from our original assumption. Therefore, it follows that Theorem (6.11) applies.

From Theorem (6.11), there exist $H > 0$ and $Z > 0$ such that, whenever we have that $h_l \leq H$, $\forall l$ such that $0 \leq l \leq N$, we can get $||z_l|| \leq Z$, $\forall l$ such that $0 \leq l \leq N$.

We see that the first part of the conclusion of our theorem is true, once we use (6.16), and define $V = \left|\left|M^{-\frac{1}{2}}\right|\right| Z$ to get $||v_l|| \leq V$, $\forall l$ such that $0 \leq l \leq N$.

In addition to the second part of Theorem 6.11 we use Lemma (6.9). This means that the second part of the conclusion of our theorem follows after we use $z_{l+1} \leq \left|\left|M^{\frac{1}{2}}\right|\right| \left|\left|v^{(l+1)}\right|\right|$, which follows from (6.16) and from choosing $C_c = \frac{1}{2} C_2^d \, ||M^{-1}|| \, ||M||$ in (6.31). ■

The algorithm we propose here achieves constraint stabilization and, in particular, the second conclusion of Theorem (6.12) actually quantifies the constraint stabilization property. This means that the discretization error from our integration process cannot overwhelm the solution. In the unstabilized schemes, the integration process may cause constraint drift, where the computed solution fails to satisfy necessary geometrical constraints.

Notice that the velocity remains bounded. That is, as we proceed with our simulation for a fixed time interval, and under some general suitable conditions on the external force (6.13), the velocity will not become infinite.

We do not need to change the step size to control the infeasibility. In fact we only need to solve one linear complementarity problem per step. This is a tremendous computational advantage, and means that in some sense, we can predict the maximum amount of computation needed.

This method, although developed to handle convex polyhedra, can easily be extended to other possibilities. For example, it is certainly possible to consider cases when the signed distance function is defined piecewise (for whatever reason) and has component functions that are, in fact, differentiable.

7.0 NUMERICAL RESULTS

We have previously shown that the solution set of the LCP subproblem may be nonconvex for arbitrarily small friction [4]. However, even in this case, we can find two iterative methods that converge linearly with a fixed convergence rate to a solution point, at least for small values of the friction coefficient [6], while solving only convex subproblems that can be solved in polynomial time, with no need to backtrack for collisions. The result is especially intriguing since problems with nonconvex solution sets rarely have polynomial time solutions.

We have also shown that our method can be applied to interesting phenomena, such as size-based segregation,. One example of size-based segregation is the Brazil Nut example where 270 bodies were simulated, including a few larger sized bodies. The large ball emerges after about 40 shakes, and this means that out results were in the same order of magnitude as typical penalty method simulations, but with 4 orders of magnitude larger time step while essentially capturing the same dynamics [28]. Figure 16 shows four frames of the Brazil Nut example.

We have also previously defined a method that achieves constraint stabilization while solving only linear complementarity problem per step [5]. Since our method does not need to stop and detect collisions explicitly, it can advance with a constant time step and predictable amount of effort per step. We proved that the velocity stays bounded and that the constraint infeasibility is uniformly bounded in terms of the size of the time step and the current value of the velocity.

In [7] we extended our method to a version with an adjustable parameter γ, and the constraint stabilization effect was shown to hold for any $\gamma \in (0, 1]$. An application of this method was used in a robotic grasp simulator [37]. In Figure 17, we see two frames of a robot simulation consisting of a glass that is within the reach of a Bartlett hand that starts

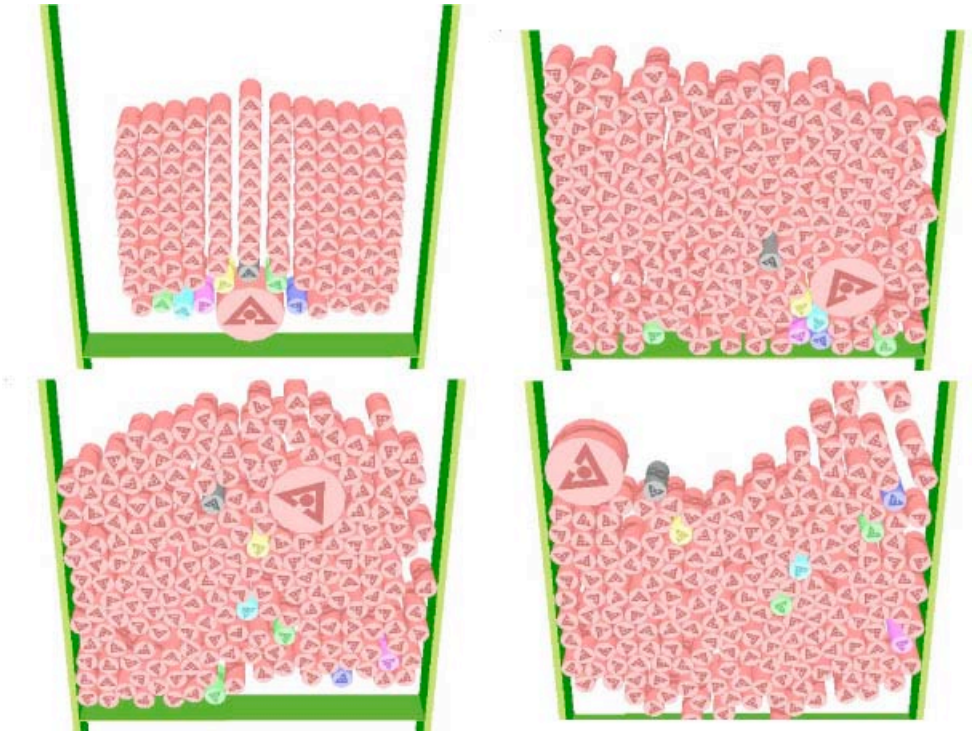

Figure 16: Four frames from the Brazil Nut example

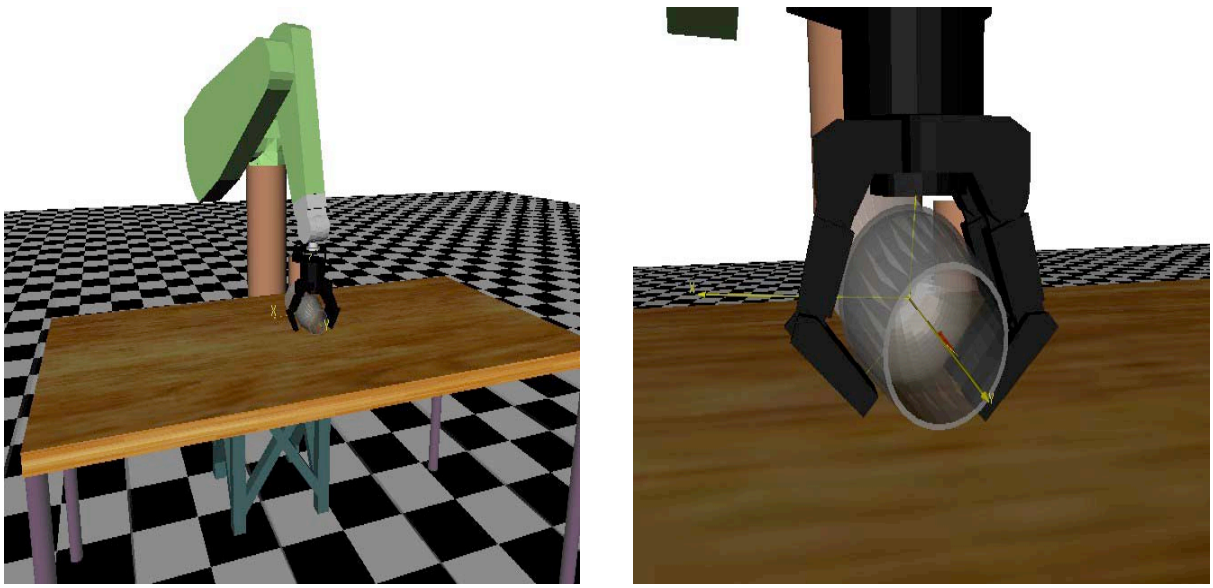

Figure 17: Two frames of a robot simulation

to close.

Finally, we show four examples of the successful implementation of our method, which was adjusted to take advantage of convex polyhedral bodies. These problems all use the Ratio Metric Penetration Depth to calculate the distance between bodies and the depth of penetration, when it exist.

We successfully implement our algorithm for numerous examples, and in all simulations, we define the following parameters:

h is the constant stepsize,

μ is the Coulomb friction coefficient,

γ is the constraint stabilization parameter.

ϵ_x is an event detection parameter,

ϵ_t is an event detection parameter,

ϵ_0 is an event detection parameter, and

δ_{max} is the maximum allowable determinant.

The parameters h, μ, γ, ϵ_x, and ϵ_t have been previously defined. However, especially in the case of checking the EoE events, we need to determine whether the matrices were singular, so if the determinant of the system exceeds δ_{max}, we conclude that the system is singular. Also, the theoretical condition $t^* \leq t \leq t^* + \epsilon_t$ is replaced by the computational condition $t^* - \epsilon_0 \leq t \leq t^* + \epsilon_t$.

Since it is impossible to compare the actual value of the maximum infeasibility for different timesteps, we instead use the average infeasibility, which is a fair comparison. The simulations were all produced from implementation of our algorithm into several MatLab routines. The numerical calculations were performed on either an Apple PowerBook running a 1.67 GHz PowerPC G4 processor with 2 GB of RAM running Mac OS X 10.4.8 or an Apple PowerMac G5 running a 1.6 GHz G5 processor with 512 MB or RAM running Mac OS X 10.4.8 and all calculations were performed by MatLab 10.0 R14 for Mac OS X.

7.1 PROBLEM: BALANCE2

This problem is two dimensional and has six bodies: two triangles, three squares, and one rectangle. With two squares and a triangle place on the rectangle and delicately balanced on the other triangle, a square is dropped at one end, disturbing the initial balance of the system.

We ran the simulation for 12 seconds with the parameters:

h	μ	γ	ϵ_x	ϵ_t	ϵ_0	δ_{max}
0.01	0.1	1.0	0.01	0.1	0.0001	1000000

In Figure 18, we show six successive frames from the simulation. They represent the situation for the values of time 0, 2, 3, 5, 6, and 12 seconds, respectively.

We demonstrate the effect of the constraint stabilization parameter γ, by running the problem for a series of values of $\gamma \in \{0, 0.25, 0.5, 0.75, 1\}$ and $h \in \{0.1, 0.05, 0.02, 0.01\}$. The results are shown in Figure 19, where we clearly see that when the stepsizes are larger, then infeasibility grows.

In Figure 20 we fixed $\gamma = 1$ and showed that, as $h \in \{0.1, 0.02, 0.01, 0.002, 0.001\}$ that, in the limit as the stepsize approaches zero, the behavior of the infeasibility is proportional to the square of the stepsize, which validates Theorem 6.12.

7.2 PROBLEM: PYRAMID1

Despite it name, this problem is two dimensional and involves a single triangle with nine rectangular bodies arranged in a row. The triangle makes contact with one rectangle, which causes a chain reaction similar to dominoes falling.

We ran the simulation for 10 seconds with the parameters:

h	μ	γ	ϵ_x	ϵ_t	ϵ_0	δ_{max}
0.01	0.2	1.0	0.01	0.1	0.0001	1000000

At the end of the simulation, the bodies were all at rest.

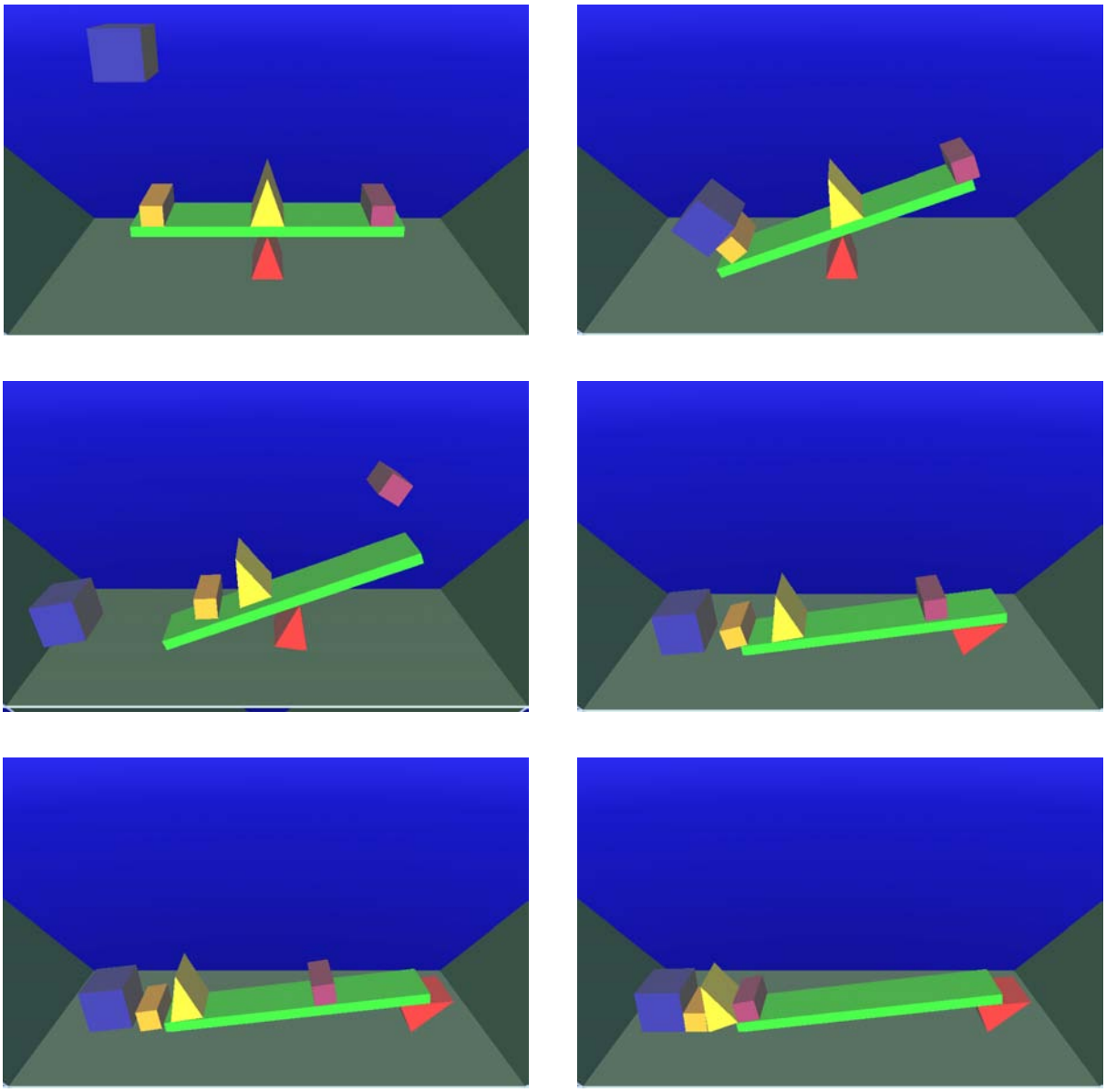

Figure 18: Six successive frames from Balance2

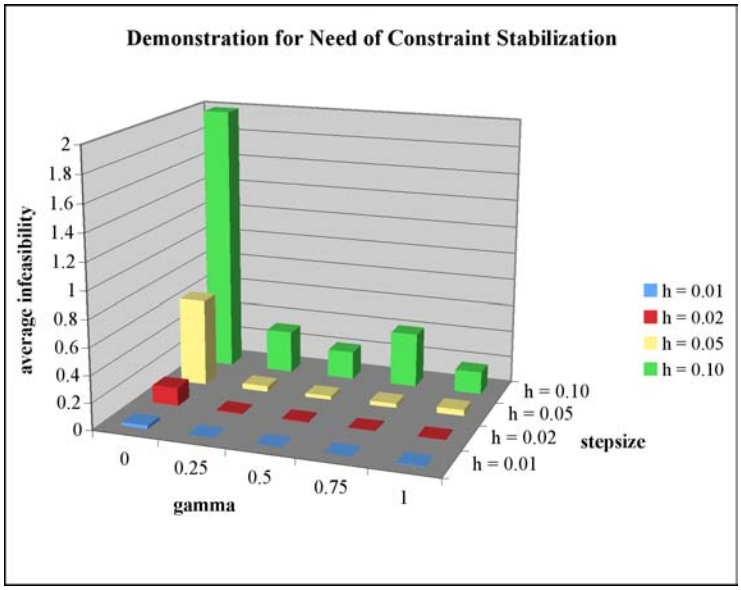

Figure 19: Problem Balance2: Effect of Constraint Stabilization Constant γ on Infeasibility

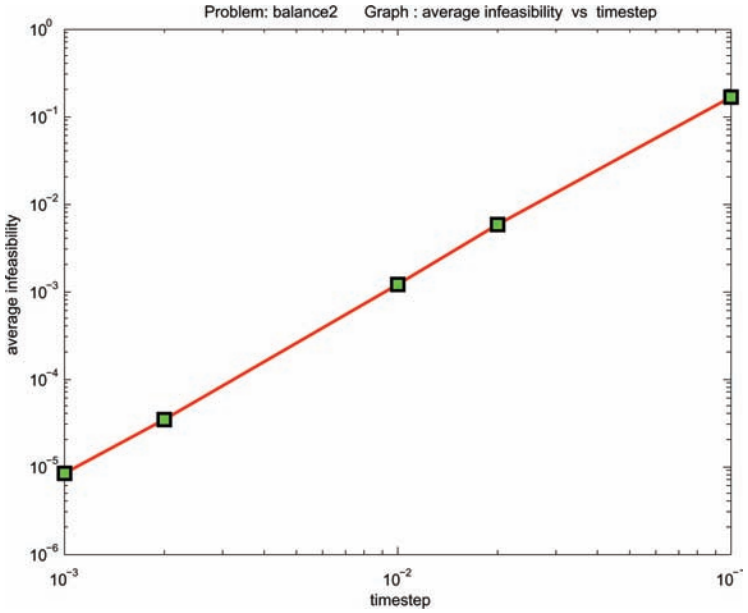

Figure 20: Problem Balance2: Infeasibility

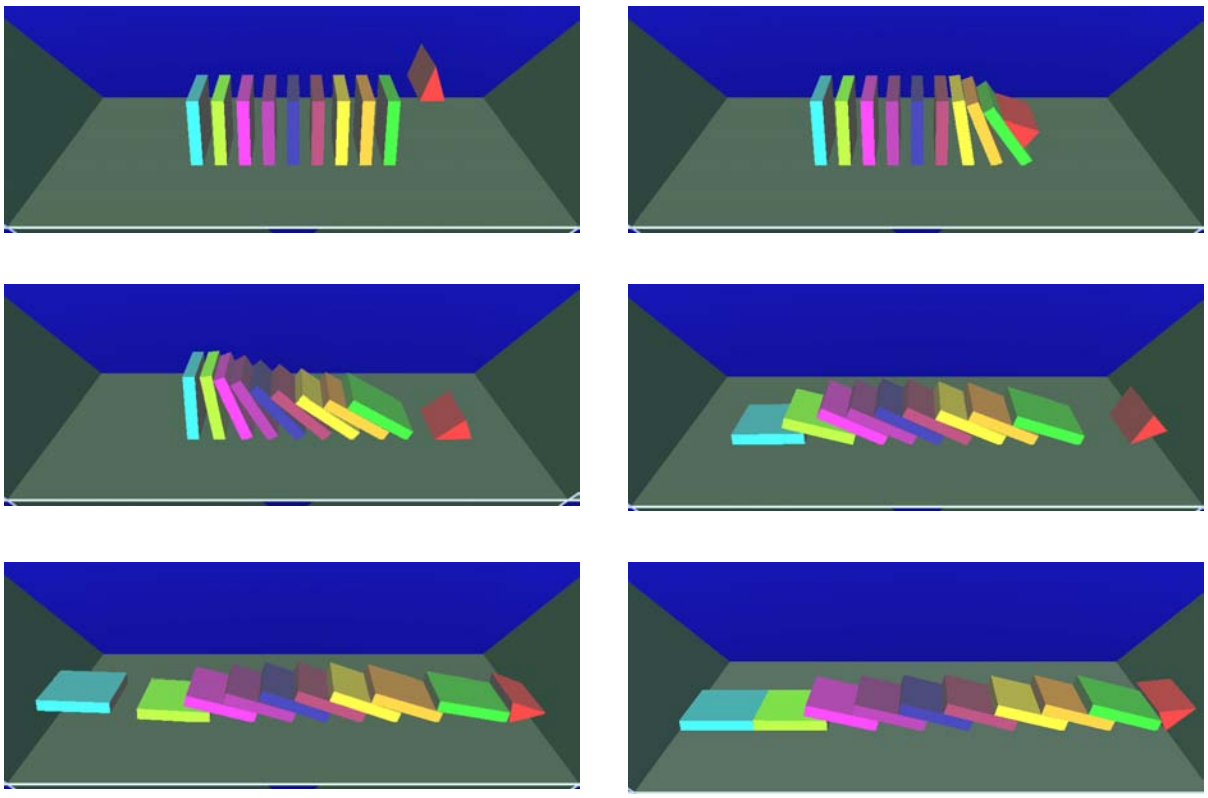

Figure 21: Six successive frames from Pyramid1

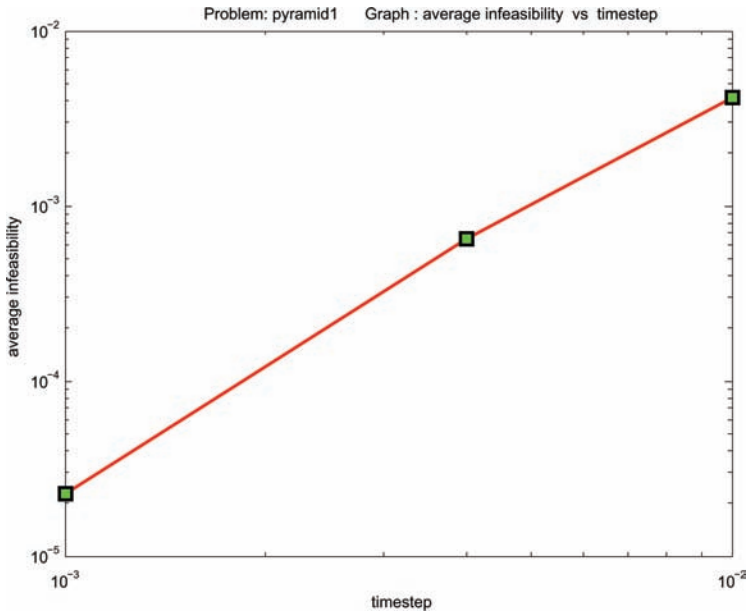

Figure 22: Problem Pyramid1: Infeasibility

In Figure 21, we show six successive frames from the simulation. They represent the situation for the values of time 0, 1, 2, 3, 4, and 10 seconds, respectively. The quadratic nature of the constraint stabilization is again demonstrated in Figure 22 when we again fixed $\gamma = 1$ and observed that, as $h \in \{0.1, 0.02, 0.01, 0.002, 0.001\}$ that the behavior of the infeasibility is proportional to the square of the stepsize in the limit, again validating Theorem 6.12.

7.3 PROBLEM: DICE3

Originally, the theory for this thesis was developed for demonstration with two dimensional problems. However, it soon became clear that the concepts easily extended to three dimensions. What followed is the extension of the theoretical analysis to three dimensionsa. This problem is precisely a three dimensional problem and two cubes, one on top of the other. Gravity causes the cube on top to fall over the edge of the bottom cube.

We ran the simulation for 3 seconds with the parameters:

h	μ	γ	ϵ_x	ϵ_t	ϵ_0	δ_{max}
0.01	0.1	0.3	0.5	0.2	$1.0e-7$	$1.0e+10$

At the end of the simulation, both of the bodies were on the floor but the one that fell was not quite at rest. In Figure 23, we show four successive frames from the simulation. They represent the situation for the values of time 0, 1, 2, and 3 seconds, respectively.

We were excited to notice the quadratic nature of the constraint stabilization for this three dimensional problem, again seen in Figure 24 when we fixed $\gamma = 1$ and observed that, as $h \in \{0.1, 0.05, 0.01, 0.005\}$ that the behavior of the infeasibility is proportional to the square of the stepsize in the limit, again validating Theorem 6.12 for a 3D case.

7.4 PROBLEM: SETUP6

This problem is another three dimensional problem and consists of two polyhedra, a cube and a tetrahedron. The cube is dropped from its initial position somewhat above the cube. Once it is dropped, it falls and collides with the tatrahedron. The collision causes the cube to fall to the floor and slide away, while the tetrahedron slides into the corner.

Note again the quadratic nature of the constraint stabilization for this three dimensional problem, again seen in Figure **??**. We fixed $\gamma = 0.3$ and observed that, as $h \in \{0.1, 0.03, 0.01, 0.003, 0.001\}$ that the behavior of the infeasibility is proportional to the square of the stepsize in the limit, again validating Theorem 6.12 for a 3D case.

We ran the simulation for 6 seconds with the parameters:

h	μ	γ	ϵ_x	ϵ_t	ϵ_0	δ_{max}
0.01	0.3	0.3	0.5	0.5	$1.0e-7$	$1.0e+10$

At the end of the simulation, both bodies were all on the floor and at rest. In Figure 26, we show four successive frames from the simulation. They represent the situation for the values of time 0, 2, 4, and 6 seconds, respectively.

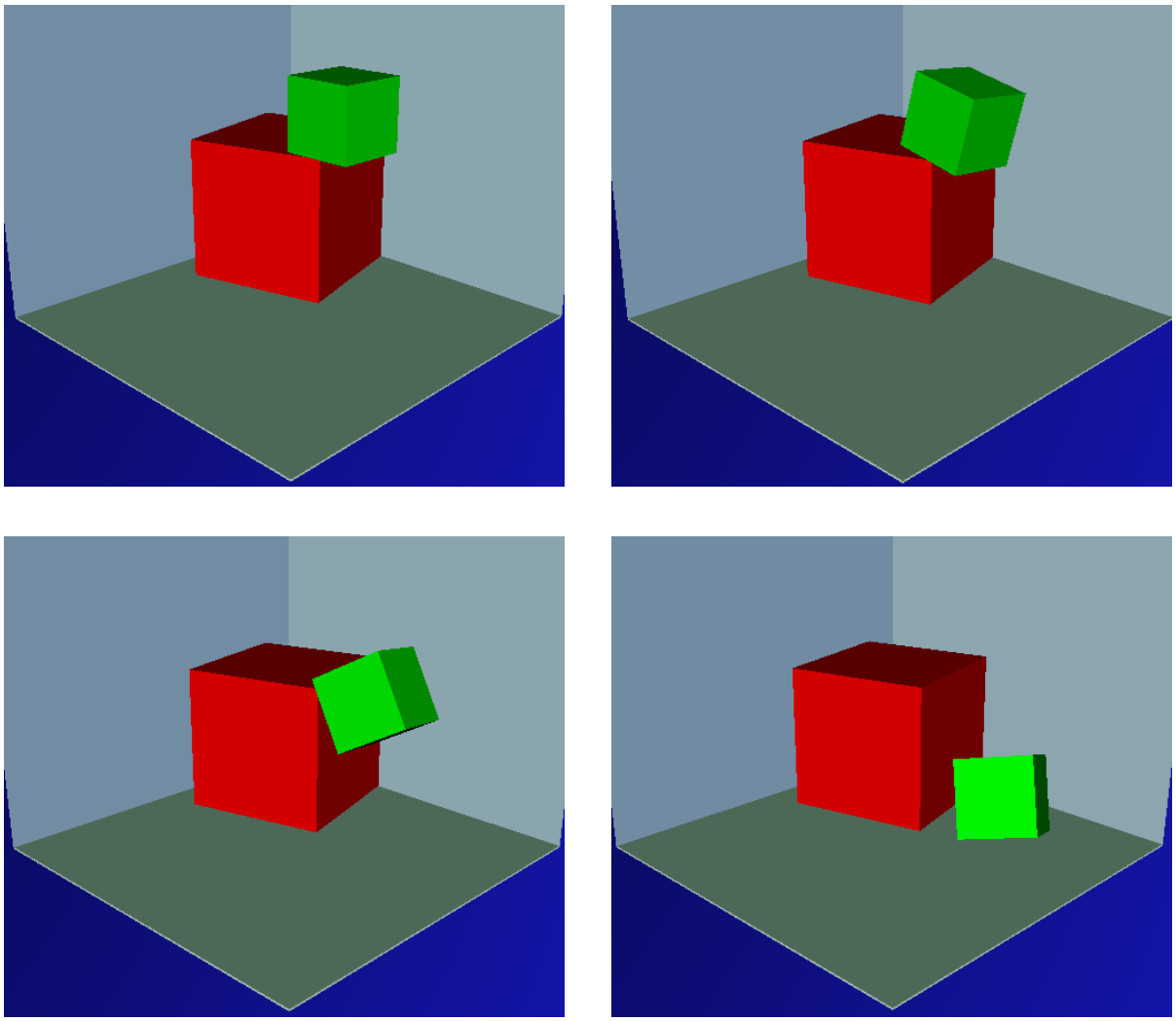

Figure 23: Four successive frames from Dice3

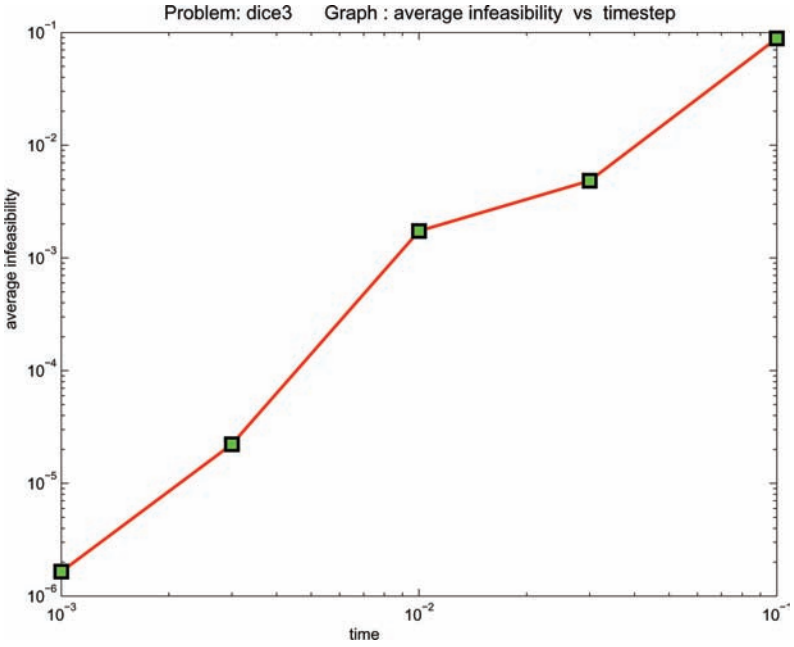

Figure 24: Problem dice3: Infeasibility

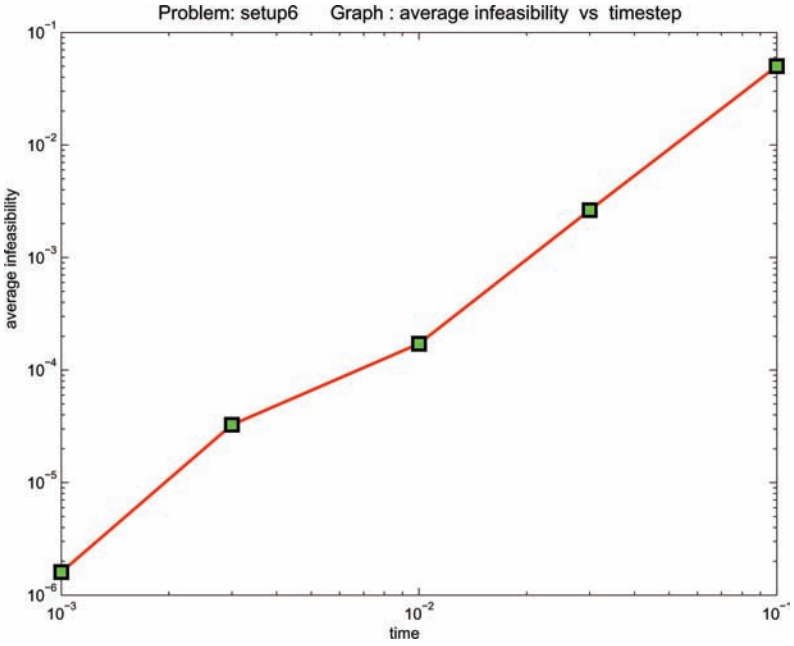

Figure 25: Problem Setup6: Infeasibility

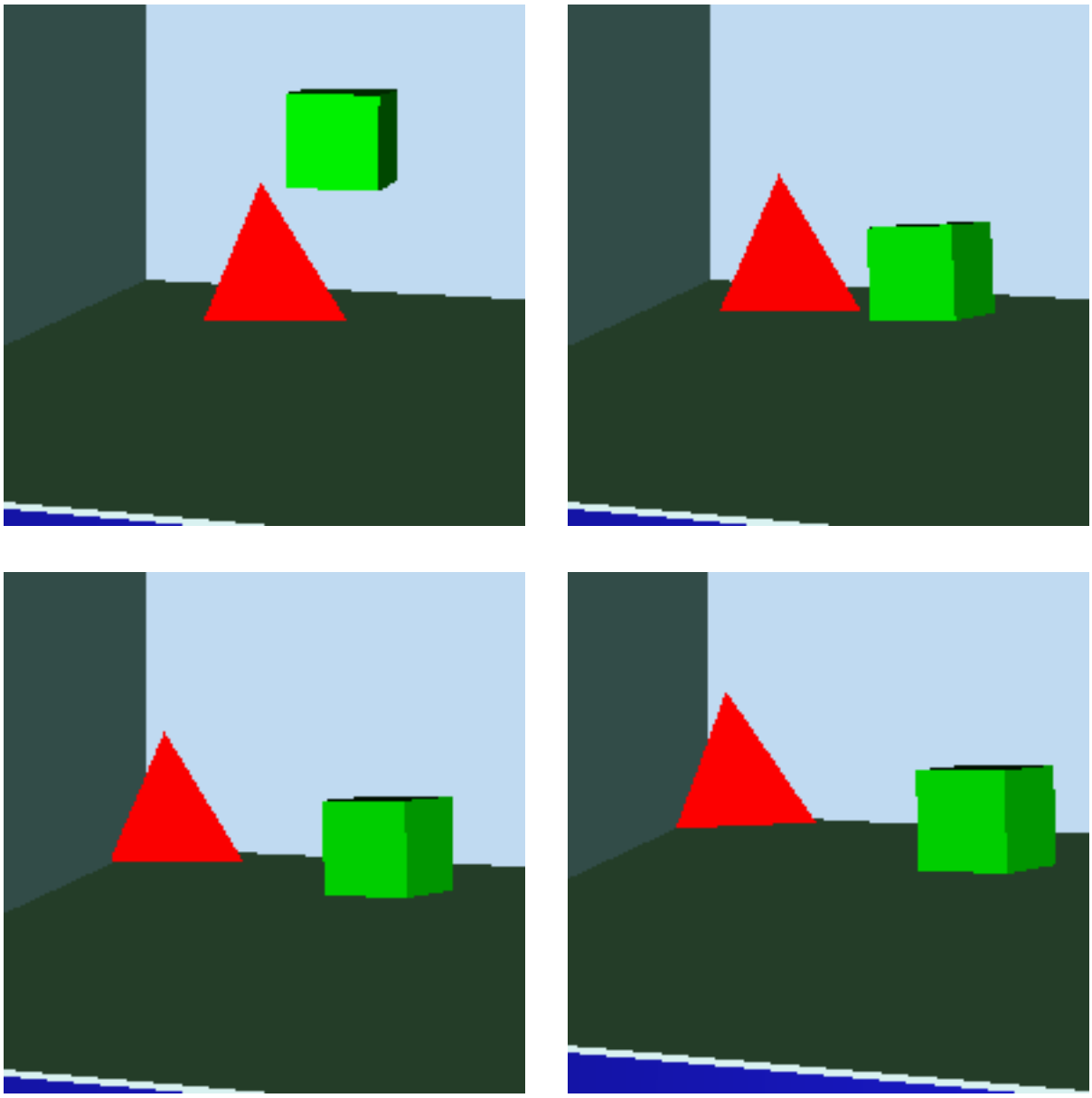

Figure 26: Four successive frames from Setup6

7.5 DISCUSSION OF RESULTS

We have successfully defined a method that achieves constraint stabilization while solving only linear complementarity problem per step [5]. Our method does not need to stop and detect collisions explicitly and can advance with a constant time step and predictable amount of effort per step. We proved that the velocity stays bounded and that the constraint infeasibility is uniformly bounded in terms of the size of the time step and the current value of the velocity.

All this is still possible for polyhedral bodies because of our newly defined Ratio Metric Penetration Depth, which we used to calculate the distance or interpenetration between bodies. The simulations all look very good, and we have shown successive frames for each simulation. The achievement of constraint stabilization appears to be validated by our numerical results, as seen in Figures 20 and 22.

8.0 CONCLUSIONS AND FUTURE WORK

In the analysis of the time-stepping scheme for multi-body dynamics with joints, contact, and friction that stabilizes constraint infeasibility while solving only one linear complementarity problem per step, local constraint stabilization has already been proved for the choice of $\gamma = 1$ [5]. It was shown that this scheme achieves constraint stabilization and that infeasibility at step l is upper bounded by $O(||h_{l-1}||^2 \left|\left|v^{(l)}\right|\right|^2)$. We have developed a scheme with $0 < \gamma \leq 1$, used it in a robotics applications, and demonstrated numerically its convergence [7]. We have now extended the convergence analysis to prove that the scheme achieves constraint stabilization. *That is*, this thesis has shown that the constraint infeasibility is of order $O(h^2)$ where h is the time step, while the accuracy of the method is order $O(h)$.

However, any body can be approximated by a finite union of convex, smooth-shaped bodies, we could extend, in principle, the analysis for approximation of any configuration, and we have now succeeded in extending the results with smooth bodies to non-smooth or non-convex bodies. Therefore, this thesis has advanced anaylsis in the specific area of convex polyhedra, which has currently not been performed to date. In order to do that, we proposed a new metric that improves upon the current method of detection of collisions or penetrations. This is a natural next step to move towards the analysis of contact with non-smooth bodies.

Specifically, we have produced a metric that is equivalent to the Minkowski-type ones proposed in [2, 32, 33], but with the huge advantage that penetration is simple to determine computationally. Our new metric is truly interesting because penetration between two bodies is easily determined. One of the truly remarkable aspects of the use of this metric is its simplicity, in that its computations only involves solving a linear programming problem, which can be done very efficiently.

Note that the major accomplishments *achieved in this thesis* can be summarizes as follows:

1. *I have successfully* developed a special signed distance function indicator, which we defined in Definition 2.12, for convex, polyhedral bodies. The function is based on solving the linear program. Recall that the advantage is that computing this indicator function has complexity $O(m+n)$, where m, n are the facets of the polyhedra, due to results on the complexity of linear programming in R^3 [35]. This compares much favorably with previous results that have a worst case complexity at best $O(n^2)$ [32, 33].
2. *We have successfully* shown from the Metric Equivalence Theorem 2.16 that this new measure of penetration depth is equivalent to the Minkowski Penetration Depth metric, at least in the limit of small penetration.
3. *We have successfully* calculated the generalized gradients of this function, which are needed in the linearization phase for implementation, by sensitivity analysis of the linear program. This was discussed in Remarks 3.12 and and 3.10 and for a CoF contact, we use equation 3.8.
4. *We have successfully* extended the convergence analysis to prove in Theorem 6.12 that, when used in conjuction with the calculated generalized gradients, the scheme achieves constraint stabilization. Particularly, we proved that *the constraint infeasibility is order* $O(h^2)$ where h is the time step, while the accuracy of the method is order $O(h)$.
5. *We have successfully* implemented the analysis into a method, namely Algorithm 6.5 that achieves constraint stabilization while solving only one linear complementarity problem per step for several problems with good results.

Some future endeavors based on this research may include:

- Optimizing program performance. Some of the programs used were previously created and optimized for smooth bodies, and adapted for polyhedral bodies. They need to be optimized for polyhedral bodies.
- Optimizing the algorithm. Worth serious investigation is the adoption of an algorithm which at each step solves a strictly convex quadratic program, as opposed to solving a mixed linear complementarity problem by conventional methods.

- Extending the results of piecewise smooth signed distance functions to piecewise smooth signed distance functions. We might get better results or sharper bounds from using piecewise smooth functions.
- Extension to higher dimensions. It might be interesting to extend all results to higher dimensions so as to include general convex polytopes, because future applications might not be limited to three dimensions.
- Evaluating the bounds of constraint stabilization. It would be interesting to explore the possibility of constraint stabilization results being useful for values of $\gamma \geq 1$. It is worth experimentation, since there are cases where extrapolation is beneficial, such as the method of successive over relaxation (SOR) in the numerical solution of systems of linear equations.
- Expansion of numerical examples. Of further interest is the implementation of this method to sized-based segregation problems, such as the Brazil Nut example, using polyhedral bodies..

BIBLIOGRAPHY

[1] L. Adhamï, E. Coste-Manière, and J.-D. Boissonnat, *Planning and simulation of robotically assisted minimal invasive surgery*, in Proc. Medical Image Computing and Compter Assisted Intervention (MICCAI'00), vol. 1935 of Lect. Notes in Comp. Sc. 1954, Springer, Oct 2000.

[2] P. K. Agarwal, L. J. Guibas, S. Har-Peled, A. Rabinovitch, and M. Sharir, *Penetration depth of two convex polytopes in 3d*, Nordic Journal in Computing, 7 (2000), pp. 227–240.

[3] M. Anitescu, J. F. Cremer, and F. A. Potra, *Formulating 3d contact dynamics problems*, Mechanics of Structures and Machines, 24 (1996), pp. 405–437.

[4] M. Anitescu and G. D. Hart, *Solving nonconvex problems of multibody dynamics with joints, contact, and small friction by successive convex relaxation*, Mechanics Based Design of Structures and Machines, 31 (2003), pp. 335–356.

[5] ——, *A constraint-stabilized time-stepping approach for rigid multibody dynamics with joints, contact and friction*, International Journal for Numerical Methods in Engineering, 60 (2004), pp. 2335–2371.

[6] ——, *A fixed-point iteration approach for multibody dynamics with contact and small friction*, Mathematical Programming, 101 (2004), pp. 3–32.

[7] M. Anitescu, A. Miller, and G. D. Hart, *Constraint stabilization for time-stepping approaches for rigid multibody dynamics with joints, contact and friction*, in Proceedings of the 2003 ASME International Design Engineering Technical Conferences, Chicago, Illinois, 2003, American Society for Mechanical Engineering. ANL/MCS-P1023-0403.

[8] M. Anitescu and F. A. Potra, *Formulating dynamic multi-rigid-body contact problems with friction as solvable linear complementarity problems*, Nonlinear Dynamics, 14 (1997), pp. 231–247.

[9] ——, *On integrating stiff rigid multibody dynamics with contact and friction*, in Contact Mechanics. Proceedings of the 3rd Contact Mechanics International Symposium, Praia

de Consola cão, Peniche, Portugal, June 17-21, 2001, Dordrecht, Netherlands, 2002, Kluwer Academic Publishers.

[10] M. Anitescu, F. A. Potra, and D. Stewart, *Time-stepping for three-dimensional rigid-body dynamics*, Computer Methods in Applied Mechanics and Engineering, 177 (1999), pp. 183–197.

[11] U. M. Ascher, H. Chin, L. R. Petzold, and S. Reich, *Stabilization of constrained mechanical systems with daes and invariant manifolds*, J. Mech. Struct. Mach, 23 (1995), pp. 135 – 158.

[12] U. M. Ascher, H. Chin, and S. Reich, *Stabilization of daes and invariant manifolds*, Numerische Mathematik, 67 (1994), pp. 131–149.

[13] U. M. Ascher and L. R. Petzold, *Computer methods for ordinary differential equations and differential-algebraic equations*, Society for Industrial and Applied Mathematics, Philadelphia, PA, 1998.

[14] Y. Baillot, J. P. Rolland, and D. L. Wright, *Automatic modeling of knee-joint motion for the virtual reality dynamic anatomy (vrda) tool"*, Presence: Teleoperators and Virtual Environments (MIT Press), 9 (3) (2000), pp. 223 – 235.

[15] D. Baraff, *Issues in computing contact forces for non-penetrating rigid bodies*, Algorithmica, 10 (1993), pp. 292–352.

[16] J. Baumgarte, *Stabilization of constraints and integrals of motion in dynamical systems*, Computer Methods in Applied Mechanics and Engineering, 1 (1972), pp. 1–16.

[17] F. H. Clarke, *Optimization and Nonsmooth Analysis*, vol. 5 of SIAM Classics in Applied Mathematics, SIAM, Philadelphia, 1990.

[18] M. B. Cline and D. K. Pai, *Post-stabilization for rigid body simulation with contact and constraints*, in Proceedings of the IEEE International Conference in Robotics and Automation, IEEE, 2003.

[19] C. A. C. Coello, *Use of a self-adaptive penalty approach for engineering optimization problems*, Computers in Industry, 41 (2000), pp. 113–127.

[20] D. W. Coit and A. E. Smith, *Penalty guided genetic search for reliability design optimization*, Computers and Industrial Engineering, 30 (2000), pp. 895–904.

[21] R. W. Cottle, J.-S. Pan, and R. E. Stone, *The Linear Complementarity Problem*, Academic Press, Boston, 1992.

[22] J. F. Cremer and D. E. Stewart, *The architecture of newton, a general purpose dynamics simulator*, in Proceedings of the IEEE International Conference in Robotics and Automation, IEEE, 2003, pp. 1806–1811.

[23] J. Difede and H. G. Hoffman, *Virtual reality exposure therapy for world trade center post traumatic stress disorder: A case report*, CyberPsychology and Behavior, 5(6) (2002), pp. 529–536.

[24] B. R. Donald and D. K. Pai, *On the motion of compliantly connected rigid bodies in contact: a system for analyzing designs for assembly*, in Proceedings of the Conf. on Robotics and Automation, IEEE, 1990, pp. 1756–1762.

[25] C. Glocker and F. Pfeiffer, *An lcp-approach for multibody systems with planar friction*, in Proceedings of the CMIS 92 Contact Mechanics Int. Symposium, Lausanne, Switzerland, 1992, pp. 13 – 30.

[26] ——, *Multiple impacts with friction in rigid multi-body systems*, Nonlinear Dynamics, 7 (1995), pp. 471–497.

[27] E. Hairer and G. Wanner, *Solving ordinary differential equations I – non-stiff problems*, vol. 8 of Springer Series in Comput. Mathematics, Springer-Verlag, Berlin, 1993.

[28] G. D. Hart and M. Anitescu, *A hard-constraint time-stepping approach for rigid multibody dynamics with joints, contact, and friction*, in Proceedings of the Richard Tapia Celebration of Diversity in Computing Conference 2003, J. Meza and B. York, eds., New York, NY, USA, 2003, ACM Press, pp. 34–41.

[29] E. J. Haug, *Computer Aided Kinematics and Dynamics of Mechanical Systems. Vol. 1: Basic Methods*, Allyn & Bacon, Inc., Needham Heights, MA, USA, 1989.

[30] L. Hodges, P. L. Anderson, G. C. Burdea, H. G. Hoffman, and B. O. Rothbaum, *Treating psychological and physical disorders with vr*, IEEE Computer Graphics and Applications, (2001), pp. 25–33.

[31] W. Huyer and A. Neumaier, *A new exact penalty function*, SIAM J. on Optimization, 13 (2002), pp. 1141–1158.

[32] Y. J. Kim, M. C. Lin, and D. Manocha, *Deep: Dual-space expansion for estimating penetration depth between convex polytopes*, in Proceedings of the 2002 International Conference on Robotics and Automation, vol. 1, Institute for Electrical and Electronics Engineering, 2002, pp. 921–926.

[33] Y. J. Kim, M. A. Otaduy, M. C. Lin, and D. Manocha, *Fast penetration depth computation for physically-based animation*, in Proceedings of the 2002 ACM Siggraph/Eurograph symposium on Computer Animation, J. Hodgins and M. van de Panne, eds., San Antonio, Texas, 2002, Association for Computing Machinery, pp. 21 – 33.

[34] U. Kühnapfel, H. Çakmak, and H. Maass, *Endoscopic surgery training using virtual reality and deformable tissue simulation*, Computers and Graphics, 24 (2000), pp. 671–682.

[35] N. Megiddo, *Linear-time algorithms for linear programming in r^3 and related problems*, SIAM Journal on Computing, 12 (1983), pp. 759–776.

[36] V. J. Milenkovic and H. Schmidl, *Optimization-based animation*, in SIGGRAPH 2001, Computer Graphics Proceedings, E. Fiume, ed., ACM Press / ACM SIGGRAPH, 2001, pp. 37– 46.

[37] A. Miller and H. I. Christensen, *Implementation of multi-rigid-body dynamics within a robotic grasping simulator*, in IEEE International Conference on Robotics and Automation, 2003, pp. 2262– 2268.

[38] T. B. Moeslund and E. Granum, *A survey of computer vision-based human motion capture*, Computer Vision and Image Understanding: CVIU, 81 (2001), pp. 231–268.

[39] F. Mourgues, F. Devernay, G. Malandain, and E. Coste-Manière, *3d+t modeling of coronary artery tree from standard non simultaneous angiograms*, in MICCAI, 2001, pp. 1320–1322.

[40] R. M. Murray, Z. Li, and S. S. Sastry, *A Mathematical Introduction to Robotic Manipulation*, CRC Press, Inc., Boca Raton, FL, 1994.

[41] D. Q. Nguyen, R. Fedkiw, and H. W. Jensen, *Physically based modeling and animation of fire*, in SIGGRAPH 2002 Annual Conference, ACM Press / ACM SIGGRAPH, 2002, pp. 721 – 728.

[42] J.-S. Pang and D. E. Stewart, *A unified approach to frictional contact problems*, International Journal of Engineering Science, 37 (1999), pp. 1747–1768.

[43] B. O. Rothbaum, L. Hodges, P. L. Anderson, L. Price, and S. Smith, *Twelve-month follow-up of virtual reality and standard exposure therapies for the fear of flying*, Journal of Consulting and Clinical Psychology, 70(2) (2002), pp. 428–432.

[44] B. O. Rothbaum, L. Hodges, D. Ready, K. Graap, and R. D. Alarcon, *Virtual reality exposure therapy for vietnam veterans with posttraumatic stress disorder*, Journal of Clinical Psychiatry, 62(8) (2001), pp. 617–622.

[45] W.-J. Shiu, F. V. Donzé, and S.-A. Magnier, *Numerical study of rockfalls on covered galleries by the discrete element method*, Electronic Journal of Geotechnical Engineering, 11 Bundle D (2006).

[46] P. Song, P. Kraus, V. Kumar, and P. Dupont, *Analysis of rigid-body dynamic models for simulation of systems with frictional contacts*, Journal of Applied Mechanics, 68 (2001), pp. 118–128.

[47] D. E. Stewart, *Convergence of a time-stepping scheme for rigid body dynamics and resolution of painleve's problems*, Archive Rational Mechanics and Analysis, 145 (1998), pp. 215–260.

[48] ——, *Rigid-body dynamics with friction and impact*, SIAM Review, 42 (2000), pp. 3–39.

[49] D. E. Stewart and J. C. Trinkle, *An implicit time-stepping scheme for rigid-body dynamics with inelastic collisions and coulomb friction*, International Journal for Numerical Methods in Engineering, 39 (1996), pp. 2673–2691.

[50] J. Trinkle, J.-S. Pang, S. Sudarsky, and G. Lo, *On dynamic multi-rigid-body contact problems with coulomb friction*, Zeithschrift fur Angewandte Mathematik und Mechanik, 77 (1997), pp. 267–279.

[51] T. Weiner, *Pentagon has sights on robot soldiers*, Feb 2005. New York Times News Service, appearing in The San Diego Union-Tribune, available online at *http://www.signonsandiego.com/uniontrib/20050216/news_1n16robot.html* .

[52] *Stanford team wins robot race.* online, Oct 2005. Associated Press, available online from MSNBC.com at *http://www.msnbc.msn.com/9621761/*"id/.

[53] *World robotics 2004*, Oct 2004. Press release, available online from UNECE.org at *http://www.unece.org/press/pr2004/04robots_ index.htm.*